Cell Type-Specific Analysis of Bcl-xL Genomic Imprinting in the Mouse Brain

Cell type-specific analysis of *Bcl-x*$_L$ genomic imprinting in the mouse brain

A dissertation presented

by

Olivia Ho-Shing

to

The Department of Molecular and Cellular Biology

in partial fulfillment of the requirements

for the degree of

Doctor of Philosophy

in the subject of

Biochemistry

Harvard University

Cambridge, Massachusetts

April 2019

Dissertation Advisor: Catherine Dulac Olivia Ho-Shing

Cell type-specific analysis of *Bcl-x*$_L$ genomic imprinting in the mouse brain

Abstract

Genomic imprinting is a form of epigenetic inheritance that causes preferential expression of one allele based on its parent of origin. Imprinted expression plays crucial roles in brain development, and is associated with growth and mental disorders in humans including Prader-Willi and Angelman syndromes. Our lab has previously used RNA sequencing to uncover a large number of genes in the post-natal mouse brain, which exhibit a parental bias in their expression instead of canonical "all-or-none" imprinted expression. While these genes have been implicated in critical cellular pathways, it has been unclear what functional effects, if any, their biased expression may have on neuronal development and mature function. Moreover, we have no information about the nature of this biased expression at the level of individual neurons. Here, we investigate the gene *Bcl2l1* (*Bcl-x*$_L$), an anti-apoptotic regulator that exhibits a 60%:40% paternal bias in the cortex. We evaluate the functional consequences from brain-specific deletion of either the maternal or paternal allele of *Bcl-x*, using various cellular analyses and electrophysiological methods. We find that paternal, but not maternal deletion of Bcl-x affects cell survival and synaptic plasticity in the cortex. We also use single molecule fluorescence *in situ* hybridization to evaluate the nature of *Bcl-x*$_L$ biased expression at the level of single cells. Interestingly, we uncover remarkable cell type specificity to the imprinted expression of *Bcl-x*$_L$ in the cortex. Our findings shed new light on the impact of imprinted regulation on neuronal cell fate and function.

Acknowledgments

I would like to thank first and foremost my Ph.D. advisor, Catherine Dulac, for her continuous support and enthusiasm. I thank the members of my Dissertation Advisory Committee – D. Haig, T. Hensch and J. Lichtman – for their patience and constructive advice in the completion of this dissertation.

I thank Y. Isogai and S. Santoro for training me in *in situ* techniques; D. Richardson for training me in microscopy; A. Raj, J. Rinn and F.E. Hacisuleyman for their support and advice on single molecule FISH. I thank my collaborator M.D. Caiati for her work on synaptic plasticity in the visual cortex. I also deeply appreciate J. Perez, N. Rubinstein, B. Bintu, and H. Chung for their companionship and critical help with various analyses. I thank L. Needleman and D. Lessing for their help with cellular analyses, S. Sullivan for her help managing unruly mice; T. Tang for his computational input; and R. Hellmiss for her guidance in graphic design.

Dedication

I dedicate this dissertation to my family, especially my sister, mother and father for their unconditional love and support. And finally, to Bailey – his companionship, warmth and loyalty has carried me through graduate school.

Table of Contents

Chapter I. Introduction

Overview of genomic imprinting

Genomic imprinting is a form of epigenetic regulation found in mammals and flowering plants, which leads to the preferential expression from either the maternally or paternally inherited allele of certain genes. Although imprinted genes represent less than one percent of the mammalian genome, imprinted gene expression has been shown to play critical roles in embryonic development and adult tissue function, particularly affecting the brain (Perez et al., 2016; Tucci et al., 2019). In humans, Prader-Willi and Angelman syndromes were among the first recognized examples of imprinting defects. Prader-Willi syndrome results from disruption of one or more paternally inherited genes on chromosome 15q11–13, and is characterized by mild retardation, impaired satiety, and compulsive behavior (Angulo et al., 2015). Angelman syndrome results from disruption of the maternally inherited copy of *Ube3a* (within the 15q11-13 cluster), and is characterized by severe mental retardation, ataxia and frequent laughter. These disorders provide striking examples of how specific parent-of-origin allelic expression is essential for normal behavior control and brain function.

In parallel to clinical studies of defects in imprinted genes, studies of chimeric embryos that contain two maternal genomes (gynogenetic) or two paternal genomes (androgenetic) bolstered our understanding of this phenomenon, and suggested that the genome inherited from each parent contributes differently to the development of the brain (Keverne et al., 1996). Specifically, it was found that gynogenetic and androgenetic cells

populate different regions of the brain throughout development. Gynogenetic cells were found in hippocampal, striatal and higher cortical regions, and chimeric embryos containing gynogenetic cells developed abnormally large brains. Androgenetic cells on the other hand were found in areas including the hypothalamus and brain stem, and chimeric embryos containing androgenetic cells developed abnormally small brains. These early findings suggested that genomic imprinting strongly influences the fate or survival of neuronal cell populations, and that imprinted gene expression may dramatically alter complex neural networks and brain function. In this chapter, we discuss how improved experimental technologies have helped to identify and characterize expression of a novel class of imprinted genes in brain tissues. We then review the roles of imprinted genes in regulating key neural pathways including neurogenesis, synaptic transmission and apoptosis. This review aims to provide a better understanding of the nature and functional significance of genomic imprinting in the normal and pathological brain.

Parent-of-origin allelic expression in the brain

Early studies of genomic imprinting established the canonical definition of imprinted regulation as the complete epigenetic silencing of one parental allele, causing monoallelic expression from the other parent-of-origin copy (Bartolomei and Ferguson-Smith, 2011). For example, *Igf2*, one of the first identified imprinted genes, was initially observed to be transcriptionally active from the paternal allele while the maternal copy was silenced in the developing embryo (DeChiara et al., 1991). However, other imprinted genes, including *Gnas* and *Ube3a* displayed a bias in their expression for one of the two

parent-of-origin alleles, rather than strict monoallelic expression (Albrecht et al., 1997; Judson et al., 2014; Yu et al., 1998).

More recent genome-wide studies however, primarily characterizing expression in genetically tractable hybrid mice, have broadened the understanding of imprinted regulation beyond canonical monoallelic expression. Indeed, although some imprinted genes such as *Impact* are strictly expressed from one parental allele across all tissues, the allelic expression profiles of other imprinted genes, such as *Igf2*, uncovers newly appreciated and more nuanced imprinted effects across the brain and in non-brain tissues (**Figure 1.1**). Particularly in the postnatal brain, one can identify parentally biased gene expression that changes dynamically across brain regions and developmental stages. Rigorous genome-wide RNA sequencing analyses have uncovered numerous genes with significant parental bias in expression throughout the brain (Andergassen et al., 2017; Babak et al., 2015; Bonthuis et al., 2015b; Crowley et al., 2015; DeVeale et al., 2012; Gregg et al., 2010a; Gregg et al., 2010b; Perez et al., 2015; Pinter et al., 2015; Sittig and Redei, 2014; Ye et al., 2015), strongly suggesting that imprinted gene expression is a rather common epigenetic mechanism employed by the brain to tightly regulate neural networks. These studies initiated by Dulac and colleagues characterize emergent patterns of parentally biased expression identified in the brain.

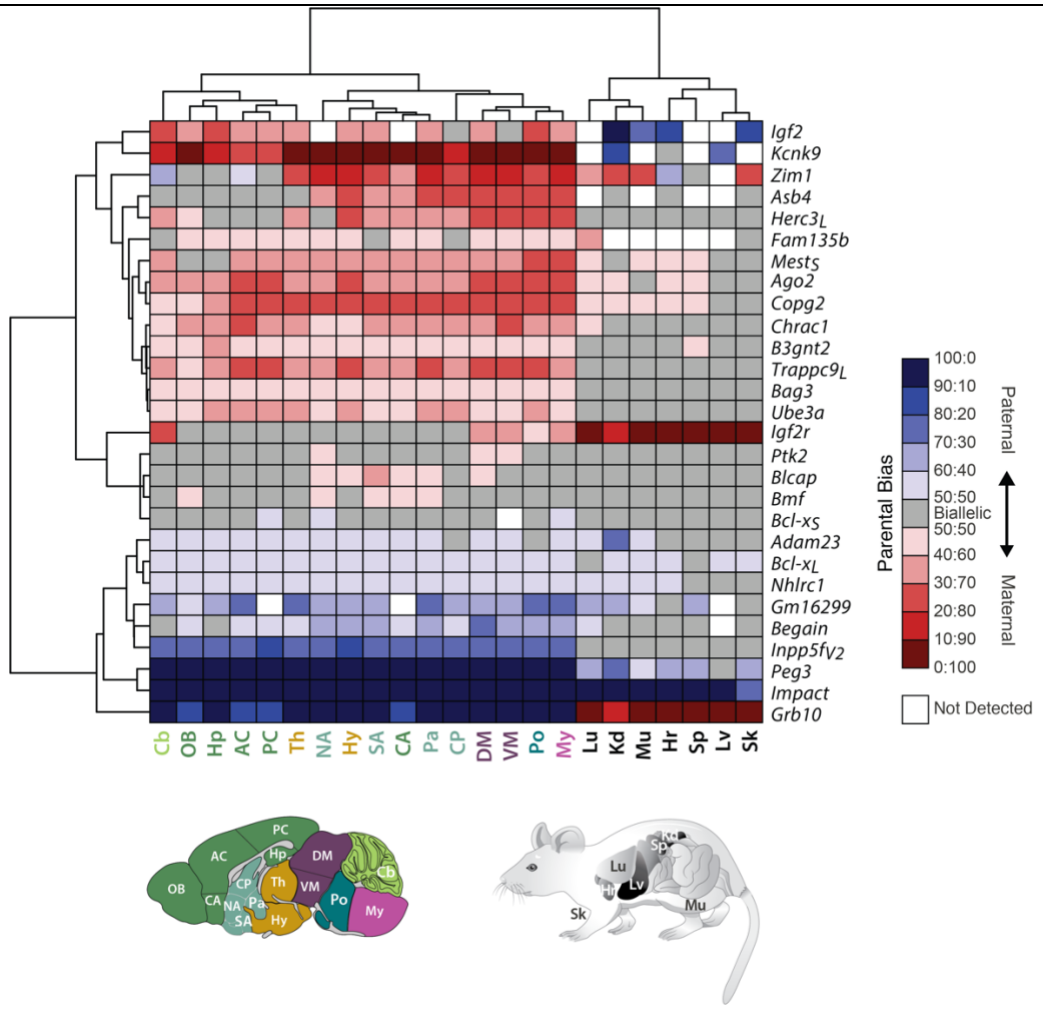

Figure 1.1: Parentally biased imprinted genes in adult mouse.

Spatial regulation of imprinting represented by a hierarchically clustered heat map of the deviation from biallelic gene expression. Panel adapted from Perez *et al*. (2015). L and S subscripts indicate long and short isoforms, respectively, and V2 indicates variant 2 isoform. Brain regions: AC, anterior cortex; CA, cortical amygdala; Cb, cerebellum; CP, caudate putamen; DM, dorsal midbrain; Hp, hippocampus; Hy, hypothalamus; My, medulla; NA, nucleus accumbens; OB, olfactory bulb; Pa, pallidum; PC, posterior cortex; Po, pons; SA, striatum-like amygdala; Th, thalamus; VM, ventral midbrain. Somatic tissues: Hr, heart; Kd, kidney; Lu, lung; Lv, liver; Mu, muscle; Sk, skin; Sp, spleen.

Next generation sequencing approaches have provided powerful new experimental platforms that enabled the detection of a large spectrum of parental biases in RNA transcripts from various biological samples. Initial studies using high-resolution sequencing provided conflicting results. While some highly stringent analyses identified only a few novel imprinted genes and failed to detect some known imprinted genes (Babak et al., 2008; Wang et al., 2008), less conservative approaches (Gregg et al., 2010a; Gregg et al., 2010b) uncovered a continuum of allelic effects in the expression of specific genes, and even specific isoforms. Both the magnitude and direction of parental bias varied across different brain regions and developmental stages. These results suggested the existence of intricate stage-specific gene regulation of the parental genomes in establishing neural pathways. Interestingly, while many strongly imprinted genes were implicated in neural circuits associated with feeding and motivated behaviors, genes that displayed a parental bias in expression often functioned in cell metabolism and signaling. Further studies strengthened the statistical methods applied to RNA sequencing results, used independent experimental methods to validate the observed parental biases, and corroborate novel imprinted genes (Andergassen et al., 2017; Bonthuis et al., 2015b; Crowley et al., 2015; Lawson et al., 2013; Perez et al., 2015). These parentally biased expression patterns revealed new intricacies of transcriptional regulation in the brain and expanded the scope of parent-of-origin-specific epigenetic regulation. Moreover, the discovery of extensive parent-of-origin expression biases prompted new questions about the range and function of this form of imprinted regulation, particularly throughout the postnatal brain.

While previously known imprinted genes were seen to be mostly expressed at high levels, genes exhibiting a parental bias appeared usually expressed at low to moderate

levels (Bonthuis et al., 2015b; Gregg et al., 2010b; Perez et al., 2015). Because of the lower expression levels and spatiotemporal specificity of parentally biased expression, some discrepancy remains between studies about the exact number of genes regulated by imprinting (Bartolomei and Ferguson-Smith, 2011; DeVeale et al., 2012; Gregg, 2014; Hayden, 2012), highlighting key issues related to the sensitivity of the RNA sequencing technique and statistical analysis (DeVeale et al., 2012; Hayden, 2012; Huang et al., 2017; Mott et al., 2014; Zou et al., 2018), and expression variations in different genetic backgrounds (Andergassen et al., 2017; Crowley et al., 2015). Perez et al. (**Figure 1.1**) and other RNA sequencing studies (Andergassen et al., 2017; Babak et al., 2015; Bonthuis et al., 2015; Crowley et al., 2015; Huang et al., 2017; Perez et al., 2015) characterized and validated imprinted expression patterns of roughly 200 genes. About one-third of monoallelic imprinted genes are protein-coding, the majority comprised of noncoding microRNAs, small nucleolar RNAs and long non-coding RNAs (lncRNAs), presumably allowing the regulation of a wide network of genes (Perez et al., 2015). On the other hand, almost 95% of parentally biased genes (exhibiting a weak to robust parent-of-origin effect between 50:50 and 90:10) are protein-coding genes clustered in loci with known strongly imprinted genes (**Figure 1.2**) (Perez et al., 2016). From these studies, a consensus has emerged that imprinted effects are more prevalent in brain than somatic tissues for mice, rats and humans (Babak et al., 2015; Huang et al., 2017; Perez et al., 2016), supporting the notion that genomic imprinting may constitute a well-conserved mechanism to instruct neural function.

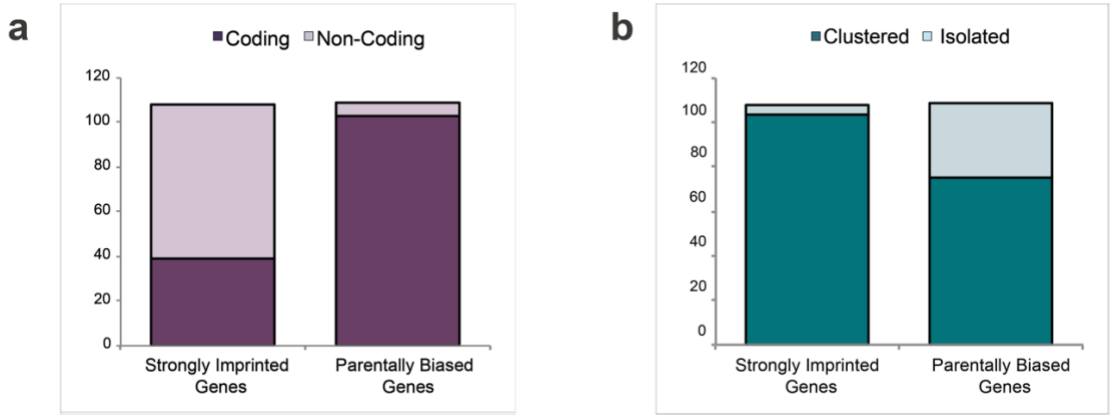

Figure 1.2: Genetic characterization of parentally-biased genes.

a): Number of coding and non-coding genes among strongly imprinted genes and parentally biased genes in the adult mouse cerebellum. b): Number of clustered and isolated genes among strongly imprinted genes and parentally biased genes in the adult mouse cerebellum. Strongly imprinted genes exhibit a 90:10 to 100:0 parental bias. Parentally biased genes include genes that exhibit a 60:40 to 90:10 parental bias. Figure adapted from Perez et al. (2015).

Spatiotemporal dynamics of imprinted genes

Multiple studies have documented a higher frequency of imprinted gene expression in the hypothalamus compared to other brain regions (Babak et al., 2015; Gregg et al., 2010b; Kroeze et al., 2017), supporting the central focus on genomic imprinting in the hypothalamus seen in early studies with chimeric embryos (Keverne, 2014; Keverne et al., 1996). The arcuate nucleus of the hypothalamus expressed 79% more imprinted genes than the dorsal raphe nucleus of the midbrain, and 100-300% more than somatic skeletal tissues (Bonthuis et al., 2015). The cortex also exhibited high frequency of biased expression patterns, with more genes preferentially expressing the maternal allele. By contrast, preference for expression of the paternal allele predominated in mid- and hindbrain regions, including the hypothalamus.

Thus, imprinted expression in both rodents and humans appears most prevalent in the brain, and gene-specific allelic effects are highly tissue-, isoform-, and age-specific (Andergassen et al., 2017; Perez et al., 2015; Prickett and Oakey, 2012). Additionally, some imprinted genes such as *Ndn, Grb10 and Ube3a* have been shown to be imprinted strictly in neuronal cells, while other genes like *Igf2r* are imprinted strictly in non-neuronal cells. The dynamic patterns of allelic expression detected in the brain may therefore result from a summation of diverse imprinted effects occurring in different cell types (Cleaton et al., 2014; Perez et al., 2016; Perez et al., 2015).

While many studies have found that imprinted expression (*i.e.* the number of imprinted genes as well as the strength of the parental bias for a given gene) is strongest in embryonic tissues and placenta, a large (though reduced) number of genes display robust allelic effects into adulthood (Andergassen et al., 2017; Perez et al., 2015). Interestingly,

many genes with a parental bias see changes in the strength of the parental bias, or even switch from a parental bias to a biallelic expression across brain regions and across developmental stages. For example, the growth suppressor gene *Grb10* exhibits biallelic expression in the cerebellum at P8 (a pivotal developmental stage for granule cell migration), but switches to monoallelic paternal expression in the adult brain. Moreover, this expression is in sharp contrast to *Grb10* in various peripheral tissues, where it exhibits monoallelic maternal expression (Crowley et al., 2015; Gregg et al., 2010b; Pinter et al., 2015). Other genes like *Zim1* exhibit even stronger region-specific shifts in allelic bias: in the cerebellum, *Zim1* switches from maternally to paternally biased as expression from the maternal allele decreases in adulthood. Expression in other hindbrain and midbrain regions, however remain strongly maternal. Interestingly *Igf2*, which is exclusively expressed from the paternal allele throughout the body, exhibits varying magnitudes of maternal preference throughout the brain (Gregg et al., 2010b; Perez et al., 2015). (**Figure 1.1**)

Imprinted regulation appears to instruct neural function by modulating the expression levels of genes within imprinted clusters (Cleaton et al., 2014). Studies of specific developmental disorders such as Rett syndrome have demonstrated how even slight changes in gene dosage in brain tissues tightly correlates with the severity of mental illness behavioral phenotypes (Chao and Zoghbi, 2012; Lu et al., 2016). Therefore, even nuanced regulation of imprinted neural genes may be highly relevant to normal brain development and function, as well as disease states. Recently studies have shown that loss of differential methylation alters expression levels within the *H19*/*Igf2* cluster (Ginart et al., 2016), and a twofold increase in imprinted gene *Cdkn1c* expression mimics

neurological and behavioral phenotypes of Silver-Russell syndrome and other associated imprinted disorders (McNamara et al., 2018b; McNamara et al., 2018c). A key question, therefore, is whether parentally-biased expression indicates a similar, though more nuanced coordinated regulation of gene dosage (Gregg, 2014). Indeed, a specific test of this hypothesis showed that for the majority of parentally biased imprinted genes uncovered in the mouse, a positive correlation is observed between the strength of the parental bias and age-regulated changes in gene expression level (Perez et al., 2015). This important result suggested that imprinted regulation may have evolved as a mechanism to provide a tight control of gene dosage, for both monoallelic and parentally biased genes. In humans, RNA profiling of imprinted expression has not demonstrated a clear correlation between imprinted status and gene dosage, though this is possibly due to confounding differences in human genetic backgrounds (Baran et al., 2015).

Roles of imprinted genes in the brain

Extensive studies have further shown that imprinted genes regulate essential neurodevelopmental processes, including neural differentiation, migration and cell survival (**Figure 1.3**) (Perez et al., 2016). Key examples of the involvement of imprinted genes in these processes are reviewed below.

Role in neural development

Neural stem cells (NSCs) originate in the ventricular zone of the developing cortex and asymmetrically proliferate to produce glia or intermediate progenitor cells, and regenerate the stem cell pool. Progenitor cells give rise to immature, then differentiated

neurons (Kriegstein and Alvarez-Buylla, 2009). NSCs highly express the paternal *Plagl1*, a zinc-finger protein that induces the expression of the maternal cyclin-dependent kinase inhibitor *Cdkn1c*. *Cdkn1c* inhibits cyclin-dependent kinases in order to prevent NSC mitosis, and thereby activates a shift from proneural to proglial differentiation (Joseph et al., 2009; Perez et al., 2016). At a later stage, *Cdkn1c promotes* neuronal migration within the cortical plate by inducing actin polymerization (Tury et al., 2012). *Igf2* and paternal *Dlk1* in the embryonic brain regulate self-renewal of NSCs and intermediate progenitors in the subgranular zone and promote fetal cortical neurogenesis in mice and humans (Giannoukakis et al., 1993). Interestingly, *Igf2* is biallelically expressed in the choroid plexus and subventricular vasculature, maternally biased in other brain regions and paternally expressed in somatic tissues (DeChiara et al., 1991; Lehtinen et al., 2011; Perez et al., 2015). Biallelic expression of *Igf2* acts as a paracrine factor that regulates NSC homeostasis in the subventricular zone, but paternal expression of *Igf2* in the hippocampus acts as an autocrine factor for neurogenesis in the subgranular zone (Ferrón et al., 2015).

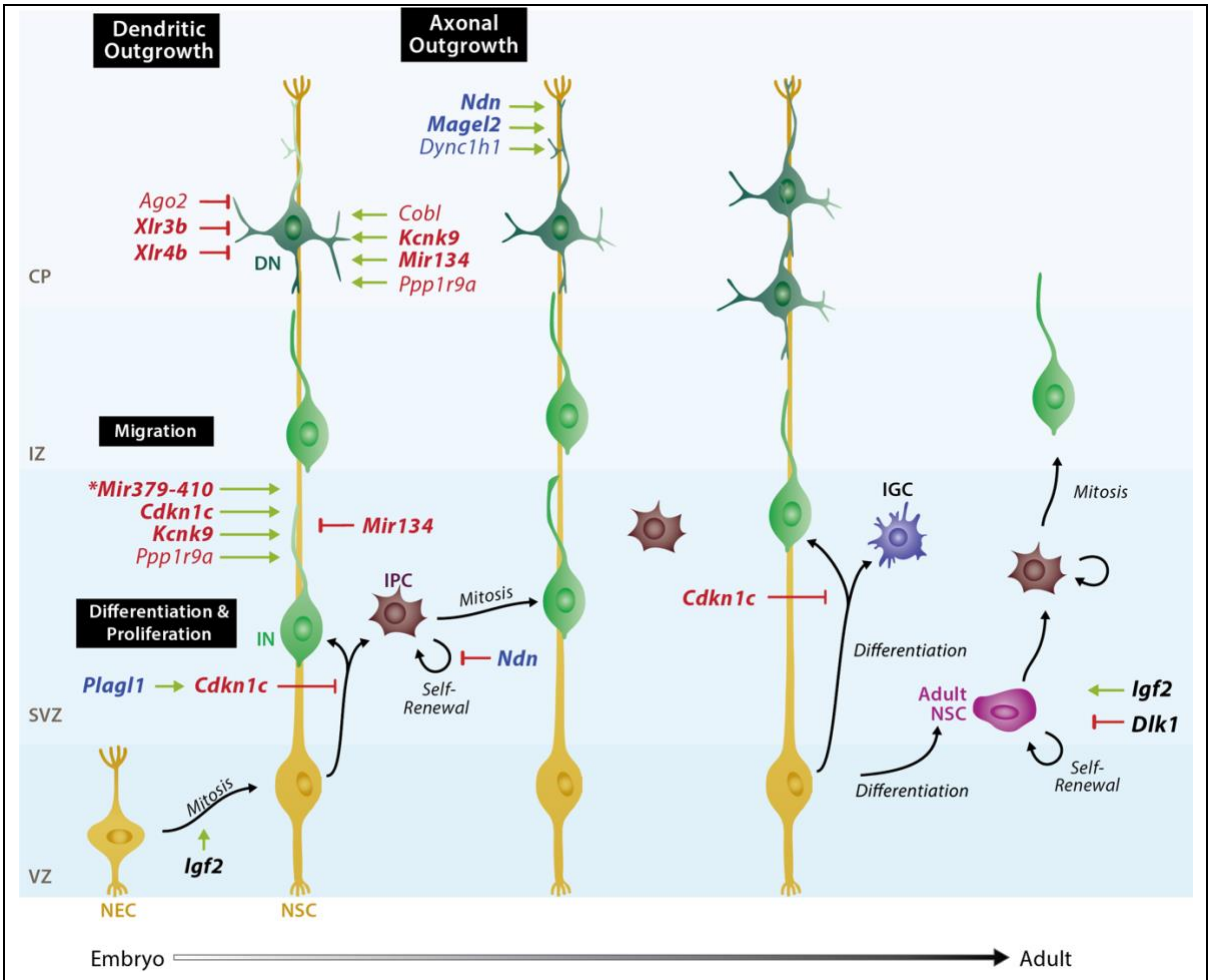

Figure 1.3: Roles of imprinted genes during cortical neurogenesis.

Genes preferentially expressed from the maternal and paternal allele appear in red and blue, respectively. In black are imprinted genes that are biallelically expressed in this context. Strongly biased and monoallelically expressed imprinted genes are in bold. Lines with arrowheads indicate enhancement, and lines with notched ends indicate reduction of the biological function. The asterisks by *Mir379-410* indicate that the corresponding biological functions are regulated by three miRNAs of this cluster: *Mir369-3p*, *Mir496*, and *Mir543*.

Igf2 expression demonstrates highly spatiotemporal imprinted regulation of transcriptional dosage to instruct adult neurogenesis. In the cerebellum, paternally biased *Dio3* regulates thyroid hormone signaling, inhibiting premature differentiation of granule cells, their migration from the external to internal layer, and the dendritic arborization of Purkinje cells (Peeters et al., 2013). Loss of imprinted expression at the *Dlk1-Dio3* locus leads to reduced neural differentiation in human stem cells (Mo et al., 2015).

Role in synaptic transmission, learning and memory

Many imprinted genes (both monoallelic and biased) play further roles in the adult brain by regulating synaptic transmission and plasticity, thus ultimately modulating the function of neural circuits (**Figure 1.4**). Deletion of maternally expressed *Kcnk9* in mice reduces membrane resting potential, altering the firing patterns in cerebellar granule cells (Brickley et al., 2007). *Ube3a* maternal deletion causes increased amplitudes of action potentials in the hippocampus, due to increased levels of α1-NaKA channels, which help maintain the membrane resting potential (Kaphzan et al., 2011; Kaphzan et al., 2013). Likewise, glutamatergic neurons derived from patients with Angelman syndrome show reduced action potential firing and synaptic activity; these are likely secondary consequences of altered resting potential (Fink et al., 2017). *Ube3a* maternal deletions also show impaired capacity to replenish presynaptic vesicles in L4 interneurons, causing weaker inhibitory postsynaptic currents (Wallace et al., 2012). Most imprinted genes known to regulate synaptic plasticity are maternally expressed, typically promoting synaptic potentiation (**Figure 1.4**). UBE3A promotes long-term potentiation (LTP) in excitatory synapses by preventing the inhibition of *N*-methyl-D-aspartate receptors

(NMDARs), and the activity-dependent internalization of α-amino-3-hydroxy-5-methyl-4-isoxazolepropionic acid receptors (AMPARs) (Greer et al., 2010; Sun et al., 2015).

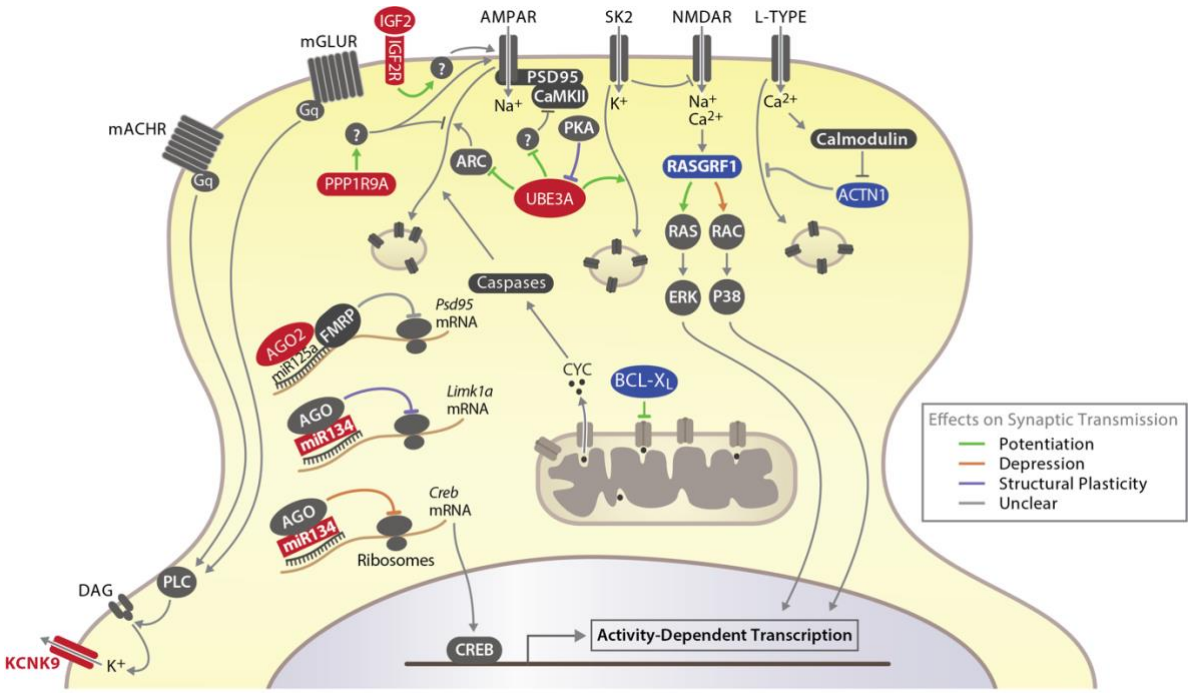

Figure 1.4: Functions of imprinted genes in synaptic transmission and plasticity.

Products of genes preferentially expressed from the maternal and paternal allele appear in red and blue, respectively. Products of biallelically expressed genes appear in dark gray. Products of strongly biased and monoallelically expressed imprinted genes are in bold. Lines with arrowheads represent stimulatory molecular interactions, whereas lines with notched ends represent inhibitory molecular interactions. The overall role of imprinted genes in synaptic plasticity is shown in green to indicate synaptic potentiation or activation, in orange to indicate synaptic depression or inhibition, in violet to indicate the induction of structural changes, and in gray when the contribution to synaptic transmission or plasticity remains unclear. White-filled circles with beige borders represent vesicles containing membrane receptors or channels.

The extensive roles of imprinted genes in neural development, synaptic function, and plasticity implicates them further in learning and memory. *Kcnk9* null mutants, for example, exhibit impaired contextual memory and fragmented sleep with reduced rapid eye movement (Gotter et al., 2011; Linden et al., 2007). *Ube3a* maternal deletions also perform poorly in contextual memory tasks (Sun et al., 2015). Monocular deprivation in *Ube3a* maternal deletion mutants fails to induce ocular dominance in the visual cortex, indicating a role in experience-dependent plasticity (Sato and Stryker, 2010). Recently, RNA sequencing of the visual system in dark-reared mice during the visual critical period uncovered up-regulation of three imprinted microRNAs: *miR882* in the retina, and *miR329* and *miR453* in the visual cortex (Hsu et al., 2018). Although there were no significant changes in the expression levels of imprinted genes identified in the visual cortex (isoform-specific *Herc3*, *Trappc9* and *H13*; and maternal *Rtl1* and maternally-biased *Ago2*), interestingly, in the suprachiasmatic nucleus of dark-reared mice one isoform of *H13* altered in imprinted status from 70:30 percent paternal:maternal expression to 60:40. These findings underline the complex tissue- and isoform-specific nature of imprinted regulation; and implicate imprinted genes in modulating plasticity during critical periods in the brain.

Role in social behaviors

Studies of knockout mice and patients with imprinted disorders highlight that appropriate regulation of imprinted genes directs various neuronal pathways that influence social behavior, particularly interactions between the offspring and mother or conspecifics. Targeted mutation of paternal *Peg3* causes a severe lack of maternal care in mothers. *Peg3* loss in the prenatal pup and placenta, though, demonstrates reduced ultrasonic

vocalizations in *Peg3*$^{-}$ pups, leading to reduced maternal behavior even in wild-type mothers (Curley et al., 2004; McNamara et al., 2018a). Furthermore, a recent study demonstrated that loss of maternal expression of *Phlda2* in offspring led to an increase in maternal care behaviors, including nursing and grooming in wild-type mothers. Interestingly, the *Phlda2* dosage from prenatal pups influences *in utero* gene expression in the mother's hypothalamus and hippocampus, showing a remarkable instance where imprinted regulation modulates through gene dosage the level of maternal investment in offspring (Creeth et al., 2018).

Studies using more elaborate crosses of inbred mice may begin to disentangle the influences of genetic background, imprinted effects and the perinatal environment on behavior (Schoenrock et al., 2017). An interesting recent study compared mice lacking maternal *Nesp* to those lacking paternal *Grb10,* two imprinted genes exhibiting similar patterns of expression in the brain. While *Nesp*$^{m-}$ mice make more impulsive choices than wild-type littermates, *Grb10*$^{p-}$ mice make fewer ones, uncovering how imprinted genes with different allelic expression profiles may affect opposing behaviors (Dent et al., 2018). Loss of *Dio3* in mice leads to increased social aggression and reduced maternal behavior (Stohn et al., 2018). Similarly, a two-fold increase in *Cdkn1c* expression – mimicking a loss of imprinting – caused in mice an increased motivation for food, increased aggression and an unstable social hierarchy (McNamara et al., 2018b; McNamara et al., 2018c).
In humans, a genome-wide association analysis of children with language impairments found significant parent-of-origin effects at two loci that were also previously associated with schizophrenia and autism (Nudel et al., 2014; Pettigrew et al., 2016). Finally, a study of children with Prader-Willi syndrome reports that the loss of paternal expression at the

Snrpn/Ube3a locus may cause the subjects' observed deficit in pitch discrimination but increased behavioral response to hearing music (Mehr et al., 2017).

Role in programmed cell death

In the developing nervous system, apoptosis is a mechanism to control the neuronal pool and synaptic matching between neurons. Internal and external stimuli regulate apoptosis by shifting the balance between pro-apoptotic and anti-apoptotic proteins. Interestingly, many genes of the apoptotic pathway are affected by imprinted regulation (**Figure 1.5**). Paternally expressed genes seem to play mostly anti-apoptotic roles, while maternally expressed genes are more pleiotropic (Broad et al., 2009; Perez et al., 2015). The maternally expressed *Kcnk9* plays a role in mediating neuronal excitability (Bando et al., 2014), and promotes apoptosis in granule cells (Lauritzen et al., 2003). Loss of the paternally expressed *Peg3* or *Magel2* causes a reduction in hypothalamic oxytocin neurons. Loss of *Peg3* also increases apoptosis in forebrain, striatal and amygdalar regions (Broad et al., 2009).

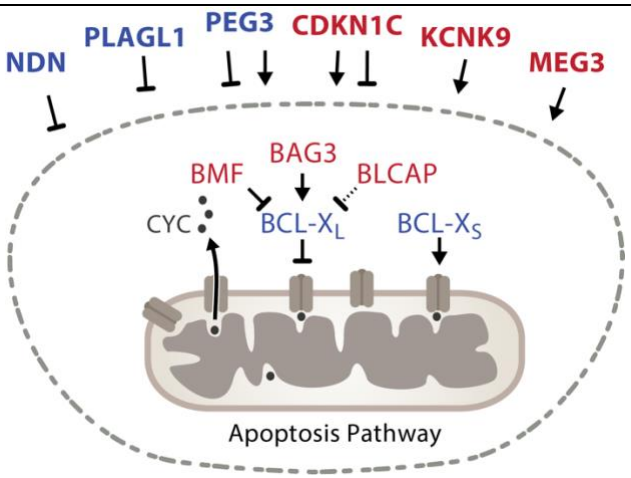

Figure 1.5: Imprinted genes involved in regulating apoptosis.

Within the ellipse are products of imprinted genes that interact directly with the apoptosis machinery, and outside the ellipse are products of imprinted genes that influence pro- or anti-apoptosis. L and S subscripts in the gene names indicate long and short isoforms, respectively.

Investigation of *Bcl-x$_L$*

Given the clear roles previously studied imprinted genes have on neuronal fate and development, here we focus our investigation on one novel parentally-biased gene involved in the apoptotic pathway, *Bcl2l1* (*Bcl-x$_L$*). Bcl-xL is a major anti-apoptotic regulator in both the mouse and human brain, the deletion of which causes massive apoptosis in postmitotic immature neurons (Motoyama et al., 1995). In the mouse brain, *Bcl-xL* exhibits a relatively modest paternal bias in expression that is consistent across brain regions (**Figure 1.1**) (Gregg et al., 2010b; Perez et al., 2015); but deeper questions about the nature and significance of its allelic expression have yet been unanswered. By investigating a conditional mutant mouse line for Bcl-x, this dissertation aims to evaluate both the effects and nature of parentally-biased gene expression in the mouse brain. In Chapter II, we evaluate the effects of parental Bcl-x expression on specific cell

populations, and utilize a single cell technique to quantify gene expression in intact cerebellar tissue. We then apply this quantification to investigate cell-type specific effects in the visual cortex (Chapter III). Finally, we investigate patterns of Bcl-x expression in non-mutant mice, within the context of its imprinted gene cluster, to analyze how this imprinted gene is transcriptionally regulated in neuronal populations (Chapter IV).

Parts of this chapter have been published in: *Ho-Shing, O., Dulac, C., Influences of genomic imprinting on brain function and behaviour. Current Opinion in Behavioral Sciences, 2019. 25: p. 66-76.*

References

Albrecht, U., Sutcliffe, J.S., Cattanach, B.M., Beechey, C.V., Armstrong, D., Eichele, G., and Beaudet, A.L. (1997). Imprinted expression of the murine Angelman syndrome gene, Ube3a, in hippocampal and Purkinje neurons. Nat Genet *17*, 75-78.

Andergassen, D., Dotter, C.P., Wenzel, D., Sigl, V., Bammer, P.C., Muckenhuber, M., Mayer, D., Kulinski, T.M., Theussl, H.-C., Penninger, J.M.*, et al.* (2017). Mapping the mouse Allelome reveals tissue-specific regulation of allelic expression. eLife *6*, e25125.

Angulo, M.A., Butler, M.G., and Cataletto, M.E. (2015). Prader-Willi syndrome: a review of clinical, genetic, and endocrine findings. J Endocrinol Invest *38*, 1249-1263.

Babak, T., Deveale, B., Armour, C., Raymond, C., Cleary, M.A., van der Kooy, D., Johnson, J.M., and Lim, L.P. (2008). Global survey of genomic imprinting by transcriptome sequencing. Curr Biol *18*, 1735-1741.

Babak, T., DeVeale, B., Tsang, E.K., Zhou, Y., Li, X., Smith, K.S., Kukurba, K.R., Zhang, R., Li, J.B., Kooy, D.v.d.*, et al.* (2015). Genetic conflict reflected in tissue-specific maps of genomic imprinting in human and mouse. Nature Genetics *47*, 544-549.

Bando, Y., Hirano, T., and Tagawa, Y. (2014). Dysfunction of KCNK potassium channels impairs neuronal migration in the developing mouse cerebral cortex. Cerebral cortex (New York, NY : 1991) *24*, 1017-1029.

Baran, Y., Subramaniam, M., Biton, A., Tukiainen, T., Tsang, E.K., Rivas, M.A., Pirinen, M., Gutierrez-Arcelus, M., Smith, K.S., Kukurba, K.R.*, et al.* (2015). The landscape of genomic imprinting across diverse adult human tissues. Genome Research *25*, 927-936.

Bartolomei, M.S., and Ferguson-Smith, A.C. (2011). Mammalian genomic imprinting. Cold Spring Harb Perspect Biol *3*.

Bonthuis, Paul J., Huang, W.-C., Hörndli, Cornelia N., Ferris, E., Cheng, T., and Gregg, C. (2015a). Noncanonical Genomic Imprinting Effects in Offspring. Cell Reports *12*, 979-991.

Brickley, S.G., Aller, M.I., Sandu, C., Veale, E.L., Alder, F.G., Sambi, H., Mathie, A., and Wisden, W. (2007). TASK-3 two-pore domain potassium channels enable sustained high-frequency firing in cerebellar granule neurons. J Neurosci *27*, 9329-9340.

Broad, K.D., Curley, J.P., and Keverne, E.B. (2009). Increased apoptosis during neonatal brain development underlies the adult behavioral deficits seen in mice lacking a functional paternally expressed gene 3 (Peg3). Dev Neurobiol *69*, 314-325.

Chao, H.T., and Zoghbi, H.Y. (2012). MeCP2: only 100% will do. Nat Neurosci *15*, 176-177.

Cleaton, M.A., Edwards, C.A., and Ferguson-Smith, A.C. (2014). Phenotypic outcomes of imprinted gene models in mice: elucidation of pre- and postnatal functions of imprinted genes. Annu Rev Genomics Hum Genet *15*, 93-126.

Creeth, H.D.J., McNamara, G.I., Tunster, S.J., Boque-Sastre, R., Allen, B., Sumption, L., Eddy, J.B., Isles, A.R., and John, R.M. (2018). Maternal care boosted by paternal imprinting in mammals. PLoS Biol *16*, e2006599.

Crowley, J.J., Zhabotynsky, V., Sun, W., Huang, S., Pakatci, I.K., Kim, Y., Wang, J.R., Morgan, A.P., Calaway, J.D., Aylor, D.L*., et al.* (2015). Analyses of allele-specific gene expression in highly divergent mouse crosses identifies pervasive allelic imbalance. Nature Genetics *47*, ng.3222.

Curley, J.P., Barton, S., Surani, A., and Keverne, E.B. (2004). Coadaptation in mother and infant regulated by a paternally expressed imprinted gene. Proc Biol Sci *271*, 1303-1309.

DeChiara, T.M., Robertson, E.J., and Efstratiadis, A. (1991). Parental imprinting of the mouse insulin-like growth factor II gene. Cell *64*, 849-859.

Dent, C.L., Humby, T., Lewis, K., Ward, A., Fischer-Colbrie, R., Wilkinson, L.S., Wilkins, J.F., and Isles, A.R. (2018). Impulsive Choice in Mice Lacking Paternal Expression of Grb10 Suggests Intragenomic Conflict in Behavior. Genetics *209*, 233-239.

DeVeale, B., Kooy, D.v.d., and Babak, T. (2012). Critical Evaluation of Imprinted Gene Expression by RNA–Seq: A New Perspective. PLoS Genetics *8*, e1002600.

Ferrón, S.R., Radford, E.J., Domingo-Muelas, A., Kleine, I., Ramme, A., Gray, D., Sandovici, I., Constancia, M., Ward, A., Menheniott, T.R*., et al.* (2015). Differential genomic imprinting regulates paracrine and autocrine roles of IGF2 in mouse adult neurogenesis. Nature communications *6*, 8265.

Fink, J.J., Robinson, T.M., Germain, N.D., Sirois, C.L., Bolduc, K.A., Ward, A.J., Rigo, F., Chamberlain, S.J., and Levine, E.S. (2017). Disrupted neuronal maturation in Angelman syndrome-derived induced pluripotent stem cells. Nature Communications *8*, ncomms15038.

Giannoukakis, N., Deal, C., Paquette, J., Goodyer, C.G., and Polychronakos, C. (1993). Parental genomic imprinting of the human IGF2 gene. Nat Genet *4*, 98-101.

Ginart, P., Kalish, J.M., Jiang, C.L., Yu, A.C., Bartolomei, M.S., and Raj, A. (2016). Visualizing allele-specific expression in single cells reveals epigenetic mosaicism in an H19 loss-of-imprinting mutant. Genes & Development *30*, 567-578.

Gotter, A.L., Santarelli, V.P., Doran, S.M., Tannenbaum, P.L., Kraus, R.L., Rosahl, T.W., Meziane, H., Montial, M., Reiss, D.R., Wessner, K.*, et al.* (2011). TASK-3 as a potential antidepressant target. Brain Res *1416*, 69-79.

Greer, P.L., Hanayama, R., Bloodgood, B.L., Mardinly, A.R., Lipton, D.M., Flavell, S.W., Kim, T.K., Griffith, E.C., Waldon, Z., Maehr, R.*, et al.* (2010). The Angelman Syndrome protein Ube3A regulates synapse development by ubiquitinating arc. Cell *140*, 704-716.

Gregg, C. (2014). Known unknowns for allele-specific expression and genomic imprinting effects. F1000Prime Reports *6*, 75.

Gregg, C., Zhang, J., Butler, J.E., Haig, D., and Dulac, C. (2010a). Sex-Specific Parent-of-Origin Allelic Expression in the Mouse Brain. Science *329*, 682-685.

Gregg, C., Zhang, J., Weissbourd, B., Luo, S., Schroth, G.P., Haig, D., and Dulac, C. (2010b). High-resolution analysis of parent-of-origin allelic expression in the mouse brain. Science *329*, 643-648.

Hayden, E.C. (2012). RNA studies under fire. Nature *484*, 428.

Hsu, C.-L., Chou, C.-H., Huang, S.-C., Lin, C.-Y., Lin, M.-Y., Tung, C.-C., Lin, C.-Y., Lai, I.P., Zou, Y.-F., Youngson, N.A.*, et al.* (2018). Analysis of experience-regulated transcriptome and imprintome during critical periods of mouse visual system development reveals spatiotemporal dynamics. Human molecular genetics *27*, 1039-1054.

Huang, W.-C., Ferris, E., Cheng, T., Hörndli, C.S., Gleason, K., Tamminga, C., Wagner, J.D., Boucher, K.M., Christian, J.L., and Gregg, C. (2017). Diverse Non-genetic, Allele-Specific Expression Effects Shape Genetic Architecture at the Cellular Level in the Mammalian Brain. Neuron *93*, 1094-1109.e1097.

Joseph, B., Andersson, E.R., Vlachos, P., Sodersten, E., Liu, L., Teixeira, A.I., and Hermanson, O. (2009). p57Kip2 is a repressor of Mash1 activity and neuronal differentiation in neural stem cells. Cell Death Differ *16*, 1256-1265.

Judson, M.C., Sosa-Pagan, J.O., Del Cid, W.A., Han, J.E., and Philpot, B.D. (2014). Allelic specificity of Ube3a expression in the mouse brain during postnatal development. J Comp Neurol *522*, 1874-1896.

Kaphzan, H., Buffington, S.A., Jung, J.I., Rasband, M.N., and Klann, E. (2011). Alterations in intrinsic membrane properties and the axon initial segment in a mouse model of Angelman syndrome. J Neurosci *31*, 17637-17648.

Kaphzan, H., Buffington, S.A., Ramaraj, A.B., Lingrel, J.B., Rasband, M.N., Santini, E., and Klann, E. (2013). Genetic reduction of the alpha1 subunit of Na/K-ATPase corrects multiple hippocampal phenotypes in Angelman syndrome. Cell Rep *4*, 405-412.

Keverne, E.B. (2014). Significance of epigenetics for understanding brain development, brain evolution and behaviour. Neuroscience *264*, 207-217.

Keverne, E.B., Fundele, R., Narasimha, M., Barton, S.C., and Surani, M.A. (1996). Genomic imprinting and the differential roles of parental genomes in brain development. Brain Res Dev Brain Res *92*, 91-100.

Kriegstein, A., and Alvarez-Buylla, A. (2009). The glial nature of embryonic and adult neural stem cells. Annu Rev Neurosci *32*, 149-184.

Kroeze, Y., Oti, M., Beusekom, E.v., Cooijmans, R.H.M., Bokhoven, H.v., Kolk, S.M., Homberg, J.R., and Zhou, H. (2017). Transcriptome Analysis Identifies Multifaceted Regulatory Mechanisms Dictating a Genetic Switch from Neuronal Network Establishment to Maintenance During Postnatal Prefrontal Cortex Development. Cerebral Cortex *28*, 833-851.

Lauritzen, I., Zanzouri, M., Honore, E., Duprat, F., Ehrengruber, M.U., Lazdunski, M., and Patel, A.J. (2003). K+-dependent cerebellar granule neuron apoptosis. Role of task leak K+ channels. J Biol Chem *278*, 32068-32076.

Lawson, H.A., Cheverud, J.M., and Wolf, J.B. (2013). Genomic imprinting and parent-of-origin effects on complex traits. Nature Reviews Genetics *14*, 609-617.

Lehtinen, M.K., Zappaterra, M.W., Chen, X., Yang, Y.J., Hill, A.D., Lun, M., Maynard, T., Gonzalez, D., Kim, S., Ye, P.*, et al.* (2011). The cerebrospinal fluid provides a proliferative niche for neural progenitor cells. Neuron *69*, 893-905.

Linden, A.-M.M., Sandu, C., Aller, M.I., Vekovischeva, O.Y., Rosenberg, P.H., Wisden, W., and Korpi, E.R. (2007). TASK-3 knockout mice exhibit exaggerated nocturnal activity, impairments in cognitive functions, and reduced sensitivity to inhalation anesthetics. The Journal of pharmacology and experimental therapeutics *323*, 924-934.

Lu, H., Ash, R.T., He, L., Kee, S.E., Wang, W., Yu, D., Hao, S., Meng, X., Ure, K., Ito-Ishida, A.*, et al.* (2016). Loss and Gain of MeCP2 Cause Similar Hippocampal Circuit Dysfunction that Is Rescued by Deep Brain Stimulation in a Rett Syndrome Mouse Model. Neuron *91*, 739-747.

McNamara, G.I., Creeth, H.D.J.D., Harrison, D.J., Tansey, K.E., Andrews, R.M., Isles, A.R., and John, R.M. (2018a). Loss of offspring Peg3 reduces neonatal ultrasonic vocalizations and increases maternal anxiety in wild-type mothers. Human molecular genetics *27*, 440-450.

McNamara, G.I., Davis, B.A., Browne, M., Humby, T., Dalley, J.W., Xia, J., John, R.M., and Isles, A.R. (2018b). Dopaminergic and behavioural changes in a loss-of-imprinting model of Cdkn1c. Genes, brain, and behavior *17*, 149-157.

McNamara, G.I.I., John, R.M., and Isles, A.R. (2018c). Territorial Behavior and Social Stability in the Mouse Require Correct Expression of Imprinted Cdkn1c. Frontiers in behavioral neuroscience *12*, 28.

Mehr, S.A., Kotler, J., Howard, R.M., Haig, D., and Krasnow, M.M. (2017). Genomic Imprinting Is Implicated in the Psychology of Music. Psychological Science, 095679761771145.

Mo, C.F., Wu, F.C., Tai, K.Y., Chang, W.C., Chang, K.W., Kuo, H.C., Ho, H.N., Chen, H.F., and Lin, S.P. (2015). Loss of non-coding RNA expression from the DLK1-DIO3 imprinted locus correlates with reduced neural differentiation potential in human embryonic stem cell lines. Stem Cell Res Ther *6*, 1.

Motoyama, N., Wang, F., Roth, K.A., Sawa, H., Nakayama, K., Nakayama, K., Negishi, I., Senju, S., Zhang, Q., Fujii, S.*, et al.* (1995). Massive cell death of immature hematopoietic cells and neurons in Bcl-x-deficient mice. Science *267*, 1506-1510.

Mott, R., Yuan, W., Kaisaki, P., Gan, X., Cleak, J., Edwards, A., Baud, A., and Flint, J. (2014). The Architecture of Parent-of-Origin Effects in Mice. Cell *156*, 332-342.

Nudel, R., Simpson, N.H., Baird, G., O'Hare, A., Conti-Ramsden, G., Bolton, P.F., Hennessy, E.R., Consortium, S.L.I., Ring, S.M., Davey Smith, G.*, et al.* (2014). Genome-wide association analyses of child genotype effects and parent-of-origin effects in specific language impairment. Genes Brain Behav *13*, 418-429.

Peeters, R.P., Hernandez, A., Ng, L., Ma, M., Sharlin, D.S., Pandey, M., Simonds, W.F., St Germain, D.L., and Forrest, D. (2013). Cerebellar abnormalities in mice lacking type 3 deiodinase and partial reversal of phenotype by deletion of thyroid hormone receptor alpha1. Endocrinology *154*, 550-561.

Perez, J.D., Rubinstein, N.D., and Dulac, C. (2016). New Perspectives on Genomic Imprinting, an Essential and Multifaceted Mode of Epigenetic Control in the Developing and Adult Brain. Annual Review of Neuroscience *39*, 1-38.

Perez, J.D., Rubinstein, N.D., Fernandez, D.E., Santoro, S.W., Needleman, L.A., Ho-Shing, O., Choi, J.J., Zirlinger, M., Chen, S.-K., Liu, J.S.*, et al.* (2015). Quantitative and functional interrogation of parent-of-origin allelic expression biases in the brain. eLife *4*, e07860.

Pettigrew, K.A., Frinton, E., Nudel, R., Chan, M.T.M., Thompson, P., Hayiou-Thomas, M.E., Talcott, J.B., Stein, J., Monaco, A.P., Hulme, C.*, et al.* (2016). Further evidence for a

parent-of-origin effect at the NOP9 locus on language-related phenotypes. Journal of Neurodevelopmental Disorders *8*, 24.

Pinter, S.F., Colognori, D., Beliveau, B.J., Sadreyev, R.I., Payer, B., Yildirim, E., Wu, C.-t., and Lee, J.T. (2015). Allelic Imbalance Is a Prevalent and Tissue-Specific Feature of the Mouse Transcriptome. Genetics *200*, 537-549.

Prickett, A.R., and Oakey, R.J. (2012). A survey of tissue-specific genomic imprinting in mammals. Mol Genet Genomics *287*, 621-630.

Sato, M., and Stryker, M.P. (2010). Genomic imprinting of experience-dependent cortical plasticity by the ubiquitin ligase gene Ube3a. Proc Natl Acad Sci U S A *107*, 5611-5616.

Schoenrock, S.A., Oreper, D., Farrington, J., McMullan, R.C., Ervin, R., Miller, D.R., Pardo-Manuel de Villena, F., Valdar, W., and Tarantino, L.M. (2017). Perinatal nutrition interacts with genetic background to alter behavior in a parent-of-origin-dependent manner in adult Collaborative Cross mice. Genes Brain Behav.

Sittig, L.J., and Redei, E.E. (2014). Fine-tuning notes in the behavioral symphony: parent-of-origin allelic gene expression in the brain. Adv Genet *86*, 93-106.

Stohn, J.P., Martinez, M.E., Zafer, M., López-Espíndola, D., Keyes, L.M., and Hernandez, A. (2018). Increased aggression and lack of maternal behavior in Dio3-deficient mice are associated with abnormalities in oxytocin and vasopressin systems. Genes, brain, and behavior *17*, 23-35.

Sun, J., Zhu, G., Liu, Y., Standley, S., Ji, A., Tunuguntla, R., Wang, Y., Claus, C., Luo, Y., Baudry, M.*, et al.* (2015). UBE3A Regulates Synaptic Plasticity and Learning and Memory by Controlling SK2 Channel Endocytosis. Cell Rep *12*, 449-461.

Tucci, V., Isles, A.R., Kelsey, G., Ferguson-Smith, A.C., and Erice Imprinting, G. (2019). Genomic Imprinting and Physiological Processes in Mammals. Cell *176*, 952-965.

Tury, A., Mairet-Coello, G., and DiCicco-Bloom, E. (2012). The multiple roles of the cyclin-dependent kinase inhibitory protein p57(KIP2) in cerebral cortical neurogenesis. Dev Neurobiol *72*, 821-842.

Wallace, M.L., Burette, A.C., Weinberg, R.J., and Philpot, B.D. (2012). Maternal loss of Ube3a produces an excitatory/inhibitory imbalance through neuron type-specific synaptic defects. Neuron *74*, 793-800.

Wang, X., Sun, Q., McGrath, S.D., Mardis, E.R., Soloway, P.D., and Clark, A.G. (2008). Transcriptome-wide identification of novel imprinted genes in neonatal mouse brain. PLoS One *3*, e3839.

Ye, X., Kohtz, A., Pollonini, G., Riccio, A., and Alberini, C.M. (2015). Insulin Like Growth Factor 2 Expression in the Rat Brain Both in Basal Condition and following Learning Predominantly Derives from the Maternal Allele. PLoS One *10*, e0141078.

Yu, S., Yu, D., Lee, E., Eckhaus, M., Lee, R., Corria, Z., Accili, D., Westphal, H., and Weinstein, L.S. (1998). Variable and tissue-specific hormone resistance in heterotrimeric Gs protein alpha-subunit (Gsalpha) knockout mice is due to tissue-specific imprinting of the gsalpha gene. Proc Natl Acad Sci U S A *95*, 8715-8720.

Zou, J., Xiang, D., Datla, R., and Wang, E. (2018). Transcriptome Data Analysis. Methods in molecular biology (Clifton, NJ) *1751*, 199-208.

Chapter II. Cellular analysis of a parentally-biased gene Bcl-x_L

Introduction

Initial imprinting studies investigated androgenetic and parthenogenetic embryos (which contained two paternally-derived or two maternally-derived chromosomes, respectively) to identify genes expressed only from one parental allele. Such early studies identified roughly one hundred "canonical" imprinted genes in which one parental allele is consistently and fully or nearly fully silenced. These genes appeared mainly clustered at various autosomal loci (Hagiwara et al., 1997; Kaneko-Ishino et al., 1995; Morison et al., 2005) and were shown to play key roles in embryonic development and maintenance of the placenta (Cleaton et al., 2014; Tunster et al., 2013). With deeper studies into human imprinted disorders such as Beckwith-Wiedemann, Prader-Willi and Angelman syndromes, several important aspects of genomic imprinting came to light. Firstly, imprinted regulation appeared to be critical for proper brain development (Keverne, 2013, 2014; Keverne et al., 1996; Wilkinson et al., 2007); and secondly, regulation of known imprinted genes seemed to be highly tissue- and age-specific (Engemann et al., 2000; Umlauf et al., 2004; Vu and Hoffman, 1997). While a canonical perspective on imprinted gene expression initially assumed a complete silencing of one parental allele, it was repeatedly observed that a substantial number of genes instead exhibit a bias in their expression in a parent-of-origin-specific manner. For example, zinc finger proteins *Zim2* and *Zim3*, and *Copg2* (a gene associated with Russell Silver syndrome) were reported to show maternal biases in expression in the mouse brain, without complete silencing of

paternal expression (Kim et al., 2001; Lee et al., 2000). An analysis of 50 reported imprinted genes across four imprinted clusters in the mouse reported that over half of the genes exhibited preferential allelic expression instead of canonical monoallelic expression (Khatib, 2007). These observed biases in parental expression may simply result from potential technical issues, including incomplete digestion of PCR products or contamination from placental tissues. Beaudet and Jiang, however, proposed that parentally-biased gene expression was a real phenomenon that could represent an evolutionary benefit by providing quantitative hypervariability – a mechanism by which a number of genes can be fine-tuned in their expression based on age and cellular identity (Beaudet and Jiang, 2002). The prevalence of parentally-biased expression in the brain, therefore, could potentially be as functionally important for mammalian development as strictly monoallelic imprinted gene expression.

The development of next-generation RNA sequencing allowed for robust and high-throughput characterization of parentally-biased expression, by utilizing tissues from F1 hybrid crosses of genetically distinct mouse strains (Babak et al., 2008; Wang et al., 2008). Dulac and colleagues used this strategy to perform a systematic survey of genomic imprinting in the mouse brain (Gregg et al., 2010a; Gregg et al., 2010b). This study validated all known imprinted genes and uncovered numerous novel imprinted genes with dynamic patterns of allelic bias. The exact number of imprinted genes uncovered by RNA sequencing has been controversial, prompting further analyses that increased the RNA sequencing read coverage, increased the number of biological replicates, and improved the statistical analyses of sequencing data (Babak et al., 2015; DeVeale et al., 2012; Hayden, 2012; Huang et al., 2017; Perez et al., 2015). Specifically, in Perez et al (2015), Perez and

Rubinstein developed a Bayesian regression allelic-imbalance model to account for all sources of variability in the experimental design, and thereby validated a large number of allelic effects initially uncovered by Gregg et al (2010a, 2010b). Many parentally-biased genes validated by this study exhibited significantly lower expression levels than strictly monoallelic imprinted genes, but maintained nuanced allelic patterns that changed dynamically between different brain regions and between different embryonic and postnatal ages. Interestingly, in this study, the apoptotic pathway emerged as a frequent target of imprinted regulation (Perez et al., 2015).

Although these RNA sequencing experiments have impacted our understanding of the scope, and spatial and temporal patterns of genomic imprinting in the brain, they were unable to address some key questions. 1 – is the allelic expression of parentally-biased genes functionally relevant for proper brain development and function? And 2 – what is the nature of the allelic expression of parentally-biased genes in the brain at the cellular level? RNA bulk sequencing analyses can only provide an averaged expression signal exhibited by the full ensemble of cells within the tissue sample (Huang, 2009; Hwang et al., 2018; Neildez-Nguyen et al., 2008), thus masking potential heterogeneity in expression that may reflect different cell identities and cell states (Eldar and Elowitz, 2010). Because every region of the mammalian brain is a mosaic of a large number of cell types, several models could explain the parentally-biased effects observed when studying genomic imprinting at the tissue level. In one model, a parental bias may arise from the complete silencing of one parental allele in a subpopulation of cells, while other populations remain biallelic. Alternatively, a parental bias may arise from the preferential expression of one allele over the other in all or most cells within the tissue (Gregg, 2014). Because cell type-specific

imprinting has been identified in both mice and humans (Blagitko et al., 2000; Ferron et al., 2011; Hu et al., 1998; Latham, 1995; Lee et al., 1997; Vu and Hoffman, 1997; Wilkinson et al., 2007), understanding which cell populations and how those populations are regulated by imprinted effects will provide significant insights into mechanisms underlying genomic imprinting across species.

In order to understand the nature of the allelic expression of *Bcl-x*$_L$, one requires a high-resolution technique that can monitor the expression patterns of *Bcl-x*$_L$ at a cellular level. Fluorescence in situ hybridization arose as an attractive approach because of the ability for spatial detection of RNA in their native cellular environment.

Conventional RNA FISH however uses long hapten-labeled probe sequences to hybridize to complementary RNA species, then applies a secondary reporter system to amplify the fluorescent signal (Huber, 2018). Although valuable for describing qualitative properties of intracellular RNA localization (Lawrence and Singer, 1986; Singer and Ward, 1982), conventional RNA FISH probes have serious limitations that make assays nearly impossible to accurately quantify, particularly when targeting rarely or lowly-expressed RNA transcripts such as *Bcl-x*$_L$. (Gaspar and Ephrussi, 2015) Singer, Raj and colleagues found a solution to this issue by developing a quantitative single cell approach (Femino et al., 1998; Raj et al., 2008), single-molecule RNA fluorescence in situ hybridization (smFISH). In contrast to conventional in situ methods, individual mRNA molecules of a given gene are targeted with a larger pool (10–50) of shorter (18–22 nt) oligonucleotide probes. Each probe is labeled with a single fluorophore at the 3' end, so that hybridization of the complete probe pool is subsequently visualized as punctate, diffraction-limited spots under a widefield microscope. Because there is no enzymatic amplification of the signal,

spots can be detected and directly counted as individual RNA transcripts using dedicated image analysis methods (Femino et al., 1998; Raj and Tyagi, 2010; Raj et al., 2008). This analysis can be conducted on individual cells, therefore providing optimal cellular resolution for quantitative expression analysis.

In this chapter, we first begin by addressing the functional relevance of a paternally-biased gene *Bcl2l1* (*Bcl-x*$_L$), by evaluating the phenotypic effects of maternal versus paternal *Bcl-x* deletion on cell survival in the adult mouse cortex and cerebellum. Then, in order to investigate the nature of the *Bcl-x*$_L$ parental bias, in this chapter we next aimed to use single molecule FISH, and quantified *Bcl-x*$_L$ expression in intact cerebellar tissue.

Results

Parental expression of Bcl-x_L differentially affects cell survival

In order to investigate the functional significance of parental bias in gene expression, we chose to study the gene *Bcl-x_L*, because of its well-characterized role in programmed cell death, and the availability of a conditional knockout line. The long isoform of *Bcl-x* (*Bcl-x_L*) is expressed in the mouse brain, exhibiting 60%:40% paternal:maternal expression, measured by RNA sequencing of tissue from Cast/EiJ and C57Bl/6J reciprocal crosses (**Figure 2.1a**). Complete deletion of *Bcl-x_L* results in embryonic lethality due to massive apoptosis, whereas loss of one allele has been reported to reduce brain weight (Kasai et al., 2003; Motoyama et al., 1995). We hypothesized that if the maternal and paternal alleles do contribute differentially to the expression of *Bcl-x_L* in the brain, loss of one parental allele will have distinct outcomes from loss of the other allele. Specifically, loss of the more highly expressed paternal allele should result in a more severe phenotype than loss of the maternal allele. To test this hypothesis, we generated mice with brain-specific deletions of the maternal and paternal alleles of *Bcl-x*, by crossing a conditional allele bearing the floxed *Bcl-x* mutation on either the mother or the father allele to a Nestin::Cre transgene (**Figure 2.1b**). The floxed *Bcl-x* allele enables Cre-dependent deletion of both the anti-apoptotic *Bcl-x_L* and pro-apoptotic *Bcl-x_S* isoforms. Since *Bcl-x_L* is the predominant isoform expressed in the brain (Krajewska et al., 2002), brain-specific deletion of *Bcl-x* is expected to nearly exclusively affect expression of *Bcl-x_L*. Control littermates also carried the Nestin::Cre transgene, and two wild-type copies of *Bcl-x*.

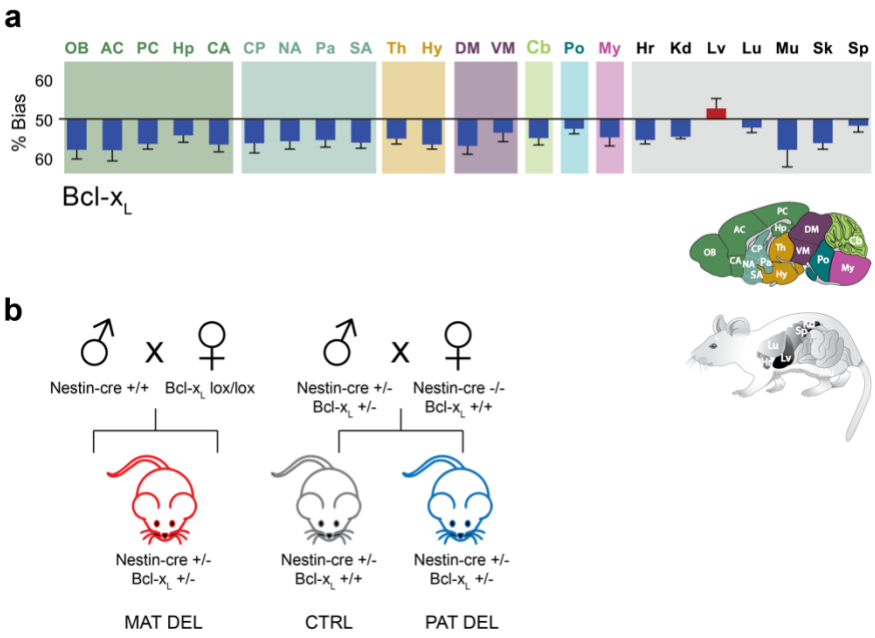

Figure 2.1: Parent-of-origin specific expression of *Bcl-x$_L$*.

a): Level of *Bcl-x$_L$* parental bias by region in the adult mouse. b): Mating scheme for generating brain-specific parental deletions of *Bcl-x$_L$*.

As expected, brain-specific deletion of *Bcl-x* had no significant effect on body weight of either maternal nor paternal deletion mice, up to age P80. We did find that mice with a paternal *Bcl-x* deletion had a roughly 15% reduction in brain weight compared to control littermates (**Figure 2.2**). In contrast, mice with a maternal *Bcl-x* deletion exhibited no significant difference in brain weight from control littermates, supporting our hypothesis that the parental alleles of *Bcl-x* contribute differentially to regulating apoptosis in the brain.

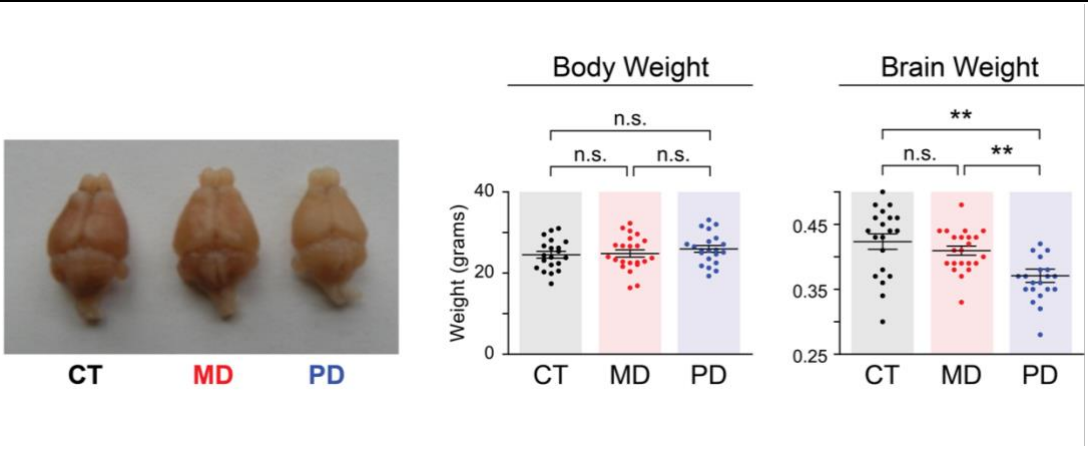

Figure 2.2: Paternal deletion of *Bcl-x* affects brain weight.

Brain and body weights of adult (P80) mice with brain-specific deletions of *Bcl-x*. Left panel shows representative images of adult brains for maternal *Bcl-x* deletion (MD) and paternal deletion (PD) compared to control (CT) littermates.

We next assessed whether the paternal *Bcl-x* deletion had observable effects on brain morphology by measuring the cross-sectional area of the cortex and cerebellum. In both structures, we found significant differences in area sizes between *Bcl-x* paternal deletion and both maternal deletion and control littermates. (**Figure 2.**3) Taken together, these results support the hypothesis that the expression of the paternal allele of *Bcl-x* does indeed make a more significant contribution to brain development than the maternal allele.

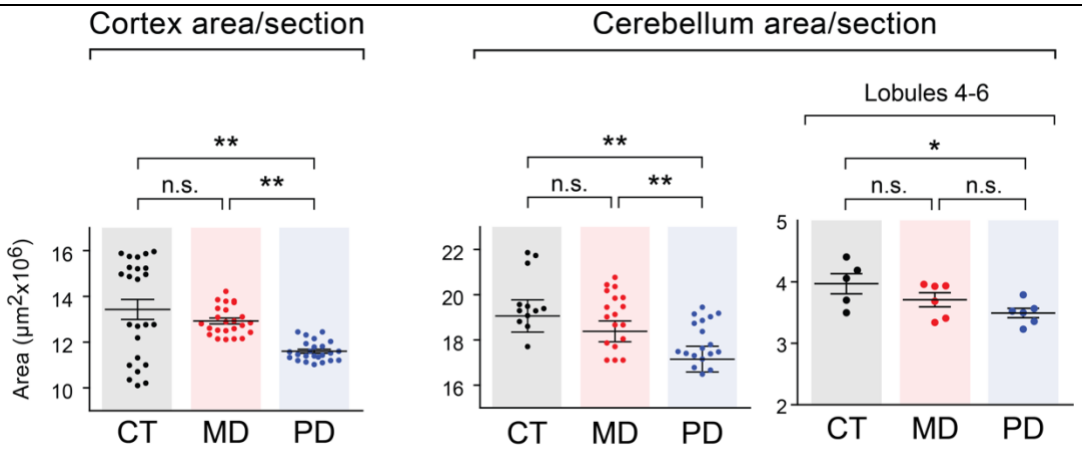

Figure 2.3: Cortical and cerebellar area differences in parental deletions.

Cross-sectional areas of the cortex, whole cerebellum, and lobules 4–6 of the cerebellum. Each data point represents a coronal section from a total of six P80 male mice.

Finally, we assessed whether the reduction in brain mass seen in the paternal deletion reflected losses in specific cell types in adult (P80) mice. We used immunofluorescence and conventional in situ hybridization assays in the cortex to quantify the total number of cells (stained with DAPI) and cells expressing the neuronal marker *NeuN*, the astroglial marker *S100ß* , a marker of excitatory neurons *Vglut1* (*Slc17a7*), and a marker of inhibitory neurons *Gad1*. Cortical cell densities did not differ significantly between genotypes. However, our data show that DAPI+, NeuN+, and Vglut1+ cells were significantly reduced in the cortices of paternal *Bcl-x* deletion, but not in maternal *Bcl-x* deletion (**Figure 2.4a**). In contrast, S100ß+ and Gad1+ cells were not significantly affected in either the paternal or maternal deletions.

Similar assays were performed on lobule 6 of the cerebellum, comparing inhibitory (Gad1+) cells found in the molecular layer to large inhibitory (Gad1+) Purkinje cells found in the Purkinje layer. Within the molecular and Purkinje layers, Gad1+ neurons were significantly reduced in number in the paternal *Bcl-x* deletion compared to control littermates (**Figure 2.4b**). Together, these results revealed that deletion of the paternal *Bcl-x* allele causes significant reductions in brain size and cell number that are not observed upon deletion of the maternal allele. Interestingly, these effects differed according to cell type and brain region, with specific subsets of neuronal cells affected in a given region. These results therefore suggest a largely unexpected role of genomic imprinting in the regulation and thereby fate of specific cell types, in distinct areas of the mouse brain.

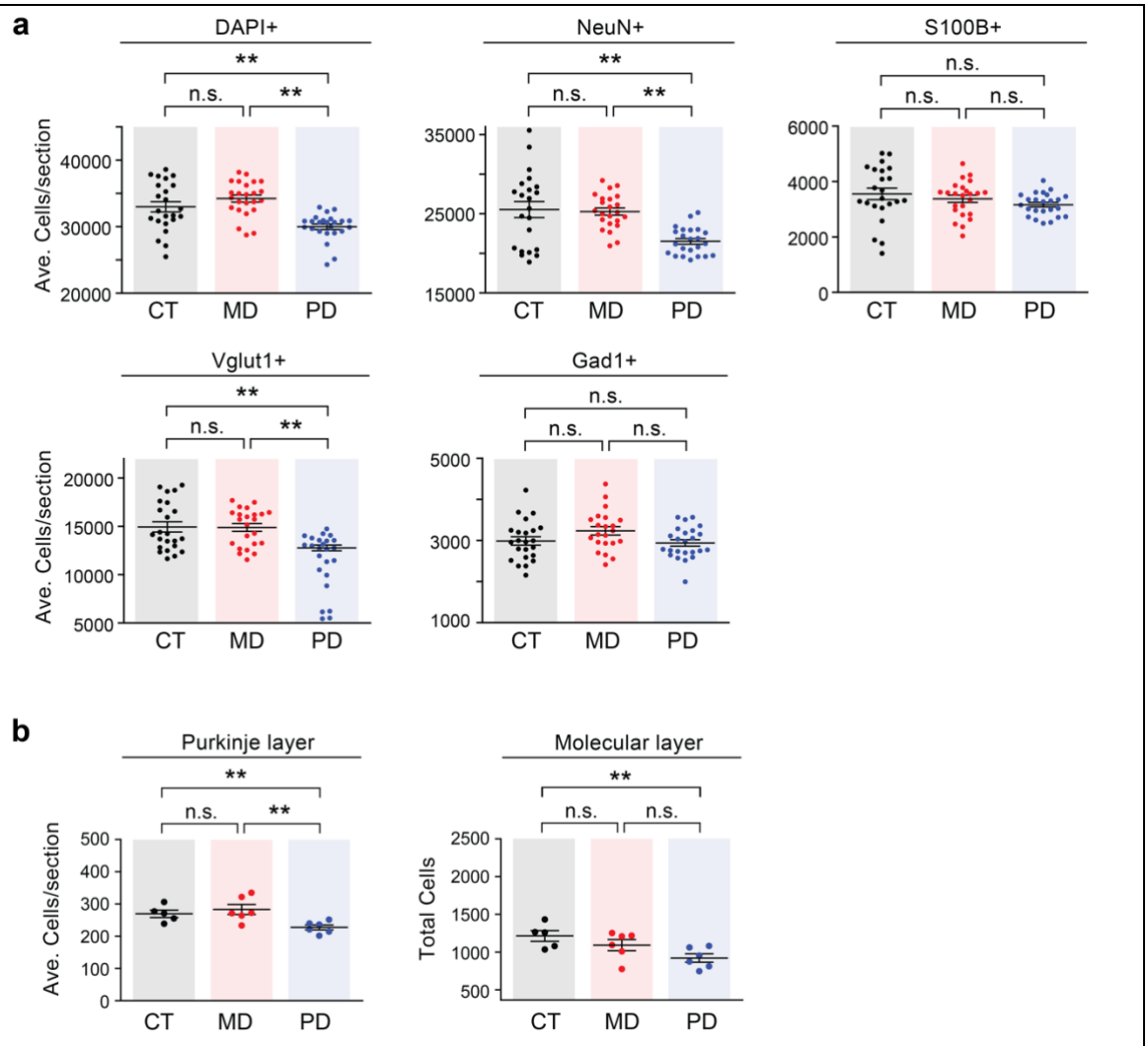

Figure 2.4: Loss of specific cell types in paternal *Bcl-x* deletion.

Quantification within the cortex of the number of cells per section labeled with cell type markers: DAPI (all cells), NEUN (neurons), S100ß (astroglia), Vglut1 (Slc17a7, subset of excitatory neurons), and Gad1 (subset of inhibitory neurons). Each data point represents a coronal section from a total of six P80 male mice.

Direct transcript quantification using smFISH

Single molecule FISH is a robust and sensitive technique to quantify RNA transcripts within single cells with high accuracy. Because cells in brain tissue are densely packed with extensive processes, neural tissues tend to display high levels of light scattering and autofluorescence. As neurons age, they also tend to accumulate lipofuscins, which are lipid-containing pigment granules left over from cellular lysosome digestion (Steiner et al., 1989). Because the signal for a single transcript is close to the diffraction limit, it was imperative to establish an appropriate pre-treatment of the tissue samples that would maintain the structure of the tissue and increase the signal to noise ratio.

In a first step forward, we found that young mouse brains up to three weeks of age (P0–P20) have not yet accumulated lipofuscin granules, which make the tissue easier to image than at older ages. Tissue from older mice can still be imaged, though the overall autofluorescence continues to increase, making it necessary to concurrently image an unused fluorescent channel and subsequently subtract the detected autofluorescent spots after image analysis. We found that the best treatment to reduce autofluorescence was to clarify tissue sections in a 2% solution of sodium dodecyl sulfate (SDS) directly before hybridization. We also increased the concentration of the probe from 5–50 nM as suggested (Raj and Tyagi, 2010) to around 200 nM in order to saturate the tissue without increasing the non-specific background signal. We were able to consistently detect transcripts for a number of parentally-biased genes, including *Ago2*, *Kcnk9*, *Trappc9* (**Figure 2.5**) and *Bcl-x*$_L$. While there is no direct way to confirm that a smFISH hybridization

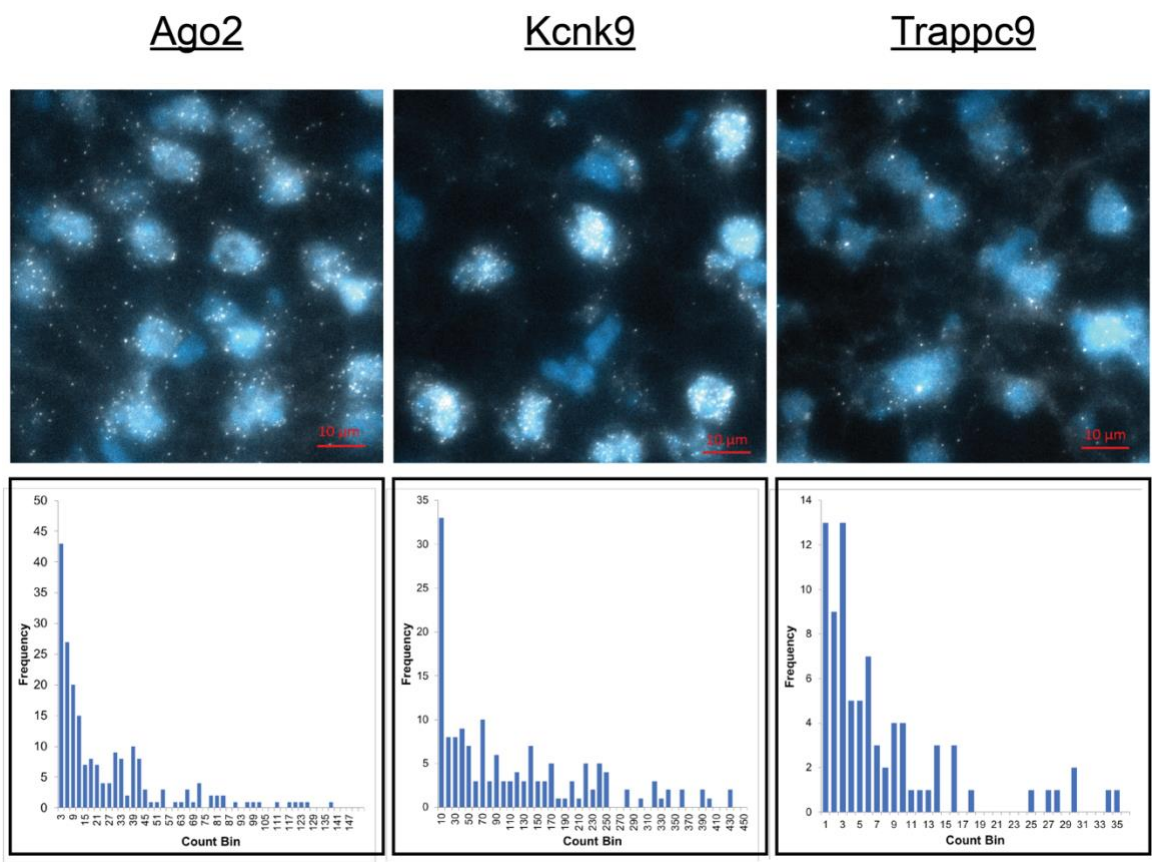

Figure 2.5: Quantifying parentally-biased genes by smFISH.

Sample images showing smFISH detection for three genes identified as parentally-biased by RNA sequencing. Nuclei are stained with DAPI (blue), and small punctate spots (white) reflect transcripts of *Ago2*, *Kcnk9*, or *Trappc9*. Below each image is a histogram showing the number of transcript spots detected in individual cells; the frequency of cells containing 0 spots are not shown. The distributions reflect spot counts from three acquisitions from the P8 anterior cortex of F1 hybrid mice.

is detecting every transcript present in the cell, one can assess the specificity of the probe as a proxy for detection efficiency by alternating the fluorophore for each oligo within the probe pool (effectively splitting the probe into two colors), and then checking the efficiency of colocalization (Raj and Tyagi, 2010) (**Figure 2.6**). We found in targeting *Bcl-x* expression, that our split *Bcl-x*$_L$ probes colocalized with high efficiency over 3 cerebellar slices, with a Pearson coefficient of 0.9983. This validated the notion that our probe was specific for the *Bcl-x*$_L$ transcript, and that half of the oligo probe used is sufficient to detect a transcript, making false negatives and particularly false positives rare events in our subsequent *Bcl-x*$_L$ quantification.

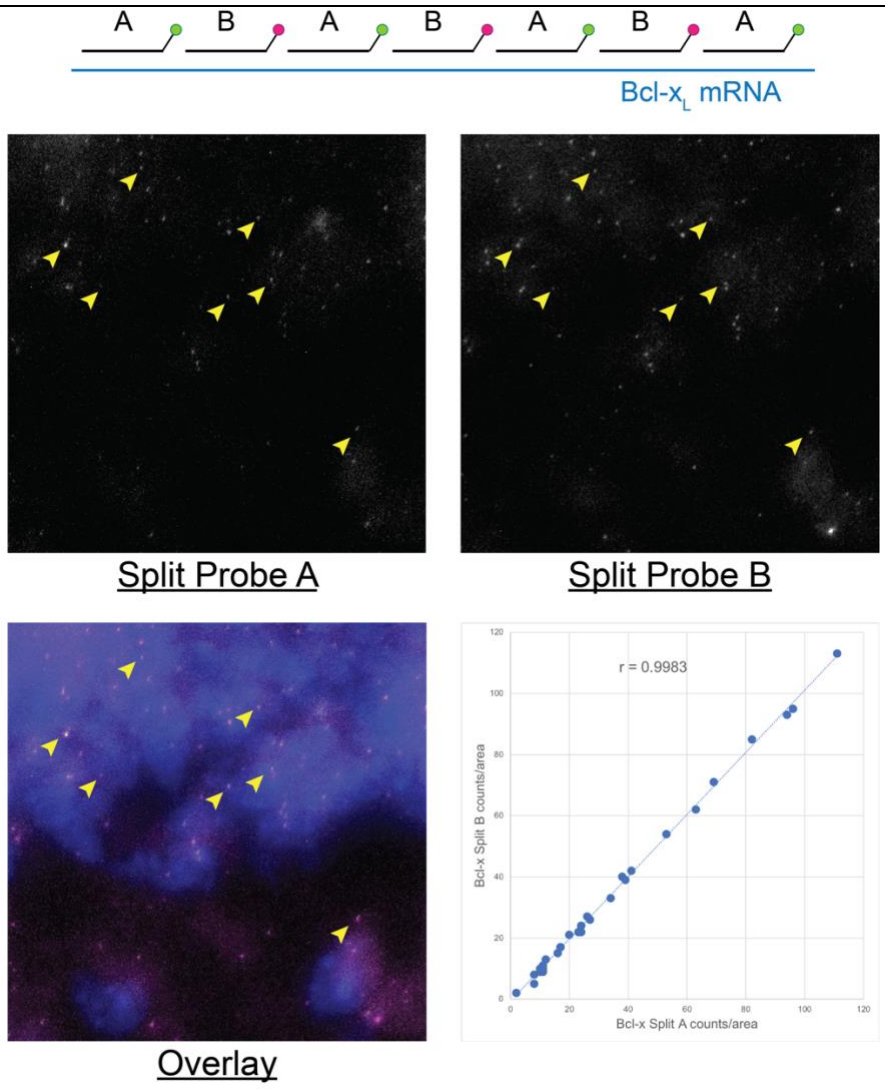

Figure 2.6: Colocalization of *Bcl-x$_L$* split probe.

Schematic illustrates the expected hybridization of *Bcl-x$_L$* split probe A and split probe B to target mRNA, to achieve colocalization. Images show smFISH signal from each split probe in P8 cerebellar tissue, and the overlay with DAPI (blue) of split probe A (white) and split probe B (red). Plot shows number of spots detected for each split probe per section area.

Bcl-x_L expression in the cerebellum

To assess the cell specificity of parental *Bcl-x* deletion in the cerebellum, we quantified *Bcl-x_L* expression in single cells within specific layers of cerebellar lobule 6. We compared *Bcl-x_L* expression levels between maternal and paternal *Bcl-x* deletions and controls in the P8 cerebellum. Postnatal day 8 (P8) is a critical developmental age for proper synaptogenesis between large inhibitory Purkinje cells and granule cells. As immature granule cells migrate past Purkinje cells to the external granule layer, the apoptotic pathway is important for clearing neurons that do not migrate to the appropriate layer, and establishing normal cerebellar morphology (Jung et al., 2008). We hypothesized that the significant loss of cells observed in the paternal *Bcl-x* deletion within the Purkinje and molecular layers could be due to a significant loss of *Bcl-x_L* expression in Purkinje or granule cells. We used smFISH to quantify the expression of *Bcl-x_L*, as well as *Gapdh*, a highly expressed gene whose expression helped delineate the soma of each neuron for cell segmentation (**Figure 2.7a**).

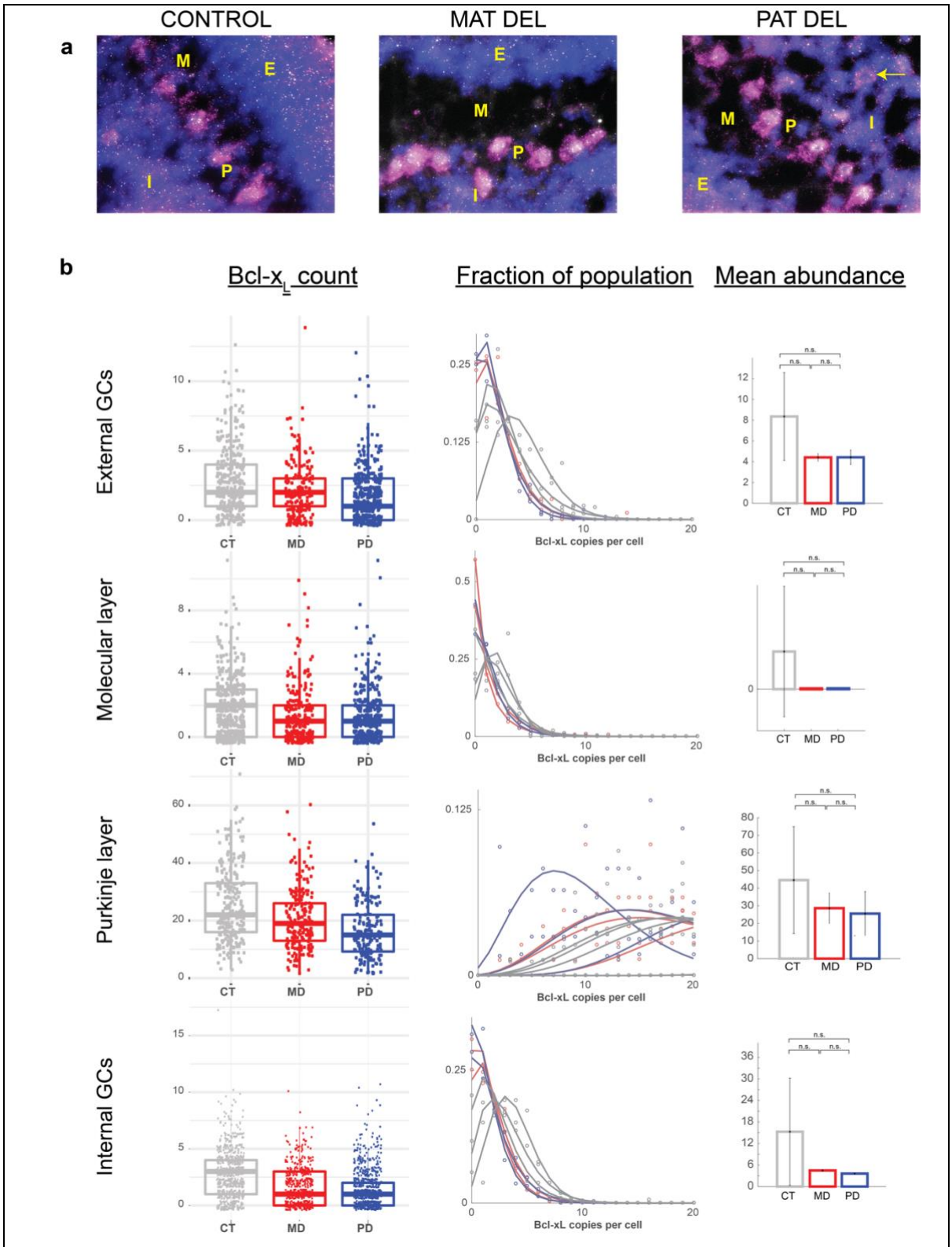

Figure 2.7: Quantification of *Bcl-x$_L$* expression in cerebellar cell populations.

(*Continued Figure 2.7*) a): Representative images of lobule 6 cerebellar layers from *Bcl-x* maternal deletion, *Bcl-x* paternal deletion, and control littermates. Nuclei are stained with DAPI (blue), *Bcl-x_L* signal is colored white, and *Gapdh* signal colored magenta. Cerebellar layers analyzed were the external granule layer (E), molecular layer (M), Purkinje layer (P), and internal granule layer (I). Arrow in paternal deletion points to a Purkinje cell within the internal granule layer. b): smFISH spot quantification of *Bcl-x_L* expression. Left panel: each data point of scatter plot reflects the number of *Bcl-x_L* transcripts detected for a single cell. Middle panel: Each curve reflects the distribution of *Bcl-x_L* expression for one mouse fitted to a negative binomial. Right panel: Mean *Bcl-x_L* transcript abundance, each bar reflecting mean and standard deviation of three mice per genotype.

When counts were compared using a zero-inflated generalized linear model (**Figure 2.6b** left panel), we found that in both maternal deletions and paternal deletions, *Bcl-x_L* expression was significantly reduced compared to control for both external granule cell (p_{MD}=4.94-e06 ; p_{PD} = 1.09e-14) and internal granule cell (p_{MD}=6.42e-15; p_{PD} <2e-16) populations. *Bcl-x_L* expression only in the paternal deletion was significantly different from control for molecular layer (p=3.87e-07) and Purkinje (p=3.87e-07) cell populations. Single-cell gene expression data, however, commonly fits best to a negative binomial distribution (Skinner et al., 2013), allowing for comparison of the distributions between genotypes that accounts for noise in single-cell expression and shows variability between individual mice within each genotype (**Figure 2.6b** middle, right panels). When we compared genotypes using the analytical means of these distributions, neither maternal nor

paternal deletion expression of *Bcl-x*$_L$ differed significantly from control expression within any cell populations examined, due to high variability in control *Bcl-x*$_L$ expression. Nonetheless, we did also qualitatively observe that Purkinje cells were more frequently found within the internal granule cell layer (**Figure 2.6a**) in paternal *Bcl-x* deletion compared to maternal deletion and control, suggesting loss of paternal *Bcl-x* does affect the proper migration or removal of Purkinje cells in the cerebellum.

Discussion

In comparing the effects of paternal versus maternal *Bcl-x* deletion, we found a surprising reduction in brain size due to loss of the paternally-inherited allele of *Bcl-x*. These results also suggest that the reduction in brain size previously reported in *Bcl-x* heterozygous knockouts (Kasai et al., 2003) is due specifically to the deletion of the paternal allele. We furthermore have found that within the adult mouse cortex, the number of Vglut1+ excitatory neurons is specifically reduced by paternal loss of *Bcl-x* expression. These results mark the first time that expression of a parentally-biased gene has been linked to effects in a specific subset of neuronal cells. Maternal expression of the imprinted gene *Ube3a* has also been shown to exhibit effects on synaptic transmission in specific neuronal subsets (Wallace et al., 2012). Therefore, our findings with the paternal deletion of *Bcl-x* instantiate the idea that both newly-uncovered parentally-biased genes and previously-known imprinted genes may play critical roles in specific neuronal pathways. In the adult mouse cerebellum, inhibitory (Gad1+) neurons including the major Purkinje neurons were also reduced in number. Because of the amount and density of the granule cells, we were unable to assess whether this excitatory cell population is also reduced in the *Bcl-x* deletions.

Using single molecule FISH, we were furthermore able to quantify *Bcl-x*$_L$ expression in single cells in the developing cerebellum. These experiments mark the first time that single molecule FISH has been used to quantify gene expression of single cells in intact vertebrate brain tissue, establishing an experimental paradigm that can be successfully used to investigate expression in the brain with high cellular resolution. Although we did observe reduced expression of *Bcl-x*$_L$ in all cell populations in maternal

and paternal deletions of the *Bcl-x*$_L$ allele, these reductions were not significantly different from *Bcl-x*$_L$ expression in control animals. Variability in *Bcl-x*$_L$ expression between individual mice was especially high in Purkinje cells for all genotypes, potentially reflecting dynamic changes that are occurring at this stage of cerebellar migration. It is also possible that cells most dramatically affected by paternal loss of *Bcl-x* expression have already undergone apoptosis at this developmental stage, complicating an interpretation on the effect of parental *Bcl-x* expression in the remaining cells. Further cellular analysis of the effects of *Bcl-x* uniparental deletions on the cerebellum could quantify the misplacement of Purkinje cells noted in the paternal deletion. This phenotype has been observed in mice lacking a pro-apoptotic Bcl-2 regulator *Bax* (Jung et al., 2008), so further analysis in *Bcl-x* deletions would give more insight into the significance of *Bcl-x*$_L$ parental expression and the apoptotic pathway overall in the proper maturation of the cerebellum.

Variability observed in *Bcl-x*$_L$ expression may also be due in part to technical issues quantifying smFISH signals in the cerebellum. Here, spot counting required labor-intensive manual segmentation of the cell bodies. Although the shape, size and location of Purkinje cells made this population very easy to individually segment, granule cells were markedly more difficult. Granule cell bodies often overlap, and *Bcl-x*$_L$ expression per cell was significantly lower than observed in Purkinje cells, so single cell counts of granule cells likely have some degree of human error. These issues with the experimental analysis were however resolved in the subsequent chapter, by switching to a more automated segmentation and spot analysis of cortical tissue. Our findings on the reduction in specific neuronal cell populations in the paternal but not maternal deletion of *Bcl-x* nonetheless

demonstrate how the parental alleles of *Bcl-x*$_L$ can contribute differently to the development and maturation of the mouse brain.

Materials and Methods

Generation of Bcl-x deletion mice and preparation of tissue for histological analyses

Mice with a nervous system-specific maternal deletion of *Bcl-x* were generated by crossing females bearing a floxed allele of *Bcl-x* (Rucker et al., 2000) with males bearing a Nestin::Cre transgene (Reichardt et al., 1999; Tronche et al., 1999). Mice with a nervous system-specific paternal deletion of *Bcl-x* were generated by crossing maternal deletion males (heterozygous for both a Nestin::Cre transgene and a floxed allele of *Bcl-x*) with wild-type females (carrying two wild-type alleles of *Bcl-x* and lacking the Nestin::Cre transgene) From those crosses, mice bearing the Nestin::Cre transgene and carrying two WT alleles of *Bcl-x* were used as control littermates (**Figure 2.1b**). Genotyping was performed by PCR as described in (Rucker et al., 2000) by a non-experimenter. This person assigned unique identifiers to each animal so that for subsequent analyses researchers were blinded to the genotype until statistical analysis of the data.

Male mice aged P78-85 were weighed and transcardially perfused with 4% paraformaldehyde (PFA) in PBS. Brains were removed, weighed, post-fixed in 4% PFA for 4 hr at 4˚C, immersed in 30% sucrose (in PBS) overnight at 4˚C, and then stored at −80˚C until being sectioned. 14-µm coronal sections of brains were prepared using a sliding microtome (Leica, Germany) and mounted in series on slides, which were also stored at −80˚C.

Area and cell type-specific quantification

Area quantifications were performed on brain sections stained using the NISSL method: sections were hydrated in a graded series of alcohol, stained with cresyl violet, dehydrated in alcohol, cleared with xylenes and mounted with DPX.

For quantification of distinct cell types, slide-mounted sections were warmed (37˚C, 5 min), equilibrated in PBS (5 min, RT), fixed in PFA (4% in PBS; 10 min, RT), washed in PBS (3 min, RT), permeabilized with Triton X-100 (0.5% in PBS; 30 min, RT), washed in TNT (3 × 5 min, RT), blocked in fetal bovine serum (FBS; 10% in TN; 30 min, RT), incubated with mouse anti-NEUN (EMD Millipore, Billerica, MA, MAB377; 1:1000) and rabbit anti-S100ß (Abcam, UK, ab41548; 1:500) antibodies (in 10% FBS; 12 hr, 4˚C), washed in TNT (3 × 5 min, RT), incubated with secondary antibodies (Alexa488- and Alexa647-labeled; Invitrogen, Carlsbad, CA; 1:1000 in 10% FBS; 12 hr, 4˚C), and washed in TNT (3 × 15 min, RT). Slides were mounted using Vectashield containing DAPI (5 µg/ml).

For conventional in situs, probe target sequences for *Vglut1* (*Slc17a7*) and *Gad1* were amplified by PCR and inserted into pCRII-TOPO vector (Life Technologies). Sequences were identical to those used by the Allen Brain Atlas (http://www.brain-map.org/). Antisense RNA probes were generated from linearized plasmid template using T7 or Sp6 polymerases (Promega, Madison, WI), and labeled with a digoxigenin RNA labeling mix (Roche, Switzerland; for Gad1) or a dinitrophenyl RNA labeling mix (Perkin Elmer, Waltham, MA; for Vglut1), treated with DNaseI (Promega), ethanol precipitated, and dissolved in a 30-µl volume of water. Slide-mounted sections were warmed (37˚C, 5 min),

washed in PBS (3 min, RT), permeabilized with Triton X-100 (0.5% in PBS; 30 min, RT), followed by Proteinase K (20 μg/ml in 50 mM Tris, 5 mM EDTA; 15 min, RT with gentle shaking), washed in PBS (3 × 3 min, RT), fixed in PFA (4% in PBS; 10 min, RT), washed in PBS (3×3 min, RT), incubated in acetylation solution (triethanolamine [0.1 M; pH 7.5], acetic anhydride [0.25%]; 10 min, RT), washed in PBS (3×3 min, RT), incubated in hybridization solution (formamide [50%], SSC [5X], Denhardts [5X], yeast tRNA [250 μg/ml], herring sperm DNA [200 μg/mL]; 30 min, RT), hybridized simultaneously with both Vglut1 and Gad1 antisense RNA probes (1:300 each in hybridization solution; 16 hr, 68˚C), washed with SSC (2×; 5 min, 68˚C), washed with SSC (0.2X; 3×30 min, 68˚C), incubated in H_2O_2 (3% in TN [Tris-HCl (0.1 M; pH 7.5), 0.15 M NaCl]; 30 min, RT), washed in TNT (Tween-20 [0.05%] in TN; 3×3 min, RT), incubated in TNB (Blocking Reagent [Perkin Elmer; 0.05% in TN]; 30 min, RT), incubated with anti-digoxigenin-POD antibody (1:1000 in TNB; 12 hr, 4˚C), and washed in TNT (3 × 20 min, RT). Fluorescent signals corresponding to the Gad1 probe were generated using the Tyramide Signal Amplification (TSA) Plus Fluorescein Kit (Perkin Elmer) according to the manufacturer's instructions, after which sections were washed in TNT (2 × 3 min, RT), incubated in H_2O_2 (3% in TN; 1 hr, RT), washed in TNT (3 × 3 min, RT), incubated with anti-dinitrophenyl-HRP antibody (Perkin Elmer; 1:500 in TNB; 12 hr at 4˚C), and washed in TNT (3 × 20 min, RT). Fluorescent signals corresponding to the Vglut1 probe were generated using the TSA Plus Cyanine5 Kit (Perkin Elmer) according to the manufacturer's instructions. Slides were mounted using Vectashield (Vector Laboratories) containing DAPI (5 μg/ml). Sections were imaged using a Zeiss (Germany) Axioscan.Z1 microscope with a 10X objective. Areas of brain regions were measured from images of NISSL-stained sections

using Zen software (Zeiss). Cell densities and numbers were quantified from two-color IF and in situ hybridization images using ImageJ software.

Five anterior cortical sections that include the somatomotor cortex (corresponding to Figures 29–33 in (Franklin and Paxinos, 2007)) were analyzed. Three coronal cerebellar sections that included lobules 4–6 of the cerebellar vermis (corresponding to Figures 86–88 in (Franklin and Paxinos, 2007)) were analyzed.

Single molecule fluorescence in situ hybridization

Brains were removed from male mice aged P8, immediately frozen in OCT compound (VWR, Franklin, MA) and stored at −80˚C. 10-µm coronal sections of brains were prepared using a Microm HM550 cryostat (Thermo Fisher, Missouri) set to −20 to −18˚C, and mounted on slides. Sections included lobules 4– 6 of the cerebellar vermis (corresponding to Figures 87–88 in (Franklin and Paxinos, 2007)). Mounted sections were fixed in PFA (4% in PBS; 10 min, RT), washed in PBS (2 × 5 min, RT), permeabilized overnight in 70% EtOH at 4˚C, and stored in 70% EtOH until hybridization.

Probes for *Bcl-xL* were generated from the GRCm38/mm10 genomic sequence for exons 2–5 (https://genome.ucsc.edu/) using the Stellaris Probe Designer software and labeled with the CalFluor 610 fluorescent dye. Probe sequences for *Bcl-xL* are listed in **Appendix 1**. Probes for *Gapdh* were ordered from Biosearch (catalog #SMF-3140-1) labeled with the Quasar 570 fluorescent dye.

Hybridization solution (2X SSC, 10% formamide, 10% dextran sulfate, 1 U/μL RNase inhibitor (Promega, catalog #N2515) contained 41 nM *Gapdh* and 215 nM *Bcl-x*$_L$ probes. 60 μL of hybridization solution was added per section, covered with a coverslip, and incubated for 14 hours at 37˚C. Slides were subsequently washed in wash buffer (2 × 30 min, RT) in the dark, stained with DAPI (2 ng/μL) during the second wash period, washed once in 2X SSC, then mounted for imaging in glucose oxidase buffer (0.4% glucose, 10 mM Tris, 2X SSC with glucose oxidase and catalase).

Images were acquired using a Zeiss (Germany) AxioImager M2 equipped with a 14-μm^2-pixel AxioCam MRm CCD camera, a 100X objective, and HXP-120C wide-field light source. Cells were imaged by taking a series of Z-stacks spaced by 0.35 μm. Exposure time for *Bcl-x*$_L$ with the given dye was 2100 ms, and for *Gapdh* 1500 ms. For spot counting, cells were segmented and thresholded using Raj lab Starsearch software (rajlab.seas.upenn.edu/StarSearch/). Each spot detect fits a two-dimensional Gaussian profile on the Z plane.

Some of this work described here has been published in: *Perez, J.D., Rubinstein, N.D., et al. (2015). Quantitative and functional interrogation of parent-of-origin allelic expression biases in the brain. eLife 4, e07860.*

References

Babak, T., Deveale, B., Armour, C., Raymond, C., Cleary, M.A., van der Kooy, D., Johnson, J.M., and Lim, L.P. (2008). Global survey of genomic imprinting by transcriptome sequencing. Curr Biol *18*, 1735-1741.

Babak, T., DeVeale, B., Tsang, E.K., Zhou, Y., Li, X., Smith, K.S., Kukurba, K.R., Zhang, R., Li, J.B., Kooy, D.v.d.*, et al.* (2015). Genetic conflict reflected in tissue-specific maps of genomic imprinting in human and mouse. Nature Genetics *47*, 544-549.

Beaudet, A.L., and Jiang, Y.H. (2002). A rheostat model for a rapid and reversible form of imprinting-dependent evolution. Am J Hum Genet *70*, 1389-1397.

Blagitko, N., Mergenthaler, S., Schulz, U., Wollmann, H.A., Craigen, W., Eggermann, T., Ropers, H.H., and Kalscheuer, V.M. (2000). Human GRB10 is imprinted and expressed from the paternal and maternal allele in a highly tissue- and isoform-specific fashion. Hum Mol Genet *9*, 1587-1595.

Cleaton, M.A., Edwards, C.A., and Ferguson-Smith, A.C. (2014). Phenotypic outcomes of imprinted gene models in mice: elucidation of pre- and postnatal functions of imprinted genes. Annu Rev Genomics Hum Genet *15*, 93-126.

DeVeale, B., Kooy, D.v.d., and Babak, T. (2012). Critical Evaluation of Imprinted Gene Expression by RNA–Seq: A New Perspective. PLoS Genetics *8*, e1002600.

Eldar, A., and Elowitz, M.B. (2010). Functional roles for noise in genetic circuits. Nature *467*, 167-173.

Engemann, S., Strodicke, M., Paulsen, M., Franck, O., Reinhardt, R., Lane, N., Reik, W., and Walter, J. (2000). Sequence and functional comparison in the Beckwith-Wiedemann region: implications for a novel imprinting centre and extended imprinting. Hum Mol Genet *9*, 2691-2706.

Femino, A.M., Fay, F.S., Fogarty, K., and Singer, R.H. (1998). Visualization of single RNA transcripts in situ. Science *280*, 585-590.

Ferron, S.R., Charalambous, M., Radford, E., McEwen, K., Wildner, H., Hind, E., Morante-Redolat, J.M., Laborda, J., Guillemot, F., Bauer, S.R.*, et al.* (2011). Postnatal loss of Dlk1 imprinting in stem cells and niche astrocytes regulates neurogenesis. Nature *475*, 381-385.

Franklin K.B.J., and Paxinos, G. (2007). The mouse brain in stereotaxic coordinates, third edition (New York: Elsevier).

Gaspar, I., and Ephrussi, A. (2015). Strength in numbers: quantitative single-molecule RNA detection assays. Wiley Interdiscip Rev Dev Biol *4*, 135-150.

Gregg, C. (2014). Known unknowns for allele-specific expression and genomic imprinting effects. F1000Prime Reports *6*, 75.

Gregg, C., Zhang, J., Butler, J.E., Haig, D., and Dulac, C. (2010a). Sex-Specific Parent-of-Origin Allelic Expression in the Mouse Brain. Science *329*, 682-685.

Gregg, C., Zhang, J., Weissbourd, B., Luo, S., Schroth, G.P., Haig, D., and Dulac, C. (2010b). High-resolution analysis of parent-of-origin allelic expression in the mouse brain. Science *329*, 643-648.

Hagiwara, Y., Hirai, M., Nishiyama, K., Kanazawa, I., Ueda, T., Sakaki, Y., and Ito, T. (1997). Screening for imprinted genes by allelic message display: identification of a paternally expressed gene impact on mouse chromosome 18. Proc Natl Acad Sci U S A *94*, 9249-9254.

Hayden, E.C. (2012). RNA studies under fire. Nature *484*, 428.

Hu, J.F., Oruganti, H., Vu, T.H., and Hoffman, A.R. (1998). Tissue-specific imprinting of the mouse insulin-like growth factor II receptor gene correlates with differential allele-specific DNA methylation. Mol Endocrinol *12*, 220-232.

Huang, S. (2009). Non-genetic heterogeneity of cells in development: more than just noise. Development *136*, 3853-3862.

Huang, W.-C., Ferris, E., Cheng, T., Hörndli, C.S., Gleason, K., Tamminga, C., Wagner, J.D., Boucher, K.M., Christian, J.L., and Gregg, C. (2017). Diverse Non-genetic, Allele-Specific Expression Effects Shape Genetic Architecture at the Cellular Level in the Mammalian Brain. Neuron *93*, 1094-1109.e1097.

Huber, D.V.v.V., L.; Kaigala, G. V. (2018). Fluorescence in situ hybridization (FISH): History, limitations and what to expect from micro-scale FISH? Micro and Nano Engineering *1*, 15-24.

Hwang, B., Lee, J.H., and Bang, D. (2018). Single-cell RNA sequencing technologies and bioinformatics pipelines. Exp Mol Med *50*, 96.

Jung, A.R., Kim, T.W., Rhyu, I.J., Kim, H., Lee, Y.D., Vinsant, S., Oppenheim, R.W., and Sun, W. (2008). Misplacement of Purkinje cells during postnatal development in Bax knock-out mice: a novel role for programmed cell death in the nervous system? J Neurosci *28*, 2941-2948.

Kaneko-Ishino, T., Kuroiwa, Y., Miyoshi, N., Kohda, T., Suzuki, R., Yokoyama, M., Viville, S., Barton, S.C., Ishino, F., and Surani, M.A. (1995). Peg1/Mest imprinted gene on chromosome 6 identified by cDNA subtraction hybridization. Nat Genet *11*, 52-59.

Kasai, S., Chuma, S., Motoyama, N., and Nakatsuji, N. (2003). Haploinsufficiency of Bcl-x leads to male-specific defects in fetal germ cells: differential regulation of germ cell apoptosis between the sexes. Dev Biol *264*, 202-216.

Keverne, E.B. (2013). Importance of the matriline for genomic imprinting, brain development and behaviour. Philos Trans R Soc Lond B Biol Sci *368*, 20110327.

Keverne, E.B. (2014). Significance of epigenetics for understanding brain development, brain evolution and behaviour. Neuroscience *264*, 207-217.

Keverne, E.B., Fundele, R., Narasimha, M., Barton, S.C., and Surani, M.A. (1996). Genomic imprinting and the differential roles of parental genomes in brain development. Brain Res Dev Brain Res *92*, 91-100.

Khatib, H. (2007). Is it genomic imprinting or preferential expression? Bioessays *29*, 1022-1028.

Kim, J., Bergmann, A., Wehri, E., Lu, X., and Stubbs, L. (2001). Imprinting and evolution of two Kruppel-type zinc-finger genes, ZIM3 and ZNF264, located in the PEG3/USP29 imprinted domain. Genomics *77*, 91-98.

Krajewska, M., Mai, J.K., Zapata, J.M., Ashwell, K.W., Schendel, S.L., Reed, J.C., and Krajewski, S. (2002). Dynamics of expression of apoptosis-regulatory proteins Bid, Bcl-2, Bcl-X, Bax and Bak during development of murine nervous system. Cell Death Differ *9*, 145-157.

Latham, K.E. (1995). Stage-specific and cell type-specific aspects of genomic imprinting effects in mammals. Differentiation *59*, 269-282.

Lawrence, J.B., and Singer, R.H. (1986). Intracellular localization of messenger RNAs for cytoskeletal proteins. Cell *45*, 407-415.

Lee, M.P., Hu, R.J., Johnson, L.A., and Feinberg, A.P. (1997). Human KVLQT1 gene shows tissue-specific imprinting and encompasses Beckwith-Wiedemann syndrome chromosomal rearrangements. Nat Genet *15*, 181-185.

Lee, Y.J., Park, C.W., Hahn, Y., Park, J., Lee, J., Yun, J.H., Hyun, B., and Chung, J.H. (2000). Mit1/Lb9 and Copg2, new members of mouse imprinted genes closely linked to Peg1/Mest(1). FEBS Lett *472*, 230-234.

Morison, I.M., Ramsay, J.P., and Spencer, H.G. (2005). A census of mammalian imprinting. Trends Genet *21*, 457-465.

Motoyama, N., Wang, F., Roth, K.A., Sawa, H., Nakayama, K., Nakayama, K., Negishi, I., Senju, S., Zhang, Q., Fujii, S.*, et al.* (1995). Massive cell death of immature hematopoietic cells and neurons in Bcl-x-deficient mice. Science *267*, 1506-1510.

Neildez-Nguyen, T.M., Parisot, A., Vignal, C., Rameau, P., Stockholm, D., Picot, J., Allo, V., Le Bec, C., Laplace, C., and Paldi, A. (2008). Epigenetic gene expression noise and phenotypic diversification of clonal cell populations. Differentiation *76*, 33-40.

Perez, J.D., Rubinstein, N.D., Fernandez, D.E., Santoro, S.W., Needleman, L.A., Ho-Shing, O., Choi, J.J., Zirlinger, M., Chen, S.-K., Liu, J.S.*, et al.* (2015). Quantitative and functional interrogation of parent-of-origin allelic expression biases in the brain. eLife *4*, e07860.

Raj, A., and Tyagi, S. (2010). Detection of individual endogenous RNA transcripts in situ using multiple singly labeled probes. Methods Enzymol *472*, 365-386.

Raj, A., van den Bogaard, P., Rifkin, S.A., van Oudenaarden, A., and Tyagi, S. (2008). Imaging individual mRNA molecules using multiple singly labeled probes. Nat Methods *5*, 877-879.

Reichardt, H.M., Kellendonk, C., Tronche, F., and Schutz, G. (1999). The Cre/loxP system--a versatile tool to study glucocorticoid signalling in mice. Biochem Soc Trans *27*, 78-83.

Rucker, E.B., 3rd, Dierisseau, P., Wagner, K.U., Garrett, L., Wynshaw-Boris, A., Flaws, J.A., and Hennighausen, L. (2000). Bcl-x and Bax regulate mouse primordial germ cell survival and apoptosis during embryogenesis. Mol Endocrinol *14*, 1038-1052.

Singer, R.H., and Ward, D.C. (1982). Actin gene expression visualized in chicken muscle tissue culture by using in situ hybridization with a biotinated nucleotide analog. Proc Natl Acad Sci U S A *79*, 7331-7335.

Skinner, S.O., Sepulveda, L.A., Xu, H., and Golding, I. (2013). Measuring mRNA copy number in individual Escherichia coli cells using single-molecule fluorescent in situ hybridization. Nat Protoc *8*, 1100-1113.

Steiner, I., Spivack, J.G., Jackson, A., Lavi, E., and Fraser, N.W. (1989). Effects of lipofuscin on in situ hybridization in human neuronal tissue. J Virol Methods *24*, 1-9.

Tronche, F., Kellendonk, C., Kretz, O., Gass, P., Anlag, K., Orban, P.C., Bock, R., Klein, R., and Schutz, G. (1999). Disruption of the glucocorticoid receptor gene in the nervous system results in reduced anxiety. Nat Genet *23*, 99-103.

Tunster, S.J., Jensen, A.B., and John, R.M. (2013). Imprinted genes in mouse placental development and the regulation of fetal energy stores. Reproduction *145*, R117-137.

Umlauf, D., Goto, Y., Cao, R., Cerqueira, F., Wagschal, A., Zhang, Y., and Feil, R. (2004). Imprinting along the Kcnq1 domain on mouse chromosome 7 involves repressive histone methylation and recruitment of Polycomb group complexes. Nat Genet *36*, 1296-1300.

Vu, T.H., and Hoffman, A.R. (1997). Imprinting of the Angelman syndrome gene, UBE3A, is restricted to brain. Nat Genet *17*, 12-13.

Wallace, M.L., Burette, A.C., Weinberg, R.J., and Philpot, B.D. (2012). Maternal loss of Ube3a produces an excitatory/inhibitory imbalance through neuron type-specific synaptic defects. Neuron *74*, 793-800.

Wang, X., Sun, Q., McGrath, S.D., Mardis, E.R., Soloway, P.D., and Clark, A.G. (2008). Transcriptome-wide identification of novel imprinted genes in neonatal mouse brain. PLoS One *3*, e3839.

Wilkinson, L.S., Davies, W., and Isles, A.R. (2007). Genomic imprinting effects on brain development and function. Nat Rev Neurosci *8*, 832-843.

Chapter III. Cell type-specific role of *Bcl-xL* imprinting in cortical plasticity

Introduction

Beyond its well-established role in programmed cell death, the apoptotic pathway is also known to modulate normal physiology in living neurons through the activation of caspases. While a global activation of caspases does lead to cell death, restricted and localized activation of caspases has been reported to regulate functions critical for neural plasticity, such as pruning of axonal and dendritic processes (D'Amelio et al., 2011; Erturk et al., 2014; Hyman and Yuan, 2012; Jiao and Li, 2011). In a mouse model for neurodegenerative Alzheimer's disease, Cecconi and colleagues (D'Amelio et al., 2011) found that the accumulation of amyloid-β proteins in hippocampal neurons caused an influx of intracellular calcium, which in turn activates caspase-3. Activation of caspase-3 in dendrites did not initiate cell death, but instead led to spine loss and long-term depression. Long-term potentiation (LTP) and long-term depression (LTD) are foundational processes of plasticity in neurons, by which calcium influx induces, respectively, the strengthening and weakening of synapses.

Morgan Sheng and colleagues built upon this work, showing that low level activation of effector caspase-3 (and of the upstream initiator caspase-9) in cultured hippocampal neurons is, in fact, necessary for internalization of α-amino-3-hydroxy-5-methyl-4-isoxazole propionate (AMPA) receptors and induction of LTD; affecting learning, memory and attention (Li et al., 2010; Lo et al., 2015). Most notably, Sheng and colleagues also found that overexpression of *Bcl-xL* inhibited long-term depression and

NMDA-induced internalization of AMPA receptor GluR2 (Li et al., 2010). Moreover, Bcl-xL is known to modulate the release and recycling of synaptic transmitters (Jonas et al., 2014), its overexpression also shown to enhance synaptic transmission and synapse number (Li et al., 2008). Altogether, these results demonstrate that the expression level of *Bcl-x*$_L$ is critical for preventing the activation of caspases, leading to non-apoptotic modulation of AMPA receptors, synaptic transmission, and long-term depression at excitatory synapses.

The apoptotic pathway in neurons has also been directly linked to microglia-mediated synaptic pruning (Gyorffy et al., 2018), a process that plays a role in experience-dependent plasticity (Schafer et al., 2012). In parallel, caspase-3 signaling within microglia has also been shown to activate microglia without triggering cell death (Burguillos et al., 2011). In human neuropathology as well, Bcl-xL marked activated microglia that colocalized with amyloid-β plaques. Taken together, these results suggest that *Bcl-x*$_L$ expression plays critical non-apoptotic roles in neuronal and non-neuronal cell types within the adult cortex.

While previous results demonstrated the essential role of Bcl-xL for the survival of glutamatergic cortical neurons (Nakamura et al., 2016), our cellular analysis in the cortex highlighted that, more specifically, paternal expression of *Bcl-x*$_L$ is essential for their survival (Perez et al., 2015). Next, in collaboration with Takao Hensch's lab, we sought to determine whether *Bcl-x*$_L$ also affects synaptic transmission and plasticity in a parent-of-origin-specific manner *in vivo*, by examining the primary visual cortex in the uniparental *Bcl-x* deletion mice. In light of the findings by Sheng and colleagues, we hypothesized that if allelic expression *of Bcl-x*$_L$ does affect synaptic plasticity, we would observe differential

effects in the maternal and paternal *Bcl-x* deletions, specifically in the induction of LTD and the composition of synaptic AMPA receptors. In this chapter, we focused our investigation of *Bcl-x*$_L$ allelic expression in the mouse primary visual cortex (V1), as an established experimental model to assess plasticity. Delma Caiati and Takao Hensch evaluated the electrophysiological effects in the V1 caused by maternal versus paternal deletion of *Bcl-x*. Because *Bcl-x*$_L$ is expressed widely in the neocortex, but loss of paternal *Bcl-x* affected cell number in a specific subset of neurons, we then used single molecule FISH to evaluate the expression of *Bcl-x*$_L$ in specific cell types of the V1.

Results

In order to investigate the role of *Bcl-x* in synaptic plasticity, we first sought to confirm that the parental bias observed in various brain regions of C57Bl/6J×Cast/EiJ hybrid mice was also present in tissue from V1 in brain-specific *Bcl-x* uniparental deletions (floxed *Bcl-x* mutant crossed to a Nestin::Cre transgenic line). We measured *Bcl-x*$_L$ expression using droplet digital PCR, a quantitative PCR method for detecting particularly low-abundance targets. As expected, in mice with maternal deletion of *Bcl-x,* the V1 exhibited nearly 40% less expression than in control littermates; and the V1 of paternal *Bcl-x* deletions exhibited on average 60% less expression. (**Figure 3.1**).

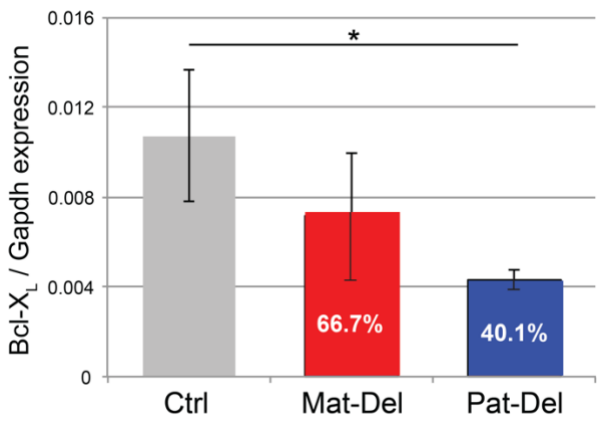

Figure 3.1: *Bcl-x*$_L$ expression in the parental deletions within the visual cortex (V1).

Bcl-x$_L$ expression measured by droplet digital PCR, relative to Gapdh expression, in P16 *Bcl-x* parental deletion mice (n_{CT} = 3, n_{MD} = 4, n_{PD} = 3). Percentages indicate the average expression level as a fraction of control expression level.

To investigate the effect parent-of-origin specific deletion of *Bcl-x* has on synaptic transmission, we performed whole-cell voltage clamp recordings in acute slices of V1. Pharmacologically isolated AMPA receptor-mediated excitatory post-synaptic currents ($EPSC_{SAMPA}$) were evoked by extracellular stimulation of layer 4 and recorded from layer 2/3 pyramidal cells. From age P16 to adulthood (P50), data from the paternal *Bcl-x* deletion showed significantly larger amplitudes and faster decay time in AMPA-mediated currents, while results from maternal deletion did not differ from control. Moreover, evoked EPSCs obtained in both the control and maternal deletion exhibited a linear I-V relationship, while currents recorded in the paternal deletion were larger at negative potentials than positive potentials, indicating inward rectification only in cells from the paternal deletion. Larger amplitudes, faster decay and inward rectification are all attributes of calcium-permeable AMPA receptors deficient in GluR2. In normal mice, calcium-permeable AMPAr are replaced by calcium-impermeable receptors around age P15 (Kumar et al., 2002), indicating that the loss of paternal but not maternal *Bcl-x* expression causes long term impairment in the maturation of AMPA synapses. Moreover, we observed that a classical conditioning pairing protocol for the induction of LTP instead elicited LTD in paternal deletion mice. We then found by two-color immunofluorescence that GluR2 is indeed expressed in both the maternal deletion and control, but not in the paternal deletion layer 2/3 pyramidal neurons, marked by the transcription factor Satb2.

These findings indicate that paternal deletion of *Bcl-x* impairs synaptic transmission in a specific cortical layer and specific neuronal cell type within the visual cortex. As previous studies show that Bcl-xL regulates long-term depression through

activation of caspase 3, we corroborated these results by selectively inhibiting caspases-3, 7, and 8 with the peptide DEVD-FMK in acute V1 slices. Inhibition of caspases rescued both the inward rectification and LTD phenotypes in the paternal *Bcl-x* deletion.

Lastly, we also found a difference in microglia between the parental *Bcl-x* deletions and controls. While microglia in a resting state show a typical ramified morphology, microglia in both of the uniparental deletions were more bushy in morphology than microglia in the control V1, indicating a more reactive state. Microglia in the paternal *Bcl-x* deletion exhibited more frequent reactivity than those in the maternal deletion. Moreover, only microglia from V1 of *Bcl-x* paternal deletion showed impairments in experience-dependent plasticity. In normal mice, short-term monocular deprivation during the V1 critical period (P14–P16) leads to hyper-ramification of microglia and robust microglia-mediated spine pruning of layer 2/3 pyramidal neurons. While microglial hyper-ramification occurred in both the maternal *Bcl-x* deletion and control mice, microglia in the *Bcl-x* paternal deletion failed to respond similarly. Moreover, microglia in the V1 of *Bcl-x* maternal deletion coupled with fewer pyramidal neurons than microglia in the control V1. Microglia in paternal *Bcl-x* deletion coupled with still fewer pyramidal neurons than in the V1 of *Bcl-x* maternal deletion, causing no spine pruning to occur in dendrites of paternal deletion pyramidal neurons. Again, inhibition of caspases by treatment with Q-VD-Oph rescued the ramification and neuronal coupling phenotypes in paternal *Bcl-x* deletion. Altogether, these findings show that paternal *Bcl-x* expression contributes differentially to the normal development of synaptic plasticity in excitatory pyramidal cells and microglia. Moreover, the effect on synaptic plasticity is mediated by activation of caspase-3, affecting

the GluR2 composition of receptors and AMPA-mediated currents, specifically in the synapses of Satb2+ pyramidal neurons.

To further investigate this layer-specific effect of paternal *Bcl-x* deletion, we used single-molecule FISH to quantify *Bcl-x*$_L$ expression in P16 *Bcl-x* deletion mice for four cell populations in the visual cortex. Cell populations were characterized by one of the following markers: Satb2, marking layer 2/3 pyramidal neurons; Ctip2, marking layer 5–6 pyramidal neurons; Pvalb, marking parvalbumin interneurons, or Iba1, marking microglia. We examined these cell types because Satb2+ neurons and Iba1+ microglia demonstrated physiological impairments in the V1, as described above, while Ctip2+ and Pvalb+ neurons showed no defects in synaptic transmission. All cell types examined, including microglia, were expected to be affected by the Nestin-specific deletion of *Bcl-x* (Dahlstrand et al., 1995; Lattin et al., 2008). We therefore hypothesized that the allelic expression of *Bcl-x* within a specific cell type could fit four potential models (**Figure 3.2**). If *Bcl-x*$_L$ is expressed equally from the maternal and paternal alleles within a cell type, we expected that the distribution of *Bcl-x*$_L$ transcripts detected by smFISH would overlap for the maternal and paternal deletions, and be roughly half of the distribution in control tissue. If *Bcl-x*$_L$ is expressed monoallelically from the paternal allele, we expected to see a complete (or near complete) collapse of the paternal distribution to 0 counts per cell, while the distribution for the maternal deletion would equal that of the control. If there is instead a uniform bias, in which all cells within the cell population express 60% paternal transcripts and 40% maternal transcripts, we expected that the distributions for the maternal and paternal deletions would shift in correspondence with the strength of the parental bias. And lastly, if *Bcl-x*$_L$ is expressed monoallelically in a significant subset of

cells within a cell type, we expected the distribution of the paternal deletion to narrow and shift significantly toward 0, while the maternal deletion distribution may shift but would maintain a similar width as the control distribution.

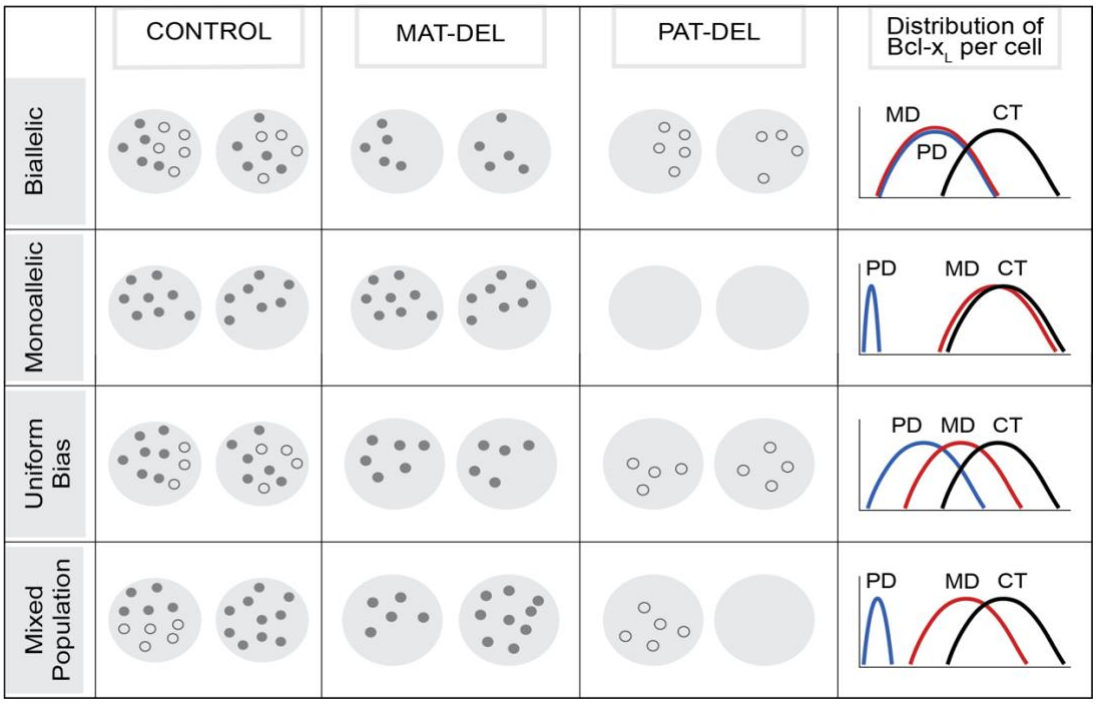

Figure 3.2: Potential models describing *Bcl-x*$_L$ expression within a cell population.

Each model illustrates potential arrangement of *Bcl-x*$_L$ transcripts in two cells defining a population. Open circles represent maternally-derived transcripts in a single cell, closed circles represent paternally-derived transcripts.

Interestingly, our results showed that *Bcl-x*$_L$ exhibited different models of allelic expression according to the cell type analyzed. We found that Satb2+ cells showed a significant loss of *Bcl-x*$_L$ expression in the paternal deletion relative to control littermates, but not in maternal *Bcl-x* deletion (**Figure 3.3**). Notably, about 40% of the Satb2+ cells in the paternal deletion showed 0 *Bcl-x* counts, compared to 4% and 5% of the Satb2+ cells in the control and maternal deletion, respectively. This significant loss of expression in the paternal deletion narrows the distribution of cells expressing *Bcl-x*$_L$ and shifts it towards 0, fitting the mixed (monoallelic and biallelic) population model.

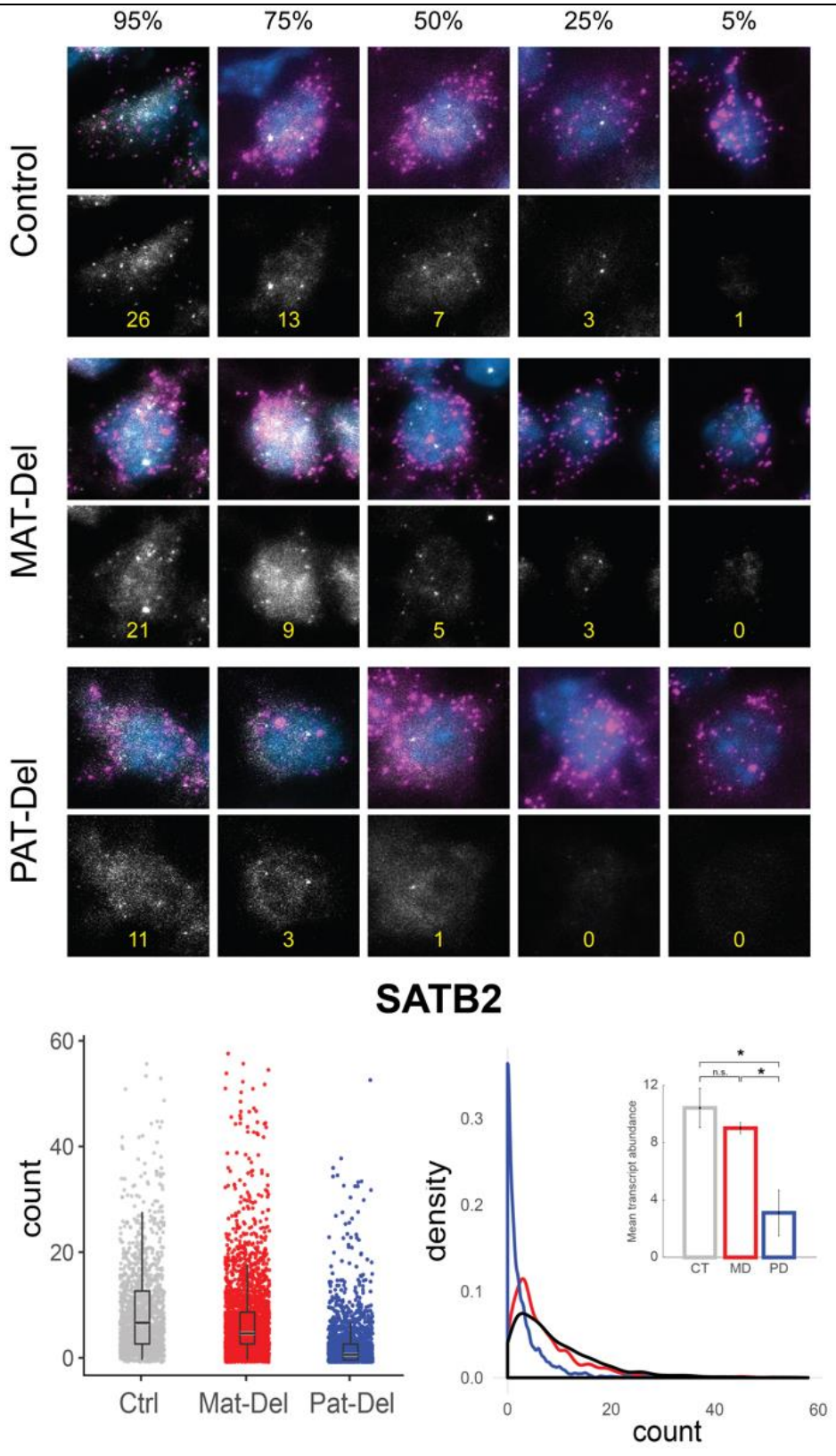

Figure 3.3: *Bcl-x*$_L$ expression in Satb2+ pyramidal neurons.

(*Continued Figure 3.3*) Each column shows a representative cell for a quantile of *Bcl-x*$_L$ expression in P16 control and parental deletions V1. Magenta spots are single transcripts of *Satb2*, white spots are single transcripts of *Bcl-x*$_L$, DAPI signal is in blue. Below each representative cell is the *Bcl-x*$_L$ channel only, and the number of spots detected. Bottom left: Scatter and box plot of *Bcl-x*$_L$ expression. Each data point reflects the number of *Bcl-x*$_L$ transcripts for a single Satb2+ cell. Bottom right: Overlaid distributions of *Bcl-x*$_L$ transcripts per cell for each genotype. Insets show mean transcript count of the distribution for each genotype, and significance by K-S test of the distributions.

In contrast, while we observed a reduction in *Bcl-x*$_L$ expression within the uniparental deletions in the other neuronal cell types, there was no significant difference in expression between genotypes for Ctip2+ neurons (**Figure 3.4**) or Pvalb+ neurons (**Figure 3.5**). These results best fit the model for biallelic expression of *Bcl-x*$_L$ in Ctip2+ and Pvalb+ neurons.

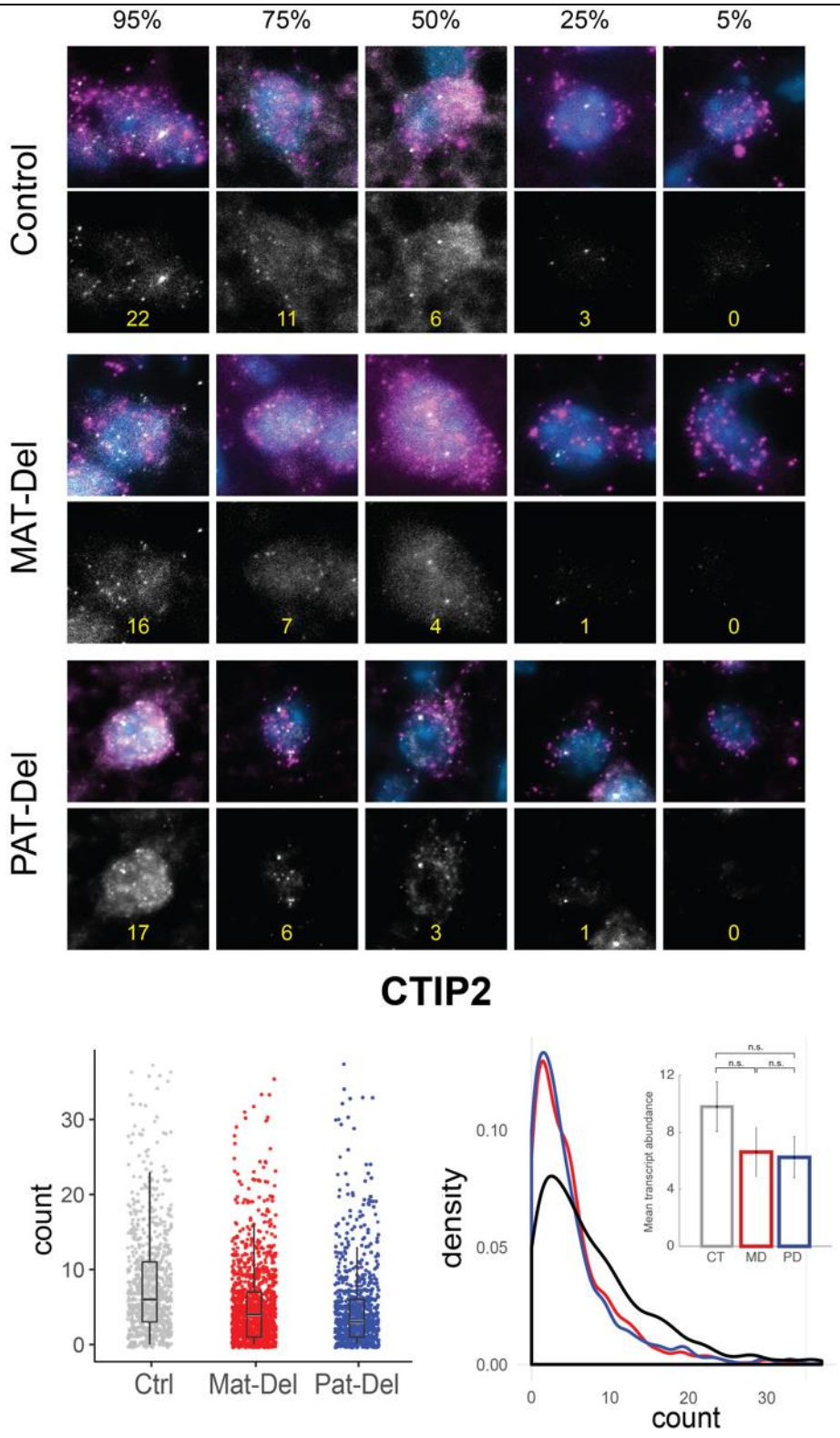

Figure 3.4: *Bcl-x$_L$* expression in Ctip2+ pyramidal neurons.

(*Continued Figure 3.4*) Each column shows a representative cell for a quantile of *Bcl-x_L* expression in P16 control and parental deletions V1. Magenta spots are single transcripts of *Ctip2*, white spots are single transcripts of *Bcl-x_L*, DAPI signal is in blue. Below each representative cell is the *Bcl-x_L* channel only, and the number of spots detected. Bottom left: Scatter and box plot of *Bcl-x_L* expression. Each data point reflects the number of *Bcl-x_L* transcripts for a single Ctip2+ cell. Bottom right: Overlaid distributions of *Bcl-x_L* transcripts per cell for each genotype. Insets show mean transcript count of the distribution for each genotype, and significance by K-S test of the distributions.

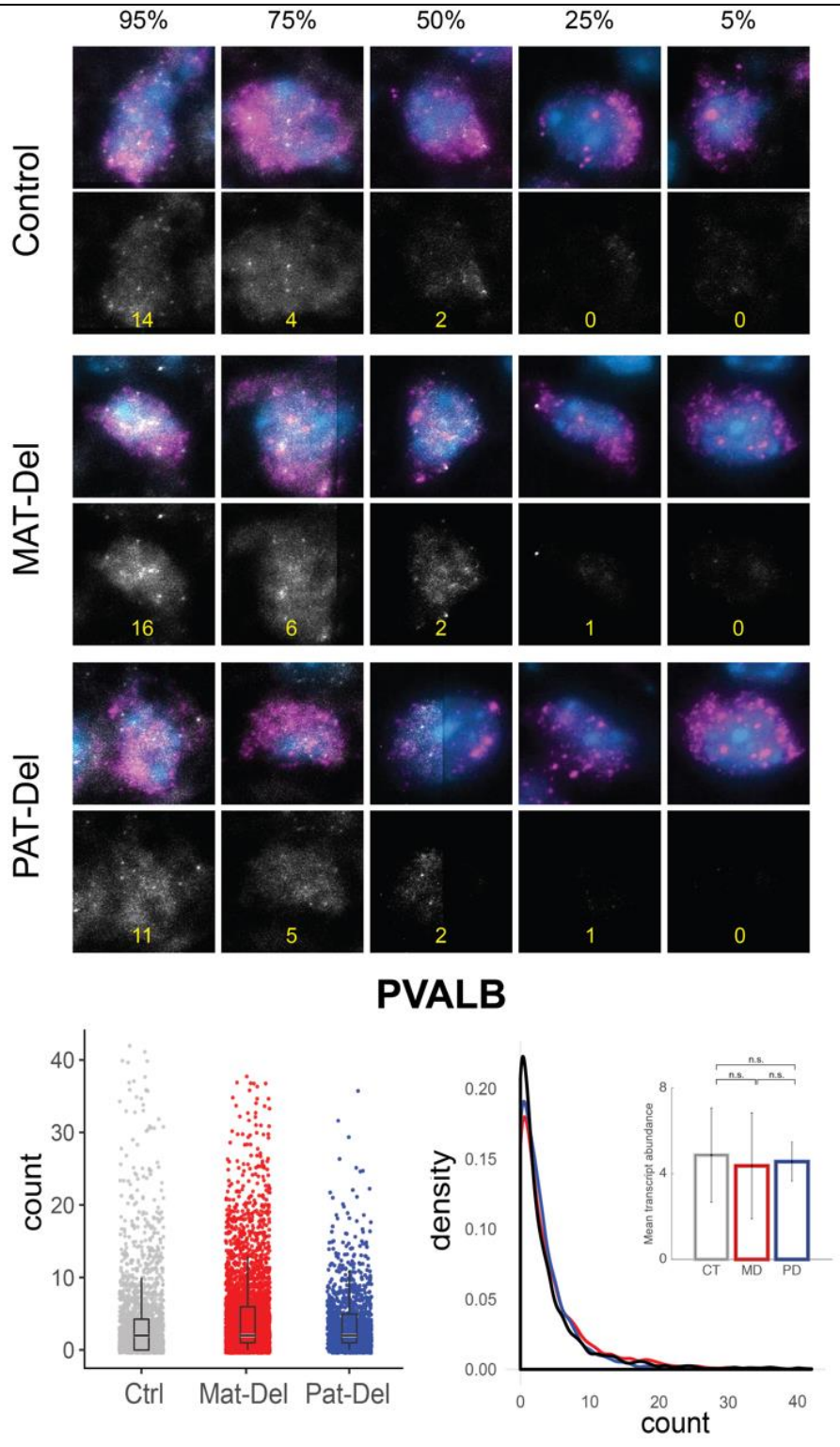

Figure 3.5: *Bcl-x*$_L$ expression in Pvalb+ interneurons.

(*Continued Figure 3.5*) Each column shows a representative cell for a quantile of *Bcl-x*$_L$ expression in P16 control and parental deletions V1. Magenta spots are single transcripts of *Pvalb*, white spots are single transcripts of *Bcl-x*$_L$, DAPI signal is in blue. Below each representative cell is the *Bcl-x*$_L$ channel only, and the number of spots detected. Bottom left: Scatter and box plot of *Bcl-x*$_L$ expression. Each data point reflects the number of *Bcl-x*$_L$ transcripts for a single Pvalb+ cell. Bottom right: Overlaid distributions of *Bcl-x*$_L$ transcripts per cell for each genotype. Insets show mean transcript count of the distribution for each genotype, and significance by K-S test of the distributions.

In Iba1+ microglia, we also observed a significant reduction in *Bcl-x*$_L$ expression in both the maternal and paternal deletions. The median number of *Bcl-x*$_L$ transcripts detected in control mice was 6, compared to 3 counts per cell in the maternal deletion, and two counts per cell in the paternal deletion (**Figure 3.6**). Thus, the *Bcl-x*$_L$ distributions for microglia would suggest that microglia either fit the model for biallelic expression of *Bcl-x*$_L$ or fit the uniform bias model. The graded reduction in mean *Bcl-x*$_L$ expression per cell – in which microglia in the V1 of paternal deletions exhibit lower expression than microglia in the V1 of maternal deletions – could explain the graded phenotypes observed in microglial reactivity and coupling to Satb2+ neurons – in which microglia in the V1 of the paternal deletion more frequently exhibit a reactive bushy morphology, and exhibit less frequent coupling than microglia in the V1 of the maternal deletion. As microglia in the maternal deletion still exhibit these effects, but to a lesser degree than in the paternal

deletion, these results would imply that even the loss of maternal *Bcl-x*$_L$ expression leads to significant effects on microglial activation and function in the V1.

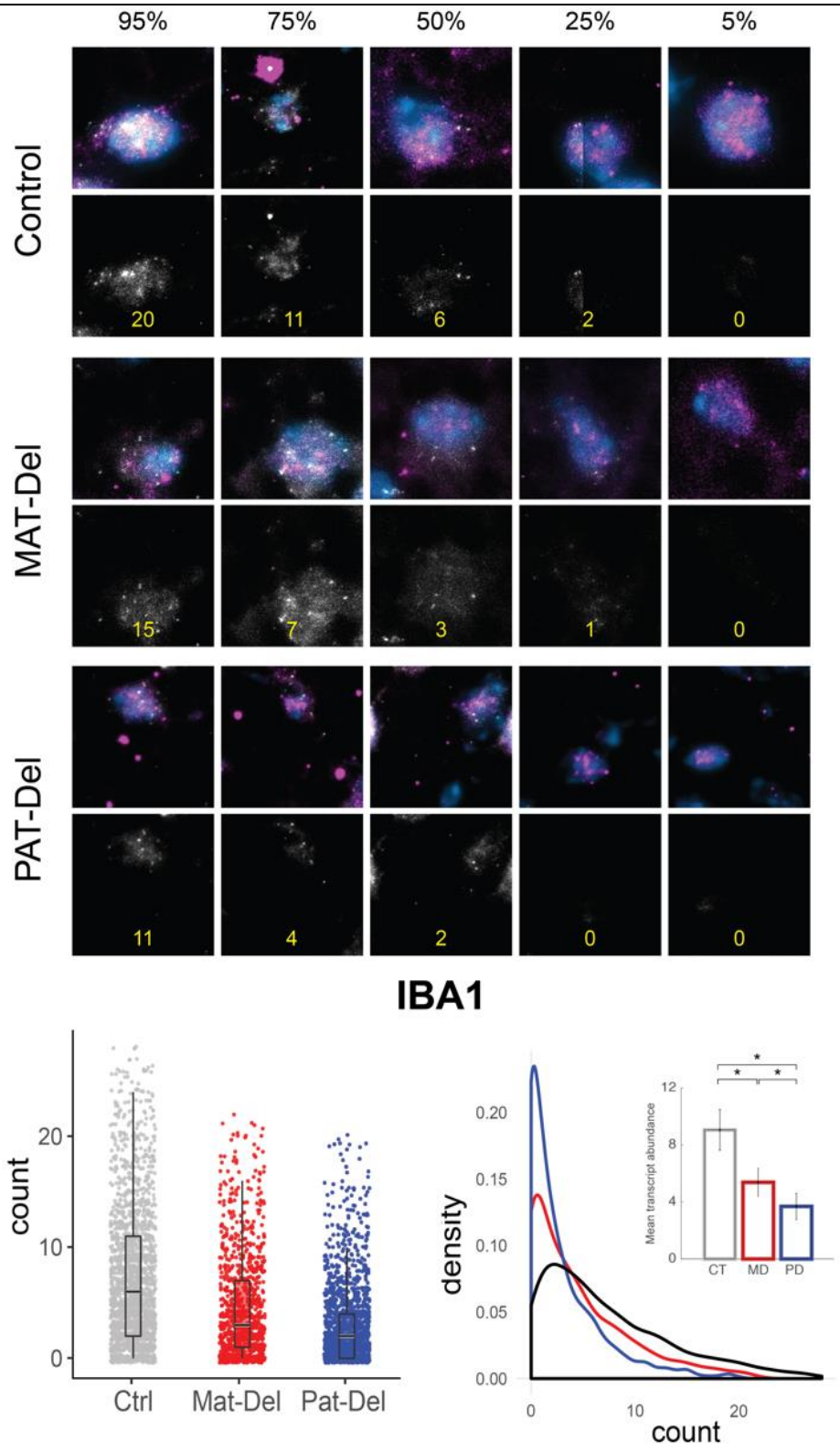

Figure 3.6: *Bcl-x$_L$* expression in Iba1+ microglia.

(*Continued Figure 3.6*) Each column shows a representative cell for a quantile of *Bcl-x*$_L$ expression in P16 control and parental deletions V1. Magenta spots are single transcripts of *Iba1*, white spots are single transcripts of *Bcl-x*$_L$, DAPI signal is in blue. Below each representative cell is the *Bcl-x*$_L$ channel only, and the number of spots detected. Bottom left: Scatter and box plot of *Bcl-x*$_L$ expression. Each data point reflects the number of *Bcl-x*$_L$ transcripts for a single Iba1+ cell. Bottom right: Overlaid distributions of *Bcl-x*$_L$ transcripts per cell for each genotype. Insets show mean transcript count of the distribution for each genotype, and significance by K-S test of the distributions.

In order to gain a better understanding of the differences in *Bcl-x*$_L$ expression seen in the various cell types, we tested for each cell type whether expression from the paternal allele is independent of the expression level from the maternal allele. For each cell type, we randomly sampled the *Bcl-x*$_L$ count from one maternal deletion cell and one paternal deletion cell, then summed these counts to produce a model control cell count. We repeated this process to form a model control distribution, and compared this distribution to the observed control *Bcl-x*$_L$ distribution for each cell type (**Figure 3.7**). Both Satb2+ and Iba1+ simulated distributions matched the observed control distributions, while they differed significantly for Ctip2+ (p=1.17e-11) and Pvalb+ (p<2.2e-16) cells. This comparison suggests that *Bcl-x*$_L$ expression in Ctip2+ and Pvalb+ neurons may involve some compensation between the two parental alleles. We also noted that the standard deviation in the mean transcript level of Ctip2+ (**Figure 3.4**) and Pvalb+ neurons (**Figure 3.5**) is higher than that of Satb2+ and Iba1+ cells, indicating that for these cell types

(which exhibited no impaired phenotypes in the deletion mice) *Bcl-x*$_L$ expression is more variable than in cell types significantly affected by paternal *Bcl-x* deletion.

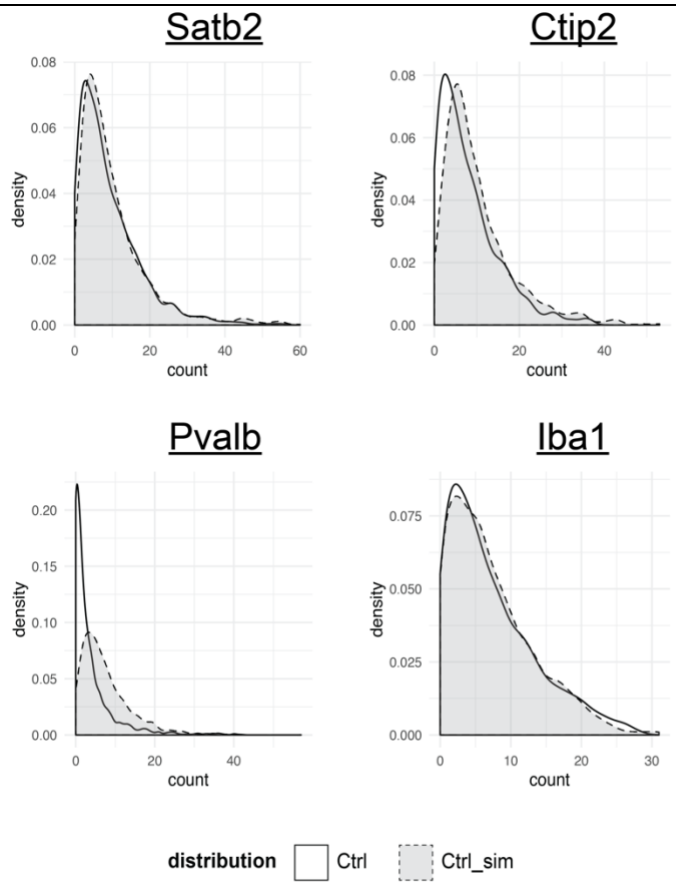

Figure 3.7: Modeled control distribution of *Bcl-x*$_L$ expression.

Observed control distribution overlaid with the experimental distribution summing MAT-del and PAT-del transcript counts per cell.

Discussion

Our study on the functional role of *Bcl-x*$_L$ parentally-biased expression in the primary visual cortex demonstrated that paternal *Bcl-x*$_L$ expression differentially affects synaptic plasticity in cortical layer 2/3. Moreover, *Bcl-x*$_L$ exhibits canonical monoallelic paternal expression in a specific subset of excitatory neurons, marked by Satb2. This parent-of-origin-specific effect of *Bcl-x*$_L$ expression builds upon the findings of Sheng and colleagues, revealing the following representation for the role of Bcl-xL, and the apoptotic pathway, in synaptic plasticity (**Figure 3.8**): In mature neurons within the V1s of control and of maternal *Bcl-x* deletion mice, glutamatergic stimulation of NMDA receptors causes an influx of calcium, but anti-apoptotic regulator Bcl-xL is sufficient to prevent the release of cytochrome C from mitochondria, inhibiting caspase-3 activation and thus inducing LTP instead of LTD. In the paternal *Bcl-x* deletion however, the complete (or near-complete) loss of Bcl-xL in a significant subset of pyramidal neurons allows for the activation of caspase-3, leading to the internalization of GluR2 subunits of AMPAr, and thus inducing LTD. Internalization of GluR2 sustains an immature AMPAr phenotype in the paternal *Bcl-x* deletion past the critical period for the visual cortex. Thus, Satb2+ neurons that survive the massive excitatory cell death in the paternal deletion retain into adulthood a phenotype of calcium-permeable glutamatergic synapses and activated caspase-3, thereby promoting LTD in response to classical LTP conditioning.

Furthermore, microglia in the V1s of control and maternal *Bcl-x* deletion more frequently showed a typical ramified morphology than microglia in the paternal *Bcl-x* deletion, and their processes couple with those of the surrounding pyramidal neurons. Microglia in the paternal *Bcl-x* deletion are bushier in morphology (a sign of increased

reactivity) and less frequently contact their neighboring Satb2+ cells (**Figure 3.8**). Altogether, expression of *Bcl-x*$_L$ is necessary for regulating microglia activation, and for functional cross-talk between Satb2+ pyramidal neurons and microglia.

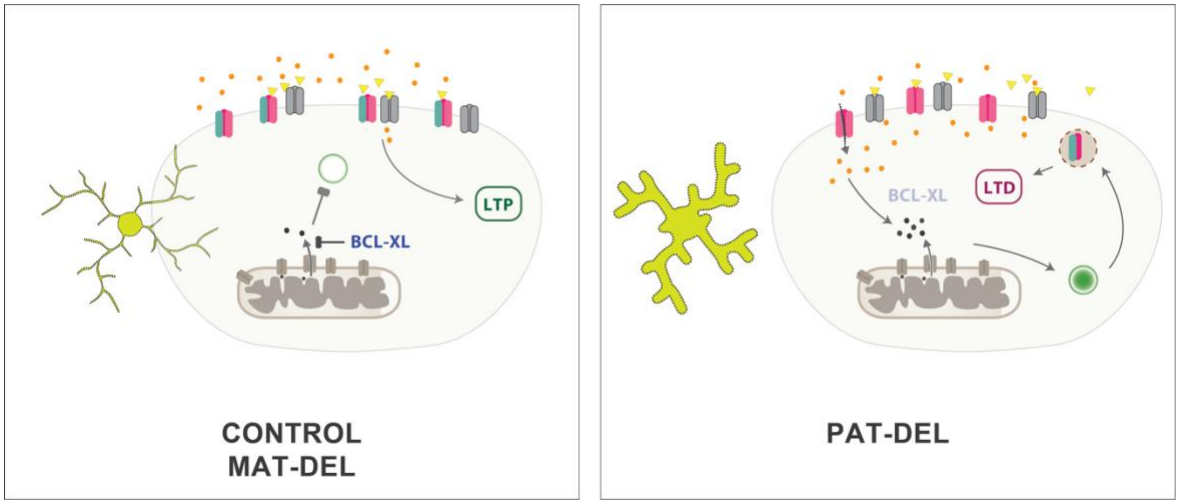

Figure 3.8: Model of cell type-specific cortical effects of *Bcl-xL* parental deletion

Schema represents synapse of a Satb2+ pyramidal neuron and adjacent microglia. Orange circles are Ca^{2+} ions, yellow triangles are glutamate released from a presynaptic neuron stimulated in layer 4. Gray receptors are NMDAr, Pink receptors are AMPAr, teal represents the GluR2 subunit of AMPAr. Black circles are cytochrome c released by the mitochondria. Green circles are caspase-3, and green fill indicates activation. Brown dashed circle is synaptic vesicle internalizing AMPAr.

Our findings quantifying expression using single molecule FISH support the hypothesis that the Satb2+ cell population exhibits our mixed population model of imprinted expression. *Bcl-x*$_L$ expression was completely absent in nearly 40% of paternal deletion Satb2+ neurons, significantly narrowing the distribution of cells that express *Bcl-x*$_L$ within this cell type. Thus, our results demonstrate that a parentally-biased gene can have multiple effects on cell fate and synaptic plasticity, interestingly in very specific subsets of neural cell types. Other strongly- and moderately-biased imprinted genes have also been reported to demonstrate cell-type specific effects on synaptic plasticity. *Ube3a* which is maternally imprinted only in neurons (Albrecht et al., 1997; Jiang et al., 1998; Wilkinson et al., 2007), has been reported to affect primarily AMPA synapses in glutamatergic neurons in an experience-dependent manner (Fink et al., 2017; Greer et al., 2010; Sato and Stryker, 2010; Yashiro et al., 2009), and only affects specific classes of inhibitory neurons (Gustin et al., 2010; Wallace et al., 2012). *MEG3* maternal expression is also induced in an experience-dependent manner and modulates AMPAr expression at synapses (Tan et al., 2017). *Nnat*, an imprinted gene residing in maternally-expressed *Blcap*, stimulates calcium release in hippocampal dendrites and is implicated in having a role in synaptic plasticity (Joseph, 2014; Oyang et al., 2011). Lastly, paternally-expressed *Plagl1* (*Zac1*) is expressed highly in cell populations with active synaptic plasticity during mouse development (Valente et al., 2004). Notably *MEG3*, *Blcap* and *Plagl1*, like *Bcl-x*$_L$ also have known roles in the apoptotic pathway (**Figure 1.5**), emphasizing the functional connections between synaptic plasticity, apoptosis, and imprinted expression in the brain.

Our results on *Bcl-x*$_L$ expression in Iba1+, Ctip2+ and Pvalb+ cells indicate that *Bcl-x*$_L$ exhibits different patterns of allelic expression in different cortical cell populations.

The results on *Bcl-xL* expression in Iba1+ microglia would suggest that *Bcl-xL* is expressed in either a biallelic or uniformly-biased fashion. In Iba1+ cells, we do observe a significant difference in Bcl-xL expression comparing expression in the control V1 to expression in both the maternal deletion and paternal deletion V1s, which would fit our expectations of a uniform bias. However, the difference in median *Bcl-xL* transcript abundance between microglia in the maternal deletion and microglia in the paternal deletion is 1, so it is difficult to rule out the possibility of expression fitting the biallelic model. Our results on *Bcl-xL* expression in Ctip2+ and Pvalb+ neurons would suggest that *Bcl-xL* in other neuronal subsets is likely biallelic. The simulations of the control distribution by summing maternal deletion and paternal deletion *Bcl-xL* counts imply that in Ctip2+ and Pvalb+ neurons, loss of *Bcl-xL* expression from one allele is compensated by increased *Bcl-xL* expression from the remaining parental allele. It is possible that in the control V1, *Bcl-xL* is regularly transcribed from only one allele during a single transcriptional burst within both Ctip2+ and Pvalb+ neurons, irrespective of the allele's parent-of-origin. This would still constitute biallelic expression over multiple periods of transcription within these cells, but would also explain why no significant difference is observed between control *Bcl-xL* expression and *Bcl-xL* expression in the uniparental deletions. Further examination of the allelic transcription of *Bcl-xL* is needed in order to definitively characterize which models best fit the allelic expression of *Bcl-xL* in Iba1+, Ctip2+ and Pvalb+ cells.

The higher variability in *Bcl-xL* expression in Pvalb+ and Ctip2+ subsets may highlight that strict paternal expression of *Bcl-xL* is a mechanism specific to Satb2+ pyramidal neurons for tightly regulating activity of the apoptotic pathway in an experience-dependent manner. Other factors beyond Bcl-xL, or different glutamatergic receptor

compositions may play more prominent roles in mediating synaptic plasticity in non-Satb2+ neuronal subtypes, including Pvalb+ interneurons. Parvalbumin is a calcium-binding protein that plays critical roles in calcium sequestration and signaling (Lichvarova et al., 2018); and through its modulation of synaptic calcium levels, parvalbumin expression can define the plastic state of Pvalb+ neurons (Collin et al., 2005; Donato et al., 2013). Furthermore, plasticity of Pvalb+ neurons is known to be triggered by external factors such as brain-derived neurotrophic factor (BDNF) and orthodenticle homeobox 2 (Otx2), which promote Pvalb+ cell maturation (Hanover et al., 1999; Sugiyama et al., 2008; Takesian and Hensch, 2013). Lastly, Pvalb+ neurons in the visual cortex have dendritic synapses, and (as opposed to pyramidal neurons) a low density of spines that contain glutamatergic receptors (Sancho and Bloodgood, 2018). Close study of long-term potentiation in the visual cortex has found that the location of the synapse, the composition of NMDA:AMPA receptors within the synapse, and the type and timing of coincident activity all contribute to the nature of calcium-mediated synaptic transmission in Pvalb+ interneurons (Le Roux et al., 2013; Sancho and Bloodgood, 2018).

Altogether, our surprising findings on *Bcl-x*$_L$ expression in the visual cortex emphasize the potential cell-type specificity of parentally-biased imprinting in the postnatal brain. *Bcl-x*$_L$ demonstrates that even modest biases in allelic expression can on the cellular level have significant and long-lasting effects on the function of neuronal populations. Moreover, our ability to rescue the mutant phenotypes by administration of caspase inhibitors underlines the potential for treating neurodegenerative disorders by targeting particularly the apoptotic pathway.

Materials and Methods

Generation of Bcl-x deletion mice and preparation of tissue for histological analyses

Mice with a nervous system-specific maternal deletion of *Bcl-x* were generated by crossing females bearing a floxed allele of *Bcl-x* (Rucker et al., 2000) with males bearing a Nestin::Cre transgene (Reichardt et al., 1999; Tronche et al., 1999). Mice with a nervous system-specific paternal deletion of *Bcl-x* were generated by crossing maternal deletion males (heterozygous for both a Nestin::Cre transgene and a floxed allele of *Bcl-x*) with wild-type females (carrying two wild-type alleles of *Bcl-x* and lacking the Nestin::Cre transgene) From those crosses, mice bearing the Nestin::Cre transgene and carrying two WT alleles of *Bcl-x* were used as control littermates. (**Figure 2.1b**) Genotyping was performed by PCR as described in (Rucker et al., 2000) by a non-experimenter. This person assigned unique identifiers to each animal so that for subsequent analyses researchers were blinded to the genotype until statistical analysis of the data.

Droplet digital PCR

Brains from control, maternal *Bcl-x* deletion and paternal *Bcl-x* deletions were dissected and frozen in OCT, and then coronally sectioned on the cryostat until reaching the V1b area according to anatomical landmarks (Allen Brain Atlas, Mouse Reference Atlas). The V1b of each hemisphere was punched out using 1mm sample corers (FST #18035-01) and collected into Trizol Reagent (ThermoFisher #15596026). RNA was purified according to manufacturer's instruction, treated with DNAse 1 (Qiagen #79254) and then cleanup using Qiagen's RNeasy Micro Kit (#74004). Reverse transcription was perform using

SuperScript III (ThermoFisher #18080093). Droplet digital PCR reactions were prepared using the Bio-Rad Supermix for Probes (Bio-rad #186-3024) and experiment performed in Bio-Rad's ddPCR platform according to manufacturer's instruction. Primer and probe sets to target *Bcl-xL* and *Gapdh* were ordered from IDT's predesigned catalog (#Mm.PT.58.28488885 (FAM) and Mm.PT.39a.1 (HEX), respectively).

Single molecule FISH

For *Bcl-xL* quantification, male mice were sacrificed at postnatal day 16 (P16), and brain tissue harvested, immediately frozen embedded in OCT (VWR, Franklin MA), and stored at −80˚C.. Brains were coronally cryosectioned using a Microm HM550 cryostat (Thermo Fisher, Missouri) set to −20 to −18˚C to the V1b area, (corresponding to Figures 56–59 in (Franklin and Paxinos, 2007)). 10-µm cryosections of the V1b were mounted on poly-D-lysine-coated coverslips (Neuvitro, #GG-18-1.5-pdl), fixed in PFA (4% in PBS; 10 min, RT), washed in PBS (2 × 5 min, RT), permeabilized overnight in 70% EtOH at 4˚C, and stored in 70% EtOH until hybridization.

Probe libraries for *Bcl-xL*, *Satb2*, *Ctip2*, *Pvalb* and *Iba1* were constructed from the GRCm38/mm10 genomic sequence from exons of each gene (https://genome.ucsc.edu/) using the Stellaris Probe Designer software as described in Raj et al (Raj et al., 2008), with one modification: cell type marker probes were designed with an encoding tail sequence and separate readout probe, conjugated with Alexa 647 dye, as described in Moffitt et al (Moffitt et al., 2016). Probe sequences are listed **Appendix 1**.

Hybridization solution (2X SSC, 10% formamide, 10% dextran sulfate, 1 U/μL RNase inhibitor (Promega, catalog #N2515) contained 100 nM of *Satb2*, *Ctip2*, *Pvalb*, or *Iba1* probe and 215 nM *Bcl-xL* probe. 60 μL of hybridization solution was added per section, covered with a coverslip, and incubated for 14 hours at 37˚C. Sections were washed three times in wash buffer, stained with DAPI (2.5 ng/μl), then hybridized at room temperature with readout probes for 30 min at RT, as described in Moffitt et al., 2016. Sections were then washed in secondary wash buffer (30% formamide in 2X SSC, 1 × 30 min, RT), and mounted in 2X SSC with glucose oxidase buffer (0.4% glucose, 10 mM Tris, 2X SSC with glucose oxidase and catalase).

Images were acquired using a Zeiss (Germany) LSM-700 confocal microscope with widefield illumination, equipped with a 63X Plan Apo objective, and a Hamamatsu C9100-14 cooled charge-coupled device camera. Cells were imaged in serial Z-stacks spaced by 0.30 μm. Images were segmented and transcript spots fitted using custom Python software, as developed for MERFISH (Moffitt et al., 2016). Each spot is fitted by size and pixel intensity to a two-dimensional Gaussian profile. Satb2-, Ctip2-, and Pvalb-positive cells were defined as cells containing minimum 15 transcript spots per cell, based on the overall distribution of expression. Iba1-positive cells were defined as cells containing minimum 7 spots per cell, based on the overall distribution of expression.

Bcl-xL distribution simulation

For each cell type, one cell was sampled randomly from both the maternal *Bcl-x* deletion distribution and the paternal *Bcl-x* deletion distribution, and summed to simulate a control

cell count. This sampling was done N times, where N is the number of cells quantified in the control *Bcl-x* distribution for the given cell type (N_{Satb2}=1522, N_{Ctip2}=835, N_{Pvalb}=2360, N_{Iba1}=1887). The density of the simulated summed up counts was plotted, and compared to the observed control distribution using the Wilcoxon rank sum test.

The work described here is part of a manuscript in preparation.

References

Albrecht, U., Sutcliffe, J.S., Cattanach, B.M., Beechey, C.V., Armstrong, D., Eichele, G., and Beaudet, A.L. (1997). Imprinted expression of the murine Angelman syndrome gene, Ube3a, in hippocampal and Purkinje neurons. Nat Genet *17*, 75-78.

Burguillos, M.A., Deierborg, T., Kavanagh, E., Persson, A., Hajji, N., Garcia-Quintanilla, A., Cano, J., Brundin, P., Englund, E., Venero, J.L.*, et al.* (2011). Caspase signalling controls microglia activation and neurotoxicity. Nature *472*, 319-324.

Collin, T., Chat, M., Lucas, M.G., Moreno, H., Racay, P., Schwaller, B., Marty, A., and Llano, I. (2005). Developmental changes in parvalbumin regulate presynaptic Ca^{2+} signaling. J Neurosci *25*, 96-107.

D'Amelio, M., Cavallucci, V., Middei, S., Marchetti, C., Pacioni, S., Ferri, A., Diamantini, A., De Zio, D., Carrara, P., Battistini, L.*, et al.* (2011). Caspase-3 triggers early synaptic dysfunction in a mouse model of Alzheimer's disease. Nat Neurosci *14*, 69-76.

Dahlstrand, J., Lardelli, M., and Lendahl, U. (1995). Nestin mRNA expression correlates with the central nervous system progenitor cell state in many, but not all, regions of developing central nervous system. Brain Res Dev Brain Res *84*, 109-129.

Donato, F., Rompani, S.B., and Caroni, P. (2013). Parvalbumin-expressing basket-cell network plasticity induced by experience regulates adult learning. Nature *504*, 272-276.

Erturk, A., Wang, Y., and Sheng, M. (2014). Local pruning of dendrites and spines by caspase-3-dependent and proteasome-limited mechanisms. J Neurosci *34*, 1672-1688.

Fink, J.J., Robinson, T.M., Germain, N.D., Sirois, C.L., Bolduc, K.A., Ward, A.J., Rigo, F., Chamberlain, S.J., and Levine, E.S. (2017). Disrupted neuronal maturation in Angelman syndrome-derived induced pluripotent stem cells. Nature Communications *8*, ncomms15038.

Franklin K.B.J., and Paxinos, G. (2007). The mouse brain in stereotaxic coordinates, third edition (New York: Elsevier).

Greer, P.L., Hanayama, R., Bloodgood, B.L., Mardinly, A.R., Lipton, D.M., Flavell, S.W., Kim, T.K., Griffith, E.C., Waldon, Z., Maehr, R.*, et al.* (2010). The Angelman Syndrome protein Ube3A regulates synapse development by ubiquitinating arc. Cell *140*, 704-716.

Gustin, R.M., Bichell, T.J., Bubser, M., Daily, J., Filonova, I., Mrelashvili, D., Deutch, A.Y., Colbran, R.J., Weeber, E.J., and Haas, K.F. (2010). Tissue-specific variation of Ube3a protein expression in rodents and in a mouse model of Angelman syndrome. Neurobiol Dis *39*, 283-291.

Gyorffy, B.A., Kun, J., Torok, G., Bulyaki, E., Borhegyi, Z., Gulyassy, P., Kis, V., Szocsics, P., Micsonai, A., Matko, J.*, et al.* (2018). Local apoptotic-like mechanisms underlie complement-mediated synaptic pruning. Proc Natl Acad Sci U S A *115*, 6303-6308.

Hanover, J.L., Huang, Z.J., Tonegawa, S., and Stryker, M.P. (1999). Brain-derived neurotrophic factor overexpression induces precocious critical period in mouse visual cortex. J Neurosci *19*, RC40.

Hyman, B.T., and Yuan, J. (2012). Apoptotic and non-apoptotic roles of caspases in neuronal physiology and pathophysiology. Nat Rev Neurosci *13*, 395-406.

Jiang, Y.H., Armstrong, D., Albrecht, U., Atkins, C.M., Noebels, J.L., Eichele, G., Sweatt, J.D., and Beaudet, A.L. (1998). Mutation of the Angelman ubiquitin ligase in mice causes increased cytoplasmic p53 and deficits of contextual learning and long-term potentiation. Neuron *21*, 799-811.

Jiao, S., and Li, Z. (2011). Nonapoptotic function of BAD and BAX in long-term depression of synaptic transmission. Neuron *70*, 758-772.

Jonas, E.A., Porter, G.A., and Alavian, K.N. (2014). Bcl-xL in neuroprotection and plasticity. Front Physiol *5*, 355.

Joseph, R.M. (2014). Neuronatin gene: Imprinted and misfolded: Studies in Lafora disease, diabetes and cancer may implicate NNAT-aggregates as a common downstream participant in neuronal loss. Genomics *103*, 183-188.

Kumar, S.S., Bacci, A., Kharazia, V., and Huguenard, J.R. (2002). A developmental switch of AMPA receptor subunits in neocortical pyramidal neurons. J Neurosci *22*, 3005-3015.

Lattin, J.E., Schroder, K., Su, A.I., Walker, J.R., Zhang, J., Wiltshire, T., Saijo, K., Glass, C.K., Hume, D.A., Kellie, S.*, et al.* (2008). Expression analysis of G Protein-Coupled Receptors in mouse macrophages. Immunome Res *4*, 5.

Le Roux, N., Cabezas, C., Bohm, U.L., and Poncer, J.C. (2013). Input-specific learning rules at excitatory synapses onto hippocampal parvalbumin-expressing interneurons. J Physiol *591*, 1809-1822.

Li, H., Chen, Y., Jones, A.F., Sanger, R.H., Collis, L.P., Flannery, R., McNay, E.C., Yu, T., Schwarzenbacher, R., Bossy, B.*, et al.* (2008). Bcl-xL induces Drp1-dependent synapse formation in cultured hippocampal neurons. Proc Natl Acad Sci U S A *105*, 2169-2174.

Li, Z., Jo, J., Jia, J.M., Lo, S.C., Whitcomb, D.J., Jiao, S., Cho, K., and Sheng, M. (2010). Caspase-3 activation via mitochondria is required for long-term depression and AMPA receptor internalization. Cell *141*, 859-871.

Lichvarova, L., Henzi, T., Safiulina, D., Kaasik, A., and Schwaller, B. (2018). Parvalbumin alters mitochondrial dynamics and affects cell morphology. Cell Mol Life Sci *75*, 4643-4666.

Lo, S.C., Wang, Y., Weber, M., Larson, J.L., Scearce-Levie, K., and Sheng, M. (2015). Caspase-3 deficiency results in disrupted synaptic homeostasis and impaired attention control. J Neurosci *35*, 2118-2132.

Moffitt, J.R., Hao, J., Wang, G., Chen, K.H., Babcock, H.P., and Zhuang, X. (2016). High-throughput single-cell gene-expression profiling with multiplexed error-robust fluorescence in situ hybridization. Proc Natl Acad Sci U S A *113*, 11046-11051.

Nakamura, A., Swahari, V., Plestant, C., Smith, I., McCoy, E., Smith, S., Moy, S.S., Anton, E.S., and Deshmukh, M. (2016). Bcl-xL Is Essential for the Survival and Function of Differentiated Neurons in the Cortex That Control Complex Behaviors. J Neurosci *36*, 5448-5461.

Oyang, E.L., Davidson, B.C., Lee, W., and Poon, M.M. (2011). Functional characterization of the dendritically localized mRNA neuronatin in hippocampal neurons. PLoS One *6*, e24879.

Perez, J.D., Rubinstein, N.D., Fernandez, D.E., Santoro, S.W., Needleman, L.A., Ho-Shing, O., Choi, J.J., Zirlinger, M., Chen, S.-K., Liu, J.S.*, et al.* (2015). Quantitative and functional interrogation of parent-of-origin allelic expression biases in the brain. eLife *4*, e07860.

Raj, A., van den Bogaard, P., Rifkin, S.A., van Oudenaarden, A., and Tyagi, S. (2008). Imaging individual mRNA molecules using multiple singly labeled probes. Nat Methods *5*, 877-879.

Reichardt, H.M., Kellendonk, C., Tronche, F., and Schutz, G. (1999). The Cre/loxP system--a versatile tool to study glucocorticoid signalling in mice. Biochem Soc Trans *27*, 78-83.

Rucker, E.B., 3rd, Dierisseau, P., Wagner, K.U., Garrett, L., Wynshaw-Boris, A., Flaws, J.A., and Hennighausen, L. (2000). Bcl-x and Bax regulate mouse primordial germ cell survival and apoptosis during embryogenesis. Mol Endocrinol *14*, 1038-1052.

Sancho, L., and Bloodgood, B.L. (2018). Functional Distinctions between Spine and Dendritic Synapses Made onto Parvalbumin-Positive Interneurons in Mouse Cortex. Cell Rep *24*, 2075-2087.

Sato, M., and Stryker, M.P. (2010). Genomic imprinting of experience-dependent cortical plasticity by the ubiquitin ligase gene Ube3a. Proc Natl Acad Sci U S A *107*, 5611-5616.

Schafer, D.P., Lehrman, E.K., Kautzman, A.G., Koyama, R., Mardinly, A.R., Yamasaki, R., Ransohoff, R.M., Greenberg, M.E., Barres, B.A., and Stevens, B. (2012). Microglia sculpt postnatal neural circuits in an activity and complement-dependent manner. Neuron *74*, 691-705.

Sugiyama, S., Di Nardo, A.A., Aizawa, S., Matsuo, I., Volovitch, M., Prochiantz, A., and Hensch, T.K. (2008). Experience-dependent transfer of Otx2 homeoprotein into the visual cortex activates postnatal plasticity. Cell *134*, 508-520.

Takesian, A.E., and Hensch, T.K. (2013). Balancing plasticity/stability across brain development. Prog Brain Res *207*, 3-34.

Tan, M.C., Widagdo, J., Chau, Y.Q., Zhu, T., Wong, J.J., Cheung, A., and Anggono, V. (2017). The Activity-Induced Long Non-Coding RNA Meg3 Modulates AMPA Receptor Surface Expression in Primary Cortical Neurons. Front Cell Neurosci *11*, 124.

Tronche, F., Kellendonk, C., Kretz, O., Gass, P., Anlag, K., Orban, P.C., Bock, R., Klein, R., and Schutz, G. (1999). Disruption of the glucocorticoid receptor gene in the nervous system results in reduced anxiety. Nat Genet *23*, 99-103.

Valente, T., Dominguez, M.I., Bellmann, A., Journot, L., Ferrer, I., and Auladell, C. (2004). Zac1 is up-regulated in neural cells of the limbic system of mouse brain following seizures that provoke strong cell activation. Neuroscience *128*, 323-336.

Wallace, M.L., Burette, A.C., Weinberg, R.J., and Philpot, B.D. (2012). Maternal loss of Ube3a produces an excitatory/inhibitory imbalance through neuron type-specific synaptic defects. Neuron *74*, 793-800.

Wilkinson, L.S., Davies, W., and Isles, A.R. (2007). Genomic imprinting effects on brain development and function. Nat Rev Neurosci *8*, 832-843.

Yashiro, K., Riday, T.T., Condon, K.H., Roberts, A.C., Bernardo, D.R., Prakash, R., Weinberg, R.J., Ehlers, M.D., and Philpot, B.D. (2009). Ube3a is required for experience-dependent maturation of the neocortex. Nat Neurosci *12*, 777-783.

Chapter IV. Transcriptional analysis of the *Bcl-x* imprinted gene cluster

Introduction

Clustering of imprinted genes is regarded as a hallmark of their genomic organization, and thought to reflect mechanisms of common imprinted regulation acting on multiple genes (Reik and Walter, 2001). In their study of genome-wide allelic biases in expression within the adult mouse brain (Perez et al., 2015), Perez and Rubinstein found that a majority of genes exhibiting parental biases in expression are located in gene clusters and within one megabase of imprinted genes that exhibit strongly-biased (near monoallelic) expression. Imprinted clusters often comprise both maternally and paternally biased genes (or gene isoforms) (Andergassen et al., 2017; Gregg et al., 2010; Perez et al., 2015), with *cis*-regulatory effects (Crowley et al., 2015), suggesting that imprinted genes within a cluster are likely regulated by shared canonical imprinting mechanisms. These imprinted mechanisms would be applied within a cluster onto strongly-biased genes, then indirectly affect allelic expression of adjacent genes. An alternative possibility is that more moderately-biased expression, like the 60% paternal bias in *Bcl-x*$_L$ expression, could be established by more direct mechanisms targeted specifically to the biased gene, independent of the adjacent imprinted genes (Perez et al., 2015). These two possibilities have different implications for the cell-type specificity, coordinated regulation, and functional relevance of parentally-biased expression.

Common mechanisms of imprinted regulation are now well established for strongly-biased imprinted genes (Bartolomei and Ferguson-Smith, 2011). DNA is

methylated at CpG dinucleotides on either the maternally- or paternally- inherited chromosomes during gametogenesis by de novo methyltransferases, establishing differentially methylated regions (DMRs) that mark (imprint) the parental alleles for differential expression after fertilization. DMRs are imprinted control regions maintained postnatally in a tissue-specific manner by the methyltransferase Dnmt1 (Bartolomei and Ferguson-Smith, 2011; Reik and Walter, 2001), applying long-range imprinted regulation that can extend parent-of-origin-specific effects to neighboring genes (Bartolomei and Ferguson-Smith, 2011; Crowley et al., 2015). In the genome, *Bcl-x* is located on mouse chromosome 2 as part of an imprinted cluster that contains the gene *H13* (**Figure 4.1**). *H13* encodes an aspartic protease, responsible for dislocating signal peptidases from the endoplasmic reticulum (Weihofen et al., 2002). Within the fourth intron of *H13* is the gene *Mcts2*, a pseudogene that originated from retrotransposition of *Mcts1* located on the X chromosome. The promoter of *Mcts2* contains the primary DMR within the cluster, differentially methylated on the maternal allele (Wood et al., 2007). Methylation of the maternal allele causes strictly paternal expression of *Mcts2*, and of a short non-enzymatic isoform of *H13* ($H13_S$). The long isoform of *H13* ($H13_L$, the predominant isoform expressed in the brain), which encodes the functional protease, is derived strictly from the maternal allele (Wood et al., 2008). Thus, the DMR in *Mcts2* establishes the imprinted control region neighboring *Bcl-x*. The cell-type specific imprinted effects that we observe for $Bcl\text{-}x_L$ in the visual cortex, could therefore arise from cell-type specific regulation of the entire imprinted cluster.

If both $H13_L$ and $Bcl\text{-}x_L$ exhibited imprinted expression through shared imprinted regulation in all of the same cell populations, one potential outcome is that the maternal

bias of *H13*$_L$ would be similar magnitude in to the paternal bias of *Bcl-x*$_L$. However, in adult mouse cortical tissue, we observed stronger maternal bias of *H13*$_L$ expression than the paternal bias of *Bcl-x*$_L$ expression (**Figure 4.1**). For most parentally-biased genes recently identified by RNA sequencing, the strength of the parental bias exhibited by a gene decays as a function of the distance from the imprinted control region of the cluster

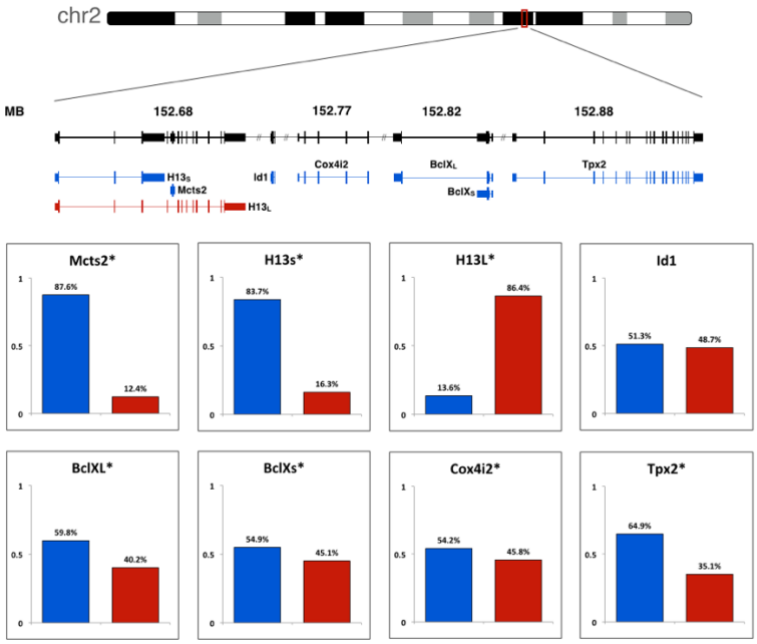

Figure 4.1: *Bcl-x* imprinted cluster.

Schematic of imprinted cluster on mouse chromosome 2, containing maternally-biased *H13*$_L$, paternally-biased *Cox4i2*, paternally-biased *Bcl-x*$_L$ and paternally-biased *Tpx2*. Bar graphs show the strength of the parental bias for each gene, measured by RNA sequencing of the adult C57xCAST mouse cortex. Courtesy of Julio Perez.

(Perez et al., 2015). In the *Bcl-x* imprinted cluster, this could reflect the fact that either the shared mechanisms of imprinted regulation within a cell type weaken with distance from the DMR. Or alternatively, the imprinted regulation of *Bcl-x* may be independent from that of *H13L*, and potentially specific to different cell populations than *H13L*. This issue highlights the observation that higher resolution cellular analyses are necessary to uncover how parent-of-origin-specific expression is maintained and coordinated within specific gene clusters.

Our cellular analyses of *Bcl-xL* in mutant mice carrying neural specific uniparental deletion indicate that the paternal bias in *Bcl-xL* expression is critical to the control of apoptosis and of synaptic plasticity in the juvenile visual cortex. Interestingly, we have found that parental *Bcl-xL* allelic expression displays a striking cell type specificity, with monoallelic paternal expression demonstrated in a subset of Satb2+ neurons, and biallelic or biased expression in other examined cell types. We were therefore interested in assessing whether the allelic regulation of *Bcl-xL* expression affects the entire *Bcl-x* imprinted cluster in Satb2+ neurons. Moreover, we sought to confirm the cell-type specificity of *Bcl-xL* allelic regulation in a non-deletion mouse background. In order to do this, we quantified the frequency of monoallelic expression of the prominent genes within the *Bcl-xL* cluster, and compared the frequencies in Satb2+ pyramidal neurons to Iba1+ microglia. Here, we used intronic smFISH in the V1 tissue of C57Bl/6J×Cast/EiJ hybrid mice to visualize active transcription sites of *Bcl-xL* and of the adjacent parentally-biased genes.

Results

To characterize the dynamics of transcription within the *Bcl-x* cluster, we designed smFISH intronic probes to target the 5' introns of the genes *H13*$_L$, *Cox4i2*, *Bcl-x*$_L$ and *Tpx2* in V1 tissue of C57Bl×Cast F1 mice (**Figure 4.2**). (We did not design intronic probes for the fifth gene in the cluster, *Id1*, because its sequence is too short to host a sufficient number of probes.) Using these intronic probes, we quantified the frequency of observing one transcription site as a readout of monoallelic expression for a given gene of the cluster in Satb2+ and Iba1+ cells (Bonthuis et al., 2015; Ginart et al., 2016). We compared these data to transcription site frequencies obtained with a control biallelic gene (*Syn2*), and with a distinct cell type-specific imprinted gene, *Ube3a,* located in a separate imprinted cluster. We reasoned that if *Bcl-x*$_L$ exhibits monoallelic paternal expression specifically in Satb2+ neurons, there should be a quantitative difference in the frequency of one active transcription site compared to Iba1+ cells in which *Bcl-x*$_L$ expression is biallelic. We also hypothesized that if the imprinted regulation of the entire *Bcl-x* imprinted cluster is cell-type specific, most or all of the genes within the cluster should display a single transcription site in Satb2+ neurons.

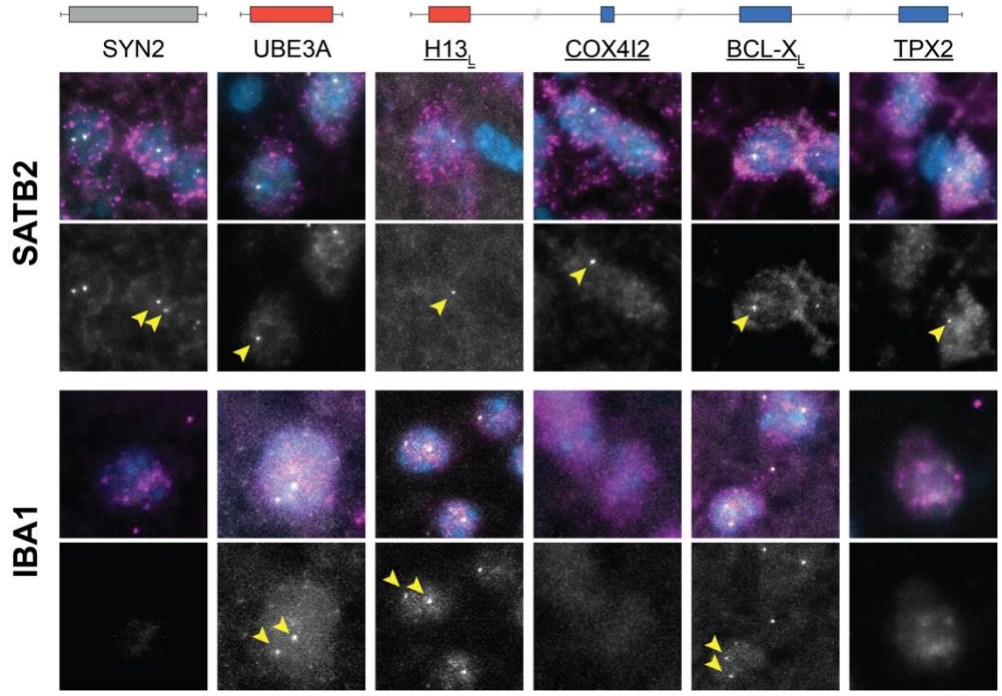

Figure 4.2: Active transcription sites in Satb2+ and Iba1+ cells.

Schematic reflects the genes targeted for transcription site activity, red genes indicate overall maternal bias in expression, blue genes indicate overall paternal bias. Overlaid images show Satb2-/Iba1-positive cells in the P16 V1 cortex, Satb2/Iba1 smFISH signal is magenta, DAPI (blue) marks the nucleus, and transcription sites targeted with intronic probes are white. Below the overlay is the intronic signal only, for each gene. Yellow arrows point to transcription sites detected within a nucleus.

We first assessed for each gene of the *Bcl-x* imprinted cluster and for control genes what fraction of cells imaged exhibited at least one site of transcription, indicating active expression in the cell (versus no active transcription). We compared the fraction of cells exhibiting at least one active transcription site at ages P8 and at P16 (**Figure 4.3**), because

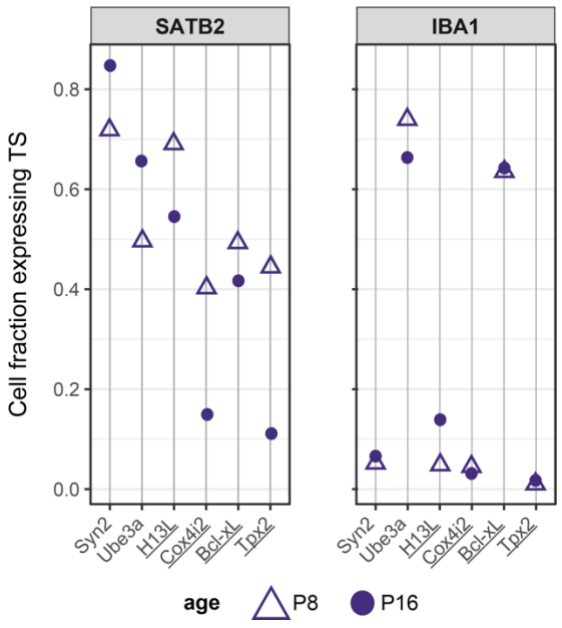

Figure 4.3: Frequency of exhibiting at least one transcription site according to cell type. Data points reflect the proportion of cells (n ~= 500, per gene per age) that exhibited either one or two transcription sites, indicating active transcription.

these ages mark two distinct and critical stages in the development of the primary visual cortex (Espinosa and Stryker, 2012). Our results show active transcription of *Ube3a* and *Syn2* in both Iba1+ and Satb2+ cells. Because *Syn2* encodes a neuron-specific phosphoprotein, we observed more frequent active transcription of *Syn2* in Satb2+ neurons; although microglia have been reported to express *Syn2* at low levels, as well (Solga et al., 2015). We found that Satb2+ neurons exhibit at least one active transcription site for all genes within the *Bcl-x* cluster, and the frequency of active transcription decreases between P8 and P16. In contrast, Iba1+ cells rarely exhibit any active

transcription of *H13L*, *Cox4i2*, or *Tpx2*. Frequency of *Bcl-xL* active transcription does not increase in Iba1+ cells between the two ages. We then assessed the number of cells exhibiting exactly one transcription site, as a fraction of the number of cells that exhibited active transcription (**Figure 4.4** left panel). By comparing the two cell types, we found that for all genes except *Cox4i2* and *Tpx2*, the fraction of cells exhibiting one transcription site was significantly different ($p<0.05$) between Satb2+ and Iba1+ cells, at both ages. In Satb2+ neurons, the frequency of one transcription site was notably high for *Ube3a*, and all genes in the *Bcl-x* cluster. By comparing the two ages, we found in Satb2+ neurons that the fraction of cells exhibiting one transcription site increased significantly between P8 and P16 for *H13L* ($p= 0.000978$), *Bcl-xL* ($p=0.00208$), and *Cox4i2* ($p=0.0133$), while the difference between ages for *Tpx2* was not significant ($p=0.0714$). In Iba1+ cells, only *Bcl-xL* showed a significant difference ($p=0.0259$) in the frequency of one transcription site between ages.

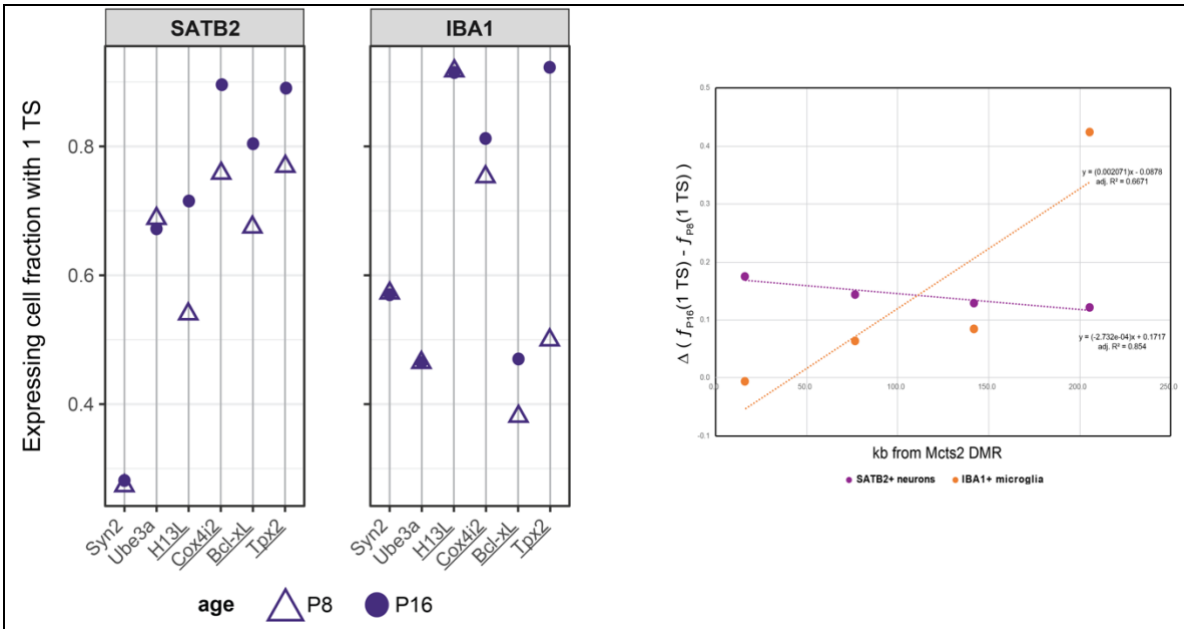

Figure 4.4: Cell type-specific frequency of exhibiting only one active transcription site.

Left panel: Data points reflect the proportion of cells (n ~= 500, per gene per age) observed that showed exactly 1 site of transcription, relative to the total number of cells that exhibited at least 1 site of transcription. *Right panel*: Linear regression analysis of the change in fraction of expression cells exhibiting exactly 1 transcription site, for each cell type. Data points reflect the delta (fraction of expressing cells with 1 TS at P16, minus the fraction at P8) for four genes in the *Bcl-x* imprinted cluster analyzed (from left to right $H13_L$, *Cox4i2*, $Bcl\text{-}x_L$, *Tpx2*; see diagram of genomic positions in Figure 4.1), with respect to their distance from the DMR in *Mcts2*.

Interestingly, for genes within the *Bcl-x* cluster, the change in frequency of 1 transcription site between ages P8 and P16 were similar (mean Δ= 0.142 ± 0.020) for Satb2+ neurons, but varied more widely for Iba1+ cells (mean Δ= 0.141 ± 0.167) (**Figure 4.4**). These results suggest that in Satb2+ (but not Iba1+) cells, the frequency of

monoallelic transcription varies together over developmental ages for all the genes within the imprinted cluster. This would imply that genes within the *Bcl-x* cluster are subject to shared imprinted regulation in Satb2+ neurons, but in Iba1+ cells there is more biallelic expression and no shared imprinted regulation within the cluster.

We plotted the change in monoallelic fraction for each gene in the *Bcl-x* cluster (*i.e.* the difference between P8 and P16 in the fraction of cells that exhibited one site of transcription) as a function of the gene's distance from the *Mcts2* DMR. We then performed a linear regression to assess for each cell type whether the distance from the imprinted control region is a significant predictor of the genes' allelic frequency patterns (**Figure 4.4** right panel). We reasoned that in a cell type in which the *Bcl-x* cluster is imprinted, the change in the monoallelic fraction would decrease for genes farther away from the imprinted control region, due to weakening of shared imprinted regulation. In a cell type in which the cluster is not imprinted, change in the monoallelic fraction for a gene would be irrespective of the distance from an imprinted control region. We found from this analysis that in Satb2+ cells, the change in monoallelic fraction was negatively correlated with distance from *Mcts2*. This indicates that the increase in active monoallelic transcription observed in Satb2+ cells between P8 and P16 does weaken for genes farther away from the DMR. The *p*-value of the linear regression was significant (p=0.04990), indicating that the gene's distance from the DMR. is a significant predictor of how frequently we observe monoallelic transcription within the *Bcl-x* cluster. Conversely, in Iba1+ cells, the genes' distance from the DMR was not a significant predictor of the observed monoallelic frequencies.

Our results show that monoallelic transcription for genes in the *Bcl*-x cluster is more frequently observed in Satb2+ cells than Iba1+ cells. These data correlated well with the smFISH analysis of *Bcl-x*$_L$ expression in the V1 of uniparental *Bcl-x* deletions. They furthermore suggest that with age, the frequency of monoallelic transcription of genes within the *Bcl-x* cluster varies together. The linear regression analysis shows that in Satb2+ but not Iba1+ cells, distance from the imprinted control region governs, at least in part, the frequency of expression from a single allele. Lastly, these results suggest that the gene located farthest away from the DMR, *Tpx2*, is less coordinated in its allelic transcriptional activity than genes located closer to *Mcts2*. Taken together, these data support the idea that in Satb2+ neurons the entire Bcl-x imprinted cluster is regulated in its allelic expression by shared imprinted mechanisms at the DMR in *Mcts2*.

Finally, we wondered whether *H13*$_L$ and *Bcl-x*$_L$ are transcriptionally active at the same time in Satb2+ cells, or whether their expression might be exclusive to separate subsets of Satb2+ cells. We found that at both P8 and P16, *Bcl-x*$_L$ and *H13*$_L$ showed active transcription at the same time in a large proportion of cells (**Figure 4.5**), further supporting the idea that transcriptional regulation allowing active transcription at the center of the imprinted cluster often corresponds with active transcription of *Bcl-x*$_L$.

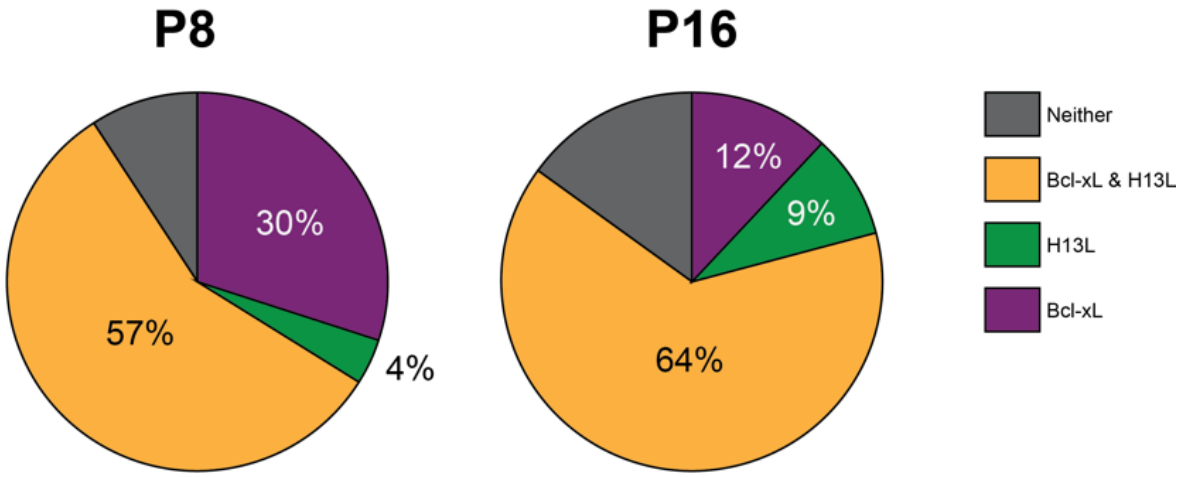

Figure 4.5: Co-expression of *Bcl-x$_L$* and *H13$_L$* in Satb2+ neurons.

Percentages of Satb2+ cells in P8 and P16 V1 cortex exhibiting expression of either *Bcl-x$_L$* only, *H13$_L$* only, and both genes (n = 1000 cells per age).

Discussion

In this chapter, we aimed to see whether monoallelic expression in Satb2+ neurons was specific to *Bcl-x*$_L$, or coordinated with adjacent genes in the imprinted cluster. By using intronic probes to detect active transcription sites, we found that *Bcl-x*$_L$ shows a high frequency of monoallelic transcription in Satb2+ neurons, and not in Iba1+ microglia. Our data on *Bcl-x*$_L$ monoallelic transcription corroborate our findings in the Bcl-x uniparental deletions, that only one allele contributes to *Bcl-x*$_L$ expression in Satb2+ cells. We also found that in Satb2+ neurons the frequency of monoallelic transcription is similarly high for other genes within the *Bcl-x* cluster. The frequency of monoallelic transcription varies significantly in a coordinated fashion, even over short but critical developmental ages. Both *H13*$_L$ and *Bcl-x*$_L$ are transcriptionally active at the same time in a majority of Satb2+ neurons, which taken together strongly suggests that the entire imprinted cluster containing *Bcl-x*$_L$ share the same imprinted mechanisms of transcriptional activation and repression. This coordinated transcriptional activity is specific to the Satb2+ neuronal subset, and not seen in Iba1+ microglia. Microglia exhibit higher frequencies of biallelic expression for both cell-type specific imprinted genes, *Ube3a* and *Bcl-x*$_L$, supporting the notion that imprinting is a more common mechanism to regulate expression in neuronal cells than non-neuronal cells. Other genes within the *Bcl-x* imprinted cluster rarely exhibited any active transcription in Iba1+ cells, suggesting that the transcriptional activity of these genes may simply be less critical for microglial cell function than Satb2+ neuronal function.

These findings uncover a remarkable cell type specificity in the transcriptional activity of parentally-biased genes, and demonstrate how allele-specific transcriptional activity can change dynamically between postnatal ages. It is important to note that this

analysis of active transcription sites does not distinguish between the maternal and paternal alleles, so it is possible that in some proportion of Satb2+ cells the active transcription site reflects expression from the maternal allele instead of the paternal allele. Future analysis of *Bcl-x*$_L$ transcriptional activity could utilize allele-specific intronic probes to distinguish the maternal and paternal transcription sites, and thus further corroborate that *Bcl-x*$_L$ and potentially other genes within the *Bcl-x* cluster are imprinted in a cell-type specific manner. Future studies could also investigate the cell-type specific mechanisms of imprinted regulation on the *Bcl-x* imprinted cluster, including cell-type specific differential DNA methylation and histone modifications.

Materials and Methods

Mice

F1 hybrids were generated by reciprocally crossing C57Bl/6J and Cast/EiJ mouse strains. For transcription site analysis, we used 16 male mice, covering both crosses and two age groups: animals sacrificed at postnatal day 8 (P8) and animals sacrificed at postnatal day 16 (P16). Immediately after sacrifice, brains were harvested, and immediately frozen embedded in OCT (VWR, Franklin MA), and stored at −80˚C.

Intronic single molecule FISH

10-µm coronal sections of brains were prepared using a Microm HM550 cryostat (Thermo Fisher, Missouri) set to −20 to −18˚C, and mounted on slides. Sections included the V1b primary visual cortex, corresponding to Figures 56–59 in (Franklin and Paxinos, 2007). Mounted sections were fixed in PFA (4% in PBS; 10 min, RT), washed in PBS (2 × 5 min, RT), permeabilized overnight in 70% EtOH at 4˚C, and stored in 70% EtOH until hybridization.

Probes for *Syn2*, *Ube3a*, *Bcl-x*$_L$, *H13*$_L$, *Cox4i2* and *Tpx2* were generated from the GRCm38/mm10 genomic sequence (https://genome.ucsc.edu/) for the most 5' intron of the given gene isoform, as described in (Levesque et al., 2013), using the Stellaris Probe Designer software. An encoding tail sequence was added to generate probe sequences, and a separate readout probe conjugated with Alexa 647 dye, was used for detected as described in (Moffitt et al., 2016). Intronic probe sequences are listed in **Appendix 2**.

Overnight hybridization was performed as described in Raj et al (Raj and Tyagi, 2010; Raj et al., 2008), with some modifications: cryosections were fixed in 4% paraformaldehyde for 15 minutes, incubated in 2% SDS (1x PBS) for 30 minutes and washed twice in wash buffer (10% formamide, 2X saline-sodium citrate) before hybridization. Sections were washed three times in wash buffer, stained with DAPI (5 ng/μl), then hybridized at room temperature with readout probes for 30 min. Sections were then washed in 30% formamide and 2x SSC, and mounted in glucose oxidase buffer (0.4% glucose, 10 mM Tris, 2X SSC with glucose oxidase and catalase).

Images were acquired using a Zeiss (Germany) LSM-700 confocal microscope with widefield illumination, equipped with a 63x Plan Apo objective, and a Hamamatsu C9100-14 cooled charge-coupled device camera. Cells were imaged in serial Z-stacks spaced by 0.30 μm. Images were segmented and spots were fitted using custom Python software, as developed for MERFISH (Moffitt et al., 2016). To detect active transcription sites, fitted size of spots was increased two-fold and the intensity threshold increased by four-fold, relative to the spot fitting for spots targeted with exonic probes for mature mRNA. Satb2-positive cells were defined as cells containing minimum 15 transcript spots per cell, based on the overall distribution of expression. Iba1-positive cells were defined as cells containing minimum 8 spots per cell, based on the overall distribution of expression. No difference was noted in transcription site frequency between the two F1 crosses, so numbers were combined.

Transcription site analysis

Frequencies of one active transcription site were calculated for each gene by dividing the number of cells exhibiting one site of transcription by the number of cells exhibiting one or two sites of transcription. Frequencies were compared between ages and between cell types using a two-tailed proportion test.

This work described here is part of a manuscript in preparation.

References

Andergassen, D., Dotter, C.P., Wenzel, D., Sigl, V., Bammer, P.C., Muckenhuber, M., Mayer, D., Kulinski, T.M., Theussl, H.-C., Penninger, J.M., *et al.* (2017). Mapping the mouse Allelome reveals tissue-specific regulation of allelic expression. eLife *6*, e25125.

Bartolomei, M.S., and Ferguson-Smith, A.C. (2011). Mammalian genomic imprinting. Cold Spring Harb Perspect Biol *3*.

Bonthuis, Paul J., Huang, W.-C., Hörndli, Cornelia N., Ferris, E., Cheng, T., and Gregg, C. (2015). Noncanonical Genomic Imprinting Effects in Offspring. Cell Reports *12*, 979-991.

Crowley, J.J., Zhabotynsky, V., Sun, W., Huang, S., Pakatci, I.K., Kim, Y., Wang, J.R., Morgan, A.P., Calaway, J.D., Aylor, D.L., *et al.* (2015). Analyses of allele-specific gene expression in highly divergent mouse crosses identifies pervasive allelic imbalance. Nature Genetics *47*, ng.3222.

Espinosa, J.S., and Stryker, M.P. (2012). Development and plasticity of the primary visual cortex. Neuron *75*, 230-249.

Franklin K.B.J., and Paxinos, G. (2007). The mouse brain in stereotaxic coordinates, third edition (New York: Elsevier).

Ginart, P., Kalish, J.M., Jiang, C.L., Yu, A.C., Bartolomei, M.S., and Raj, A. (2016). Visualizing allele-specific expression in single cells reveals epigenetic mosaicism in an H19 loss-of-imprinting mutant. Genes Dev *30*, 567-578.

Gregg, C., Zhang, J., Weissbourd, B., Luo, S., Schroth, G.P., Haig, D., and Dulac, C. (2010). High-resolution analysis of parent-of-origin allelic expression in the mouse brain. Science *329*, 643-648.

Levesque, M.J., Ginart, P., Wei, Y., and Raj, A. (2013). Visualizing SNVs to quantify allele-specific expression in single cells. Nat Methods *10*, 865-867.

Moffitt, J.R., Hao, J., Wang, G., Chen, K.H., Babcock, H.P., and Zhuang, X. (2016). High-throughput single-cell gene-expression profiling with multiplexed error-robust fluorescence in situ hybridization. Proc Natl Acad Sci U S A *113*, 11046-11051.

Perez, J.D., Rubinstein, N.D., Fernandez, D.E., Santoro, S.W., Needleman, L.A., Ho-Shing, O., Choi, J.J., Zirlinger, M., Chen, S.-K., Liu, J.S., *et al.* (2015). Quantitative and functional interrogation of parent-of-origin allelic expression biases in the brain. eLife *4*, e07860.

Raj, A., and Tyagi, S. (2010). Detection of individual endogenous RNA transcripts in situ using multiple singly labeled probes. Methods Enzymol *472*, 365-386.
Raj, A., van den Bogaard, P., Rifkin, S.A., van Oudenaarden, A., and Tyagi, S. (2008). Imaging individual mRNA molecules using multiple singly labeled probes. Nat Methods *5*, 877-879.

Reik, W., and Walter, J. (2001). Genomic imprinting: parental influence on the genome. Nat Rev Genet *2*, 21-32.

Solga, A.C., Pong, W.W., Walker, J., Wylie, T., Magrini, V., Apicelli, A.J., Griffith, M., Griffith, O.L., Kohsaka, S., Wu, G.F*., et al.* (2015). RNA-sequencing reveals oligodendrocyte and neuronal transcripts in microglia relevant to central nervous system disease. Glia *63*, 531-548.

Weihofen, A., Binns, K., Lemberg, M.K., Ashman, K., and Martoglio, B. (2002). Identification of signal peptide peptidase, a presenilin-type aspartic protease. Science *296*, 2215-2218.

Wood, A.J., Roberts, R.G., Monk, D., Moore, G.E., Schulz, R., and Oakey, R.J. (2007). A screen for retrotransposed imprinted genes reveals an association between X chromosome homology and maternal germ-line methylation. PLoS Genet *3*, e20.

Wood, A.J., Schulz, R., Woodfine, K., Koltowska, K., Beechey, C.V., Peters, J., Bourc'his, D., and Oakey, R.J. (2008). Regulation of alternative polyadenylation by genomic imprinting. Genes Dev *22*, 1141-1146.

Chapter V. Conclusion and future directions

This dissertation investigated the function and cell type-specificity of the parental allelic expression of *Bcl-x*$_L$ in the postnatal mouse brain. Previous RNA sequencing analysis of *Bcl-x*$_L$ allelic expression in brain and somatic tissues from C57Bl×Cast hybrids had revealed a modest paternal bias in *Bcl-x*$_L$ expression. A main goal of my PhD work was to assess *Bcl-x*$_L$ parental allelic expression at the single cell level. Using single molecule FISH in brain-specific uniparental deletions of *Bcl-x*, we were able to quantify *Bcl-x* expression from each parental allele in specific cortical cell types. These experiments revealed that a subset of Satb2+ pyramidal neurons in layer 2/3 of the visual cortex express only the paternal allele of *Bcl-x*$_L$, while other cell types appear to express *Bcl-x*$_L$ from both parental alleles. These findings demonstrate that a parental bias in gene expression detected at the tissue level may result from canonically imprinted monoallelic expression within a specific cell population. The full scope of *Bcl-x*$_L$ allelic expression patterns exhibited by different cell types is not yet clear, but it is possible that in addition to monoallelic and biallelic expression, cells in other subsets of neuronal populations exhibit a clear parental bias in *Bcl-x*$_L$ expression. Even within Satb2+ cells, we do see diversity in the pattern of allelic expression; although a significant fraction exhibited no *Bcl-x*$_L$ expression in the V1 of paternal *Bcl-x* deletion, in a majority of Satb2+ neurons the maternal allele also contributes to the expression level of *Bcl-x*. The overall 60% bias for paternal expression of *Bcl-x*$_L$ that we observe at the tissue level therefore results from a mixture of allelic expression patterns in various subsets of cells.

Our cell type-specific analyses of *Bcl-x*$_L$ in the cortex provide a new case study that demonstrates parentally-biased expression in the brain can be functionally relevant for the

survival, maturation and plasticity of neurons. Because epigenetic marks, including differential DNA methylation, must be actively maintained by the cell, one might expect that cell populations that maintain parent-of-origin specific monoallelic expression of *Bcl-x*$_L$ have a functionally relevant reason to tightly regulate its expression. The lack of *Bcl-x*$_L$ monoallelic expression in other neuronal cell types such as Pvalb+ and Ctip2+ neurons may reflect less stringent needs to regulate Bcl-xL dosage in the modulation of synaptic plasticity. If such cell type specificity of genomic imprinting accounts for the wide diversity of imprinted effects identified throughout the brain, one may be able to conclude that genomic imprinting of other parentally-biased genes provides a flexible mechanism to yield highly-regulated parental expression in some cell populations, and more variable biallelic expression in other cell populations. Beaudet and Jiang liken this proposed role for imprinted regulation to a rheostat (Beaudet and Jiang, 2002), allowing substantial, rapid and reversible changes in the level of gene expression, in an age- and cell type-specific manner.

In our approach, we have established single molecule FISH as an effective method to analyze gene expression of lowly- to moderately-expressed genes in single cells, within intact brain tissue. By taking this approach in our investigation of *Bcl-x*$_L$, we were able to further uncover nuances of its imprinted regulation in the cortex. Our methods of analysis therefore carry significant potential to elucidate the nature and cell type-specificity of the imprinted expression of other parentally-biased genes. Ideally, future experiments can rely less on the availability of conditional mutants to analyze parental expression, and instead investigate allelic expression in a diversity of F1 hybrid mouse strains. One attractive method for further study of parentally-biased expression is allele-specific single molecule FISH. To distinguish maternal and paternal transcripts, allele-specific FISH targets single nucleotide polymorphisms in cells from

hybrid crosses, and quantifies the colocalization of an allele-specific signal with a "guide probe" signal targeting the rest of the mRNA molecule. (Levesque et al., 2013) While this method has proven successful for investigating a highly-expressed imprinted gene in cell cultures and somatic tissues (Ginart et al., 2016), it showed very minimal success in our attempts to investigate parentally-biased genes in C57/Cast brain tissue, due to several confounding factors. While Raj and colleagues have reported that 10 oligos can be sufficient to detect a signal above background fluorescence, we and others have found that at least 15 oligos are needed to potentially detect a signal in brain tissue (Moffitt et al., 2016a; Moffitt et al., 2016b). Because allele-specific probes target just one nucleotide instead of roughly 20, the hybridization is far less efficient than the guide probe, so more than 15 probes are likely needed. Many parentally-biased genes validated in the brains of C57/Cast reciprocal crosses have fewer than 15 polymorphisms in their coding regions, including *Bcl-x*$_L$ which has only 5. And finally, most parentally-biased genes exhibit low to moderate expression levels, so the lower hybridization efficiency of allele-specific probes leaves a more significant fraction of the guide probe signals unassigned to either allele than if the gene is very highly expressed. An alternative approach going forward would be to perform allele-specific intronic FISH, which could distinguish maternal and paternal nascent RNAs in single cells (Bonthuis et al., 2015). This approach is more likely to be successful than targeting mature RNAs because there is a higher frequency of polymorphisms to target in intronic sequences, and the localization of nascent RNAs at active transcription sites affords a brighter detectable signal. Although this approach alone would not be directly quantifying total expression, experiments using allele-specific intronic FISH in combination with regular guide probes can provide information about the level of expression and parent-of-origin specific dynamics of transcription in individual neurons.

By examining active transcription sites, our data here also reveal cell type-specificity in the frequency of monoallelic expression for the *Bcl-x* imprinted cluster as a whole. In Satb2+ neurons we observed an increase in the frequency of monoallelic transcription of the cluster genes from P8 to P16, but a decrease in the fraction of cells expressing the clustered genes. In Perez et al. (2015), Perez and Rubinstein observe for parentally-biased genes expressed in the cerebellum that the overall strength of allelic bias and the overall expression level tend to decrease from P8 to P60. As P16 marks a critical period in the development of the primary visual cortex, and P8 marks a critical period in development of the cerebellum, it may be notable that we observe greater magnitudes of allelic bias at these stages, according to brain region. Our transcriptional analysis does not quantify the expression level of genes in the *Bcl-x* cluster, but does note a decrease from P8 to P16 in the frequency of Satb2+ cells exhibiting active transcription. Conversely, the analysis in Perez et al. notes that it is possible the enhanced expression and the parental bias observed in the P8 cerebellum originate from different cell populations in the cerebellum. Therefore, a deeper investigation of the dynamics of the imprinting at the *Bcl-x* cluster in the cortex should firstly distinguish the maternal and paternal transcription sites with allele-specific probes, to determine whether the monoallelic transcription is from the paternally-derived allele for *Bcl-x*$_L$. We can then assess the frequency of paternal *Bcl-x*$_L$ expression in Satb2+ cells at later stages up to P60, to determine whether the strength of paternal bias continues to increase into adulthood, and whether the fraction of cells expressing paternal *Bcl-x*$_L$ diminishes. Furthermore, we can perform this analysis of transcription sites while quantifying overall *Bcl-x*$_L$ expression with regular smFISH guide probes. This analysis would provide insights into both the cell type-specificity of longer-term patterns of *Bcl-x* imprinting, and provide insights into the correlation between allelic bias and expression level within a

defined cell type. Such an analysis could also of course be repeated to investigate other cell types, brain regions or other parentally-biased genes. Ctip2+ and Pvalb+ neurons could be valuable cell types to further investigate, in order to better understand at least the imprinted status of *Bcl-x*$_L$ for other neuronal subsets in the V1. Further analysis of *Bcl-x*$_L$ as well as *H13*$_L$ could provide some interesting data on how the strength and direction of parental biases within an imprinted cluster correlate over time.

A recent study (Hsu et al., 2018) examined experience-dependent plasticity in the visual system of C57/Cast mice, and assessed the allelic expression of parentally-biased genes in response to light experience. These authors used RNA sequencing to profile the expression of imprinted genes in the retina, suprachiasmatic nucleus (SCN) and visual cortex (V1) after rearing mice either in normal light conditions or complete dark until P28 (past the critical period for the visual system). Although some imprinted miRNAs primarily from the *Dlk-Dio3* imprinted cluster were up-regulated in the retina and visual cortex of dark-reared mice, most imprinted genes showed little or no visual system-specific changes in response to dark rearing. Interestingly, the authors did find that light experience altered in the SCN the allelic bias of the short isoform of *H13* (*H13*$_S$). In the SCN of dark-reared mice, the bias of *H13*$_S$ shifted from 70:30% paternal:maternal expression to 60:40%. Maternally-biased *H13*$_L$ isoforms were not affected in their allelic bias or expression level. As we have investigated here the role of paternal *Bcl-x*$_L$ in synaptic plasticity, it could be interesting to investigate changes in *Bcl-x*$_L$ and *H13* allelic expression in specific cell types of the visual cortex before and after dark rearing. This could elucidate further the functional role imprinting of the *Bcl-x* cluster has in experience-dependent plasticity.

While we show in this dissertation that parentally-biased expression of *Bcl-x*$_L$ does have a differential functional role in the V1 synaptic plasticity, it is not clear whether our findings fit with any existing theory of genomic imprinting. The evolutionary theory that has been most successful in explaining functional roles and the phylogenetic distribution of imprinted genes is the kinship theory (Haig, 2014; Wilkins and Haig, 2003). This theory proposes that imprinting reflects a conflict between the parental genomes over the allocation of maternal resources to offspring. Generally, maternally-expressed genes tend to reduce offspring demand for maternal resources while paternally-expressed genes tend to increase demand. Another primary theory (Keverne, 2013, 2014) proposes that imprinted genes act in a co-adaptive manner in the brain and placenta to optimize both fetal development and the mother's ability to nurture postnatally. While this and other hypotheses could explain a subset of imprinted genes, none have fully provided an interpretation of the complex brain functions in which we observe parent-of-origin-specific expression.

A critical direction moving forward is to investigate the mechanisms that establish and maintain the imprinted expression of *Bcl-x*$_L$ in Satb2+ neurons, and potentially in other neuronal subtypes. At the tissue level, Gregg and colleagues used chromatin immunoprecipitation of hypothalamic tissue to identify an enrichment of the repressive histone modification H3K9me3 on the *Bcl-x*$_L$ maternal allele (Bonthuis et al., 2015). A cell-type-specific analysis of differential DNA and histone modifications at loci of parentally-biased genes would provide some valuable insight into which neuronal subtypes in the brain frequently maintain imprinted regulation, and thereby potentially uncover further roles played by parentally-biased genes in critical neuronal functions.

This dissertation emphasizes apoptosis and synaptic plasticity as two significant neuronal functions affected by imprinted regulation. Further, other studies of imprinting have proposed that imprinted genes form vast regulatory networks that influence common cellular functions (Al Adhami et al., 2015; Lopez et al., 2017; Lui et al., 2008; Varrault et al., 2006). Future investigations therefore could also take more systems-level approaches to elucidate the wider imprinted gene network of *Bcl-x*$_L$, and thereby potentially improve our understanding of neural disorders. For example, the apoptotic pathway has been implicated in the pathology of Alzheimer's, Parkinson's and Huntington's diseases (D'Amelio et al., 2012), and Perez et al. has established that the apoptotic pathway is a frequent target of imprinted regulation. Further high-resolution investigations of imprinted genes are likely to elucidate more nuances of imprinted expression in neuronal circuits, which could open new avenues for targeted treatment of specific imprinted disorders like Angelman syndrome (Meng et al., 2015).

References

Al Adhami, H., Evano, B., Le Digarcher, A., Gueydan, C., Dubois, E., Parrinello, H., Dantec, C., Bouschet, T., Varrault, A., and Journot, L. (2015). A systems-level approach to parental genomic imprinting: the imprinted gene network includes extracellular matrix genes and regulates cell cycle exit and differentiation. Genome Res *25*, 353-367.

Beaudet, A.L., and Jiang, Y.H. (2002). A rheostat model for a rapid and reversible form of imprinting-dependent evolution. Am J Hum Genet *70*, 1389-1397.

Bonthuis, Paul J., Huang, W.-C., Hörndli, Cornelia N., Ferris, E., Cheng, T., and Gregg, C. (2015). Noncanonical Genomic Imprinting Effects in Offspring. Cell Reports *12*, 979-991.

D'Amelio, M., Sheng, M., and Cecconi, F. (2012). Caspase-3 in the central nervous system: beyond apoptosis. Trends Neurosci *35*, 700-709.

Ginart, P., Kalish, J.M., Jiang, C.L., Yu, A.C., Bartolomei, M.S., and Raj, A. (2016). Visualizing allele-specific expression in single cells reveals epigenetic mosaicism in an H19 loss-of-imprinting mutant. Genes Dev *30*, 567-578.

Haig, D. (2014). Coadaptation and conflict, misconception and muddle, in the evolution of genomic imprinting. Heredity (Edinb) *113*, 96-103.

Hsu, C.L., Chou, C.H., Huang, S.C., Lin, C.Y., Lin, M.Y., Tung, C.C., Lin, C.Y., Lai, I.P., Zou, Y.F., Youngson, N.A.*, et al.* (2018). Analysis of experience-regulated transcriptome and imprintome during critical periods of mouse visual system development reveals spatiotemporal dynamics. Hum Mol Genet *27*, 1039-1054.

Keverne, E.B. (2013). Importance of the matriline for genomic imprinting, brain development and behaviour. Philos Trans R Soc Lond B Biol Sci *368*, 20110327.

Keverne, E.B. (2014). Significance of epigenetics for understanding brain development, brain evolution and behaviour. Neuroscience *264*, 207-217.

Levesque, M.J., Ginart, P., Wei, Y., and Raj, A. (2013). Visualizing SNVs to quantify allele-specific expression in single cells. Nat Methods *10*, 865-867.

Lopez, S.J., Dunaway, K., Islam, M.S., Mordaunt, C., Vogel Ciernia, A., Meguro-Horike, M., Horike, S.I., Segal, D.J., and LaSalle, J.M. (2017). UBE3A-mediated regulation of imprinted genes and epigenome-wide marks in human neurons. Epigenetics *12*, 982-990.

Lui, J.C., Finkielstain, G.P., Barnes, K.M., and Baron, J. (2008). An imprinted gene network that controls mammalian somatic growth is down-regulated during postnatal growth deceleration in multiple organs. Am J Physiol Regul Integr Comp Physiol *295*, R189-196.

Meng, L., Ward, A.J., Chun, S., Bennett, C.F., Beaudet, A.L., and Rigo, F. (2015). Towards a therapy for Angelman syndrome by targeting a long non-coding RNA. Nature *518*, 409-412.

Moffitt, J.R., Hao, J., Bambah-Mukku, D., Lu, T., Dulac, C., and Zhuang, X. (2016a). High-performance multiplexed fluorescence in situ hybridization in culture and tissue with matrix imprinting and clearing. Proc Natl Acad Sci U S A *113*, 14456-14461.

Moffitt, J.R., Hao, J., Wang, G., Chen, K.H., Babcock, H.P., and Zhuang, X. (2016b). High-throughput single-cell gene-expression profiling with multiplexed error-robust fluorescence in situ hybridization. Proc Natl Acad Sci U S A *113*, 11046-11051.

Perez, J.D., Rubinstein, N.D., Fernandez, D.E., Santoro, S.W., Needleman, L.A., Ho-Shing, O., Choi, J.J., Zirlinger, M., Chen, S.-K., Liu, J.S.*, et al.* (2015). Quantitative and functional interrogation of parent-of-origin allelic expression biases in the brain. eLife *4*, e07860.

Varrault, A., Gueydan, C., Delalbre, A., Bellmann, A., Houssami, S., Aknin, C., Severac, D., Chotard, L., Kahli, M., Le Digarcher, A.*, et al.* (2006). Zac1 regulates an imprinted gene network critically involved in the control of embryonic growth. Dev Cell *11*, 711-722.

Wilkins, J.F., and Haig, D. (2003). What good is genomic imprinting: the function of parent-specific gene expression. Nat Rev Genet *4*, 359-368.

Table A1: Sequences for probes used in Chapters 2 & 3

Sequence	Sequence Name	Synthesis Scale	5' modification
cgcaacgcttgggacggttccaatcggatc	B1_Stv_1	100 nmol	Alexa 647

	Sequence	Sequence Name	Synthesis Scale	3' modification
Ago2 Probe	atctgttggtctgagtgtag	Ago2_exon_01	5 nmol	CAL Fluor Red 610
	ccaaagacgtctcatgttcg	Ago2_exon_02	5 nmol	CAL Fluor Red 610
	agtgagcagcttataggttt	Ago2_exon_03	5 nmol	CAL Fluor Red 610
	cactgagagaagtgcactct	Ago2_exon_04	5 nmol	CAL Fluor Red 610
	cttcagtgcatagatcctat	Ago2_exon_05	5 nmol	CAL Fluor Red 610
	cacacaagagaaggctcgtc	Ago2_exon_06	5 nmol	CAL Fluor Red 610
	aacagtttgagaaggtgcca	Ago2_exon_07	5 nmol	CAL Fluor Red 610
	tcactagtttaaccagttcc	Ago2_exon_08	5 nmol	CAL Fluor Red 610
	ttgcatgactaagatcccat	Ago2_exon_09	5 nmol	CAL Fluor Red 610
	ctaggtgtgagctctgatag	Ago2_exon_10	5 nmol	CAL Fluor Red 610
	tactttggcccatcagaaag	Ago2_exon_11	5 nmol	CAL Fluor Red 610
	tttggtctggggatacattt	Ago2_exon_12	5 nmol	CAL Fluor Red 610
	ctgcaccatcagacatgtaa	Ago2_exon_13	5 nmol	CAL Fluor Red 610
	aaagcaaggcacaccttact	Ago2_exon_14	5 nmol	CAL Fluor Red 610
	gatggatgtcatgatgggtt	Ago2_exon_15	5 nmol	CAL Fluor Red 610
	aaatctatggaatggggcct	Ago2_exon_16	5 nmol	CAL Fluor Red 610
	gggagttttgctagtatcac	Ago2_exon_17	5 nmol	CAL Fluor Red 610
	gggcttaaaacacgcagtga	Ago2_exon_18	5 nmol	CAL Fluor Red 610
	tttcagacttgatggggact	Ago2_exon_19	5 nmol	CAL Fluor Red 610
	ctgactagaagtacaggcgt	Ago2_exon_20	5 nmol	CAL Fluor Red 610
	aatctggagaaggcagagca	Ago2_exon_21	5 nmol	CAL Fluor Red 610
	ctctaccatatccatctatc	Ago2_exon_22	5 nmol	CAL Fluor Red 610
	cattagcaagcctgaaggta	Ago2_exon_23	5 nmol	CAL Fluor Red 610
	gggaggtcacagaaaggttg	Ago2_exon_24	5 nmol	CAL Fluor Red 610
	catgggtgtgagagatgagt	Ago2_exon_25	5 nmol	CAL Fluor Red 610
	ccaaggaagtgtagcttcta	Ago2_exon_26	5 nmol	CAL Fluor Red 610
	aacttacaggagtcggcatg	Ago2_exon_27	5 nmol	CAL Fluor Red 610
	tggggagttggacgcaataa	Ago2_exon_28	5 nmol	CAL Fluor Red 610
	aaatgtgtgttgggatggca	Ago2_exon_29	5 nmol	CAL Fluor Red 610
	atgctgtcctgtatagagag	Ago2_exon_30	5 nmol	CAL Fluor Red 610

	tctgttacattcaagccttc	Ago2_exon_31	5 nmol	CAL Fluor Red 610
	tgacaaaggccacacggaac	Ago2_exon_32	5 nmol	CAL Fluor Red 610
	aacactgactgggctattca	Ago2_exon_33	5 nmol	CAL Fluor Red 610
	ttgaggggctgaccaaagaa	Ago2_exon_34	5 nmol	CAL Fluor Red 610
	acagaccatgtacttaggtc	Ago2_exon_35	5 nmol	CAL Fluor Red 610
Bcl-x_L Probe	aaggcgacagaggaattgcg	Bclx_exon_01	5 nmol	CAL Fluor Red 610
	cttttgtatcataggtcggg	Bclx_exon_02	5 nmol	CAL Fluor Red 610 *
	attcaaatctatctccggcg	Bclx_exon_03	5 nmol	CAL Fluor Red 610
	ctgtgtttagcgattctctt	Bclx_exon_04	5 nmol	CAL Fluor Red 610 *
	ccaaaacacctgctcactta	Bclx_exon_05	5 nmol	CAL Fluor Red 610
	atagagatgggctcaaccag	Bclx_exon_06	5 nmol	CAL Fluor Red 610 *
	gagagaaagtcgaccaccag	Bclx_exon_07	5 nmol	CAL Fluor Red 610
	atcctttctgggaaagcttg	Bclx_exon_08	5 nmol	CAL Fluor Red 610 *
	tcactaaactgactccagct	Bclx_exon_09	5 nmol	CAL Fluor Red 610
	taccgcagttcaaactcatc	Bclx_exon_10	5 nmol	CAL Fluor Red 610 *
	ggttatgtgaagctgggatg	Bclx_exon_11	5 nmol	CAL Fluor Red 610
	ctgctcaaagctctgatacg	Bclx_exon_12	5 nmol	CAL Fluor Red 610 *
	tttactccatcccgaaagag	Bclx_exon_13	5 nmol	CAL Fluor Red 610
	cccgccaaaggagaaaaagg	Bclx_exon_14	5 nmol	CAL Fluor Red 610 *
	caacttgcaatccgactcac	Bclx_exon_15	5 nmol	CAL Fluor Red 610
	ctctaggtggtcattcagat	Bclx_exon_16	5 nmol	CAL Fluor Red 610 *
	tcccgtagagatccacaaaa	Bclx_exon_17	5 nmol	CAL Fluor Red 610
	tcacttccgactgaagagtg	Bclx_exon_18	5 nmol	CAL Fluor Red 610 *
	gaagagagagttgtggtggg	Bclx_exon_19	5 nmol	CAL Fluor Red 610
	tgagttgcatgtagtggttc	Bclx_exon_20	5 nmol	CAL Fluor Red 610 *
	aagctaattgcaggggactc	Bclx_exon_21	5 nmol	CAL Fluor Red 610
	agagaactgagatgtggggg	Bclx_exon_22	5 nmol	CAL Fluor Red 610 *
	ggagctggtttaggggaaaa	Bclx_exon_23	5 nmol	CAL Fluor Red 610
	agaggctcaggggtaattag	Bclx_exon_24	5 nmol	CAL Fluor Red 610 *
	aagggctaaaagcacctcac	Bclx_exon_25	5 nmol	CAL Fluor Red 610
	ctagcaaggtggactttcag	Bclx_exon_26	5 nmol	CAL Fluor Red 610 *
	tgaggcagctgaagtcatta	Bclx_exon_27	5 nmol	CAL Fluor Red 610
	aacacccaaggcaaagatgc	Bclx_exon_28	5 nmol	CAL Fluor Red 610 *
	aatatgtacagcagagagcc	Bclx_exon_29	5 nmol	CAL Fluor Red 610
	tactgaactgcactttcacc	Bclx_exon_30	5 nmol	CAL Fluor Red 610 *
	tcaggaaccagcggttgaag	Bclx_exon_31	5 nmol	CAL Fluor Red 610
	gaggtgagaggtgagtggac	Bclx_exon_32	5 nmol	CAL Fluor Red 610 *

Ctip2 Probe	aatgtagctggaaggctcat	Ctip2_B1_01	25 nmol	gatccgattggaaccgtccc
	agaactcacaggacttgctc	Ctip2_B1_02	25 nmol	gatccgattggaaccgtccc
	tgctctggaacttgaaggtc	Ctip2_B1_03	25 nmol	gatccgattggaaccgtccc
	tacacgttctcagatgggat	Ctip2_B1_04	25 nmol	gatccgattggaaccgtccc
	gaatgggtccttcatgaagt	Ctip2_B1_05	25 nmol	gatccgattggaaccgtccc
	aggaatgttccgacgatgtg	Ctip2_B1_06	25 nmol	gatccgattggaaccgtccc
	catgccacttttcatttcag	Ctip2_B1_07	25 nmol	gatccgattggaaccgtccc
	ctccaatgcgatgctaagac	Ctip2_B1_08	25 nmol	gatccgattggaaccgtccc
	acacaattgcaggatgtggg	Ctip2_B1_09	25 nmol	gatccgattggaaccgtccc
	tgggatttatctgtaggctg	Ctip2_B1_10	25 nmol	gatccgattggaaccgtccc
	gacacagtcaagttaccact	Ctip2_B1_11	25 nmol	gatccgattggaaccgtccc
	cacagaaacggaagcagcgt	Ctip2_B1_12	25 nmol	gatccgattggaaccgtccc
	aagctttaaagtgcgggtca	Ctip2_B1_13	25 nmol	gatccgattggaaccgtccc
	cactgacactcaatctcagc	Ctip2_B1_14	25 nmol	gatccgattggaaccgtccc
	tattgtgaatgccacgctta	Ctip2_B1_15	25 nmol	gatccgattggaaccgtccc
	tggcagtagagaaactgtcc	Ctip2_B1_16	25 nmol	gatccgattggaaccgtccc
	ggaagatcggttttcaaggc	Ctip2_B1_17	25 nmol	gatccgattggaaccgtccc
	actggtcttatggcattttc	Ctip2_B1_18	25 nmol	gatccgattggaaccgtccc
	cccttgtatgtatccaatac	Ctip2_B1_19	25 nmol	gatccgattggaaccgtccc
	gtggcattctgtataaccta	Ctip2_B1_20	25 nmol	gatccgattggaaccgtccc
	tacaggttgctgtgacagag	Ctip2_B1_21	25 nmol	gatccgattggaaccgtccc
	gaaccgaccaatagatccat	Ctip2_B1_22	25 nmol	gatccgattggaaccgtccc
	aatacagcgagagcctacat	Ctip2_B1_23	25 nmol	gatccgattggaaccgtccc
	ctttcttttctccactcaac	Ctip2_B1_24	25 nmol	gatccgattggaaccgtccc
	gacattccaagggaacagga	Ctip2_B1_25	25 nmol	gatccgattggaaccgtccc
	gaaggcacagaattccttca	Ctip2_B1_26	25 nmol	gatccgattggaaccgtccc
	gtgagacagactctgcattt	Ctip2_B1_27	25 nmol	gatccgattggaaccgtccc
	gtgtcaaaagggcagggtaa	Ctip2_B1_28	25 nmol	gatccgattggaaccgtccc
	ccaatagggagcaactttgg	Ctip2_B1_29	25 nmol	gatccgattggaaccgtccc
	tcacggaatcaaacctcgga	Ctip2_B1_30	25 nmol	gatccgattggaaccgtccc
	ccttgccagtacaaaagcaa	Ctip2_B1_31	25 nmol	gatccgattggaaccgtccc
	gctgtaagagacaaaccctc	Ctip2_B1_32	25 nmol	gatccgattggaaccgtccc
	ctgtgcagaccacatcagag	Iba1_B1_01	25 nmol	gatccgattggaaccgtccc
	caggaatggggtgagctgag	Iba1_B1_02	25 nmol	gatccgattggaaccgtccc
	aggaggactggctgactttc	Iba1_B1_03	25 nmol	gatccgattggaaccgtccc
	atgcaggttaagacaggcag	Iba1_B1_04	25 nmol	gatccgattggaaccgtccc
	ttgaaatctcctcaggcttc	Iba1_B1_05	25 nmol	gatccgattggaaccgtccc

Iba1 Probe	aggcatcacttccacatcag	Iba1_B1_06	25 nmol	gatccgattggaaccgtccc
	actcattcccttgctaactc	Iba1_B1_07	25 nmol	gatccgattggaaccgtccc
	tcagacgctggttgtcttag	Iba1_B1_08	25 nmol	gatccgattggaaccgtccc
	aaatccctgctttggctcat	Iba1_B1_09	25 nmol	gatccgattggaaccgtccc
	cagcagtccaaaagcttttc	Iba1_B1_10	25 nmol	gatccgattggaaccgtccc
	ttgggatcatcgaggaattg	Iba1_B1_11	25 nmol	gatccgattggaaccgtccc
	cagatcctcatcattgctgt	Iba1_B1_12	25 nmol	gatccgattggaaccgtccc
	cttgaaggcttcaagtttgg	Iba1_B1_13	25 nmol	gatccgattggaaccgtccc
	atcaaactccatgtacttca	Iba1_B1_14	25 nmol	gatccgattggaaccgtccc
	cgatatctccatttccattc	Iba1_B1_15	25 nmol	gatccgattggaaccgtccc
	gcattcgcttcaaggacata	Iba1_B1_16	25 nmol	gatccgattggaaccgtccc
	ttgggaaccccaagtttctc	Iba1_B1_17	25 nmol	gatccgattggaaccgtccc
	atctcttcagctctaggtgg	Iba1_B1_18	25 nmol	gatccgattggaaccgtccc
	ccactggacacctctctaat	Iba1_B1_19	25 nmol	gatccgattggaaccgtccc
	cagagtagctgaacgtctcc	Iba1_B1_20	25 nmol	gatccgattggaaccgtccc
	cccagcatcattctgagaaa	Iba1_B1_21	25 nmol	gatccgattggaaccgtccc
	tctcaagatggcagatctct	Iba1_B1_22	25 nmol	gatccgattggaaccgtccc
	ctcggagatagctttcttgg	Iba1_B1_23	25 nmol	gatccgattggaaccgtccc
	tgacatccacctccaatcag	Iba1_B1_24	25 nmol	gatccgattggaaccgtccc
	atcagaagctcctcactcag	Iba1_B1_25	25 nmol	gatccgattggaaccgtccc
	tatttagtctgactctggct	Iba1_B1_26	25 nmol	gatccgattggaaccgtccc
Kcnk9 Probe	tttaagtttctcctcctcgc	Kcnk9_exon_01	5 nmol	CAL Fluor Red 610
	ctctgagacggacttcttcg	Kcnk9_exon_02	5 nmol	CAL Fluor Red 610
	catcggagctgatgttgtac	Kcnk9_exon_03	5 nmol	CAL Fluor Red 610
	tcagactgcaggattaccag	Kcnk9_exon_04	5 nmol	CAL Fluor Red 610
	aatttccactggacaccagc	Kcnk9_exon_05	5 nmol	CAL Fluor Red 610
	ggcgaagtagaaggaaccgg	Kcnk9_exon_06	5 nmol	CAL Fluor Red 610
	cgatagttgtgatgacagtg	Kcnk9_exon_07	5 nmol	CAL Fluor Red 610
	aggtgcagcatgtccatatc	Kcnk9_exon_08	5 nmol	CAL Fluor Red 610
	agcacagcgtagaacataca	Kcnk9_exon_09	5 nmol	CAL Fluor Red 610
	aggctctggaacataaccag	Kcnk9_exon_10	5 nmol	CAL Fluor Red 610
	tagcgcacgaaggtgttcat	Kcnk9_exon_11	5 nmol	CAL Fluor Red 610
	gcacttcttgatacgtttca	Kcnk9_exon_12	5 nmol	CAL Fluor Red 610
	gaaacttcagtgttgcgcat	Kcnk9_exon_13	5 nmol	CAL Fluor Red 610
	caggaaaagaagccgacggt	Kcnk9_exon_14	5 nmol	CAL Fluor Red 610
	tgttatgaagcagtagtagt	Kcnk9_exon_15	5 nmol	CAL Fluor Red 610
	caaaatcgccgaaccctata	Kcnk9_exon_16	5 nmol	CAL Fluor Red 610

	tgaaggccacatagaatggc	Kcnk9_exon_17	5 nmol	CAL Fluor Red 610
	cccaccaggatatacatgaa	Kcnk9_exon_18	5 nmol	CAL Fluor Red 610
	tgaggaaggcaccgatgacg	Kcnk9_exon_19	5 nmol	CAL Fluor Red 610
	aggaatcgcaggaccacaag	Kcnk9_exon_20	5 nmol	CAL Fluor Red 610
	ctcctcatcggtattcatgg	Kcnk9_exon_21	5 nmol	CAL Fluor Red 610
	caagaatctccgcaacttct	Kcnk9_exon_22	5 nmol	CAL Fluor Red 610
	ctgaggaagtacatggcgtg	Kcnk9_exon_23	5 nmol	CAL Fluor Red 610
	gaagcagagatagcacaggg	Kcnk9_exon_24	5 nmol	CAL Fluor Red 610
	ggaaacggtgtggacggtag	Kcnk9_exon_25	5 nmol	CAL Fluor Red 610
	tctggagggatctcttcaac	Kcnk9_exon_26	5 nmol	CAL Fluor Red 610
	ccgaaaacggaccggaagta	Kcnk9_exon_27	5 nmol	CAL Fluor Red 610
	tgtgcattccaggaggaatg	Kcnk9_exon_28	5 nmol	CAL Fluor Red 610
	tagatggacttgcgacggag	Kcnk9_exon_29	5 nmol	CAL Fluor Red 610
Pvalb Probe	tgagcacgtctgtcatcgac	Pvalb_B1_01	25 nmol	gatccgattggaaccgtccc
	ctcctatcgccttcttgatg	Pvalb_B1_02	25 nmol	gatccgattggaaccgtccc
	gtggtcgaaggagtctgcag	Pvalb_B1_03	25 nmol	gatccgattggaaccgtccc
	ccaccatctggaagaacttt	Pvalb_B1_04	25 nmol	gatccgattggaaccgtccc
	tccgggttctttttcttcag	Pvalb_B1_05	25 nmol	gatccgattggaaccgtccc
	atggaacaccttcttcacct	Pvalb_B1_06	25 nmol	gatccgattggaaccgtccc
	cacttttgtctttgtccaga	Pvalb_B1_07	25 nmol	gatccgattggaaccgtccc
	agctcatcctcctcaatgaa	Pvalb_B1_08	25 nmol	gatccgattggaaccgtccc
	agaagcccttcagaatggac	Pvalb_B1_09	25 nmol	gatccgattggaaccgtccc
	agacaagtctctggcatctg	Pvalb_B1_10	25 nmol	gatccgattggaaccgtccc
	cagaagcgtctttgtttctt	Pvalb_B1_11	25 nmol	gatccgattggaaccgtccc
	agccaccagagtggagaatt	Pvalb_B1_12	25 nmol	gatccgattggaaccgtccc
	cgagaaggactgagatgggg	Pvalb_B1_13	25 nmol	gatccgattggaaccgtccc
	gaacagaaactcaggagggc	Pvalb_B1_14	25 nmol	gatccgattggaaccgtccc
	catagaggatgggggagtaa	Pvalb_B1_15	25 nmol	gatccgattggaaccgtccc
	agaagaatggcgtcatccga	Pvalb_B1_16	25 nmol	gatccgattggaaccgtccc
	ctttattgtttctccagcat	Pvalb_B1_17	25 nmol	gatccgattggaaccgtccc
	ctacaggtggtgtccgattg	Pvalb_B1_18	25 nmol	gatccgattggaaccgtccc
	aaacttgccaaaccaacacc	Pvalb_B1_19	25 nmol	gatccgattggaaccgtccc
	cccactgccctaaaaagaaa	Pvalb_B1_20	25 nmol	gatccgattggaaccgtccc
	caggagatatcggggcgttg	Pvalb_B1_21	25 nmol	gatccgattggaaccgtccc
	catgagcactcagtaccaag	Pvalb_B1_22	25 nmol	gatccgattggaaccgtccc
	agagattgaacgaggtggcc	Pvalb_B1_23	25 nmol	gatccgattggaaccgtccc

	catctccttgtgggaaaggt	Pvalb_B1_24	25 nmol	gatccgattggaaccgtccc
	aagatggacgatccatcacc	Pvalb_B1_25	25 nmol	gatccgattggaaccgtccc
	ccttctgctctttaaaaggc	Pvalb_B1_26	25 nmol	gatccgattggaaccgtccc
	ctgaaggactcaacccttc	Pvalb_B1_27	25 nmol	gatccgattggaaccgtccc
	gagtcctttgatctagctag	Pvalb_B1_28	25 nmol	gatccgattggaaccgtccc
Satb2 Probe	tctgtccatggagcaaaagt	Satb2_B1_01	25 nmol	gatccgattggaaccgtccc
	ggtcgcaataaaacgcgcag	Satb2_B1_02	25 nmol	gatccgattggaaccgtccc
	ctcggttgtcgtattcaaga	Satb2_B1_03	25 nmol	gatccgattggaaccgtccc
	accagctggctaaaaagcac	Satb2_B1_04	25 nmol	gatccgattggaaccgtccc
	gcgtcacaacgtgatagaca	Satb2_B1_05	25 nmol	gatccgattggaaccgtccc
	tctggttcatttctttgagc	Satb2_B1_06	25 nmol	gatccgattggaaccgtccc
	acttggttgctgacacattg	Satb2_B1_07	25 nmol	gatccgattggaaccgtccc
	cagctggttcatatttggta	Satb2_B1_08	25 nmol	gatccgattggaaccgtccc
	aagaactgctggttgatggc	Satb2_B1_09	25 nmol	gatccgattggaaccgtccc
	tatcaggagagacttccaca	Satb2_B1_10	25 nmol	gatccgattggaaccgtccc
	actcatctctaacttgctgg	Satb2_B1_11	25 nmol	gatccgattggaaccgtccc
	tctctgacaataatccctgt	Satb2_B1_12	25 nmol	gatccgattggaaccgtccc
	catcctggtaaatgcgatca	Satb2_B1_13	25 nmol	gatccgattggaaccgtccc
	cgtcataaatggcagctgtg	Satb2_B1_14	25 nmol	gatccgattggaaccgtccc
	ccaacgaagcagttcgcaaa	Satb2_B1_15	25 nmol	gatccgattggaaccgtccc
	actgtggtgatgtcgagatt	Satb2_B1_16	25 nmol	gatccgattggaaccgtccc
	tctagtccttcggattgtaa	Satb2_B1_17	25 nmol	gatccgattggaaccgtccc
	attacccattaaaagctgcc	Satb2_B1_18	25 nmol	gatccgattggaaccgtccc
	aagtttcctctgcactgaac	Satb2_B1_19	25 nmol	gatccgattggaaccgtccc
	actcattgagactgcgctaa	Satb2_B1_20	25 nmol	gatccgattggaaccgtccc
	tctaaccgggcagaaacttc	Satb2_B1_21	25 nmol	gatccgattggaaccgtccc
	tggaggtgcatgattccaaa	Satb2_B1_22	25 nmol	gatccgattggaaccgtccc
	tgactctgctgaaatcgctt	Satb2_B1_23	25 nmol	gatccgattggaaccgtccc
	tggcattagttctgctttac	Satb2_B1_24	25 nmol	gatccgattggaaccgtccc
	tgtggtagattgcagcttta	Satb2_B1_25	25 nmol	gatccgattggaaccgtccc
	tgtcactggaactggaaggt	Satb2_B1_26	25 nmol	gatccgattggaaccgtccc
	tgtattgcaacgtgtcttct	Satb2_B1_27	25 nmol	gatccgattggaaccgtccc
	gctcatgtcaagggtaactg	Satb2_B1_28	25 nmol	gatccgattggaaccgtccc
	actctcggattaaagctgca	Satb2_B1_29	25 nmol	gatccgattggaaccgtccc
	tgtacagagtgacttcagca	Satb2_B1_30	25 nmol	gatccgattggaaccgtccc
	acctgtaagagcttggcaaa	Satb2_B1_31	25 nmol	gatccgattggaaccgtccc
	aaatgcccacagattcactt	Satb2_B1_32	25 nmol	gatccgattggaaccgtccc

Trappc9 Probe	acggacatgtggtagtgtac	Trappc9_exon_01	5 nmol	CAL Fluor Red 610
	aggaagtcattcactgagcg	Trappc9_exon_02	5 nmol	CAL Fluor Red 610
	atgactgaagccgagcacaa	Trappc9_exon_03	5 nmol	CAL Fluor Red 610
	cttctgagggaagtgagctg	Trappc9_exon_04	5 nmol	CAL Fluor Red 610
	caatgagaacttcttgcgcc	Trappc9_exon_05	5 nmol	CAL Fluor Red 610
	tgctggtgtcaggatttatg	Trappc9_exon_06	5 nmol	CAL Fluor Red 610
	tttgtcaatgatgtcctcgg	Trappc9_exon_07	5 nmol	CAL Fluor Red 610
	aataggagatggcctctttg	Trappc9_exon_08	5 nmol	CAL Fluor Red 610
	ctgaagaaactccgaagcct	Trappc9_exon_09	5 nmol	CAL Fluor Red 610
	ccggagattgatgtacacag	Trappc9_exon_10	5 nmol	CAL Fluor Red 610
	ggattttctcttcttccgaa	Trappc9_exon_11	5 nmol	CAL Fluor Red 610
	cgtagagctcagacaggatg	Trappc9_exon_12	5 nmol	CAL Fluor Red 610
	aagaatgctgacttgcggtg	Trappc9_exon_13	5 nmol	CAL Fluor Red 610
	gtctccaaaaggagcttgta	Trappc9_exon_14	5 nmol	CAL Fluor Red 610
	cagacaggaagtccagcatg	Trappc9_exon_15	5 nmol	CAL Fluor Red 610
	caacttggtaaacggcacgg	Trappc9_exon_16	5 nmol	CAL Fluor Red 610
	atagatgaaggggctcttgg	Trappc9_exon_17	5 nmol	CAL Fluor Red 610
	cggttatgtgcgatgattgg	Trappc9_exon_18	5 nmol	CAL Fluor Red 610
	tcagctgaacttcacacaca	Trappc9_exon_19	5 nmol	CAL Fluor Red 610
	aaagcgctgcaggaagagac	Trappc9_exon_20	5 nmol	CAL Fluor Red 610
	cattcacagtgatcattcct	Trappc9_exon_21	5 nmol	CAL Fluor Red 610
	ccaaagactgtggtatggta	Trappc9_exon_22	5 nmol	CAL Fluor Red 610
	cagaaggcagtcgctgaaga	Trappc9_exon_23	5 nmol	CAL Fluor Red 610
	tgatctgcagtcttggcaag	Trappc9_exon_24	5 nmol	CAL Fluor Red 610
	cttggtggtgagaagctttg	Trappc9_exon_25	5 nmol	CAL Fluor Red 610
	agtttccagctcaagaagtc	Trappc9_exon_26	5 nmol	CAL Fluor Red 610
	gaaaggactggacaggggaa	Trappc9_exon_27	5 nmol	CAL Fluor Red 610
	agggagaggttcctgtaata	Trappc9_exon_28	5 nmol	CAL Fluor Red 610
	tgtccacttgaatagccatt	Trappc9_exon_29	5 nmol	CAL Fluor Red 610
	atgcacgctgggtaagcaaa	Trappc9_exon_30	5 nmol	CAL Fluor Red 610
	gaggtcgctcagcataatag	Trappc9_exon_31	5 nmol	CAL Fluor Red 610
	agatcagaaaggctcctctg	Trappc9_exon_32	5 nmol	CAL Fluor Red 610

* 3’ modification was Quasar 570 for split Bcl-x_L experiment

Table A2: Sequences for probes used in Chapter 4

For co-expression of *Bcl-x$_L$* and *H13$_L$* introns in Satb2+ cells, *H13$_L$* probes were modified with the B3 (5'-CCCATGATCGTCCGATCTGG-3') tail sequence instead of B11.

Sequence	Sequence Name	Synthesis Scale	5' modification
ccgtcgtctccggtccaccgttgcgcttac	B11_Stv_10	1 µmole	CAL Fluor Red 610
acaaatccgaccagatcggacgatcatggg	B3_Stv_3	1 µmole	Alexa 647

	Sequence	Sequence Name	Synthesis Scale	3' modification
Bcl-x$_L$ intronic probe	ctcctgaacaatcggtatct	Bclx_B11_intron_01	25 nmole	gcagattccgctacgctccg
	ggatgaaagatacaggtccc	Bclx_B11_intron_02	25 nmole	gcagattccgctacgctccg
	aagggctctacaaacaagcc	Bclx_B11_intron_03	25 nmole	gcagattccgctacgctccg
	tctctttatctttgggtcac	Bclx_B11_intron_04	25 nmole	gcagattccgctacgctccg
	aagggtaacaaacgcctacc	Bclx_B11_intron_05	25 nmole	gcagattccgctacgctccg
	ttgcctttacaagagctact	Bclx_B11_intron_06	25 nmole	gcagattccgctacgctccg
	taggaccactcagtcaacta	Bclx_B11_intron_07	25 nmole	gcagattccgctacgctccg
	cagtttagcatttttccagg	Bclx_B11_intron_08	25 nmole	gcagattccgctacgctccg
	caagttaccaggtatgttgc	Bclx_B11_intron_09	25 nmole	gcagattccgctacgctccg
	tggaacatgtgaatggccac	Bclx_B11_intron_10	25 nmole	gcagattccgctacgctccg
	ggcatggatggaaagagtct	Bclx_B11_intron_11	25 nmole	gcagattccgctacgctccg
	gagtttctatgctactctgt	Bclx_B11_intron_12	25 nmole	gcagattccgctacgctccg
	tttctataggcatgctgttc	Bclx_B11_intron_13	25 nmole	gcagattccgctacgctccg
	gtttccacacatttgggaac	Bclx_B11_intron_14	25 nmole	gcagattccgctacgctccg
	tgcctgagttttcttagtac	Bclx_B11_intron_15	25 nmole	gcagattccgctacgctccg
	agcgaagggcttttattctg	Bclx_B11_intron_16	25 nmole	gcagattccgctacgctccg
	ctcagtgaacaggcttagtt	Bclx_B11_intron_17	25 nmole	gcagattccgctacgctccg
	taagagtagagctgcagctt	Bclx_B11_intron_18	25 nmole	gcagattccgctacgctccg
	gaggtgcttcaactaagcac	Bclx_B11_intron_19	25 nmole	gcagattccgctacgctccg
	gaatttctgtgttggggttt	Bclx_B11_intron_20	25 nmole	gcagattccgctacgctccg
	gaggcatgagagaaggatgc	Bclx_B11_intron_21	25 nmole	gcagattccgctacgctccg
	aaaagcaagtcctgtggtgg	Bclx_B11_intron_22	25 nmole	gcagattccgctacgctccg
	agggacaacaggattcggag	Bclx_B11_intron_23	25 nmole	gcagattccgctacgctccg
	gtgggactctttttatcact	Bclx_B11_intron_24	25 nmole	gcagattccgctacgctccg
	ggctaagataaccagtgagc	Bclx_B11_intron_25	25 nmole	gcagattccgctacgctccg
	taactgggtcaaaggaggcg	Bclx_B11_intron_26	25 nmole	gcagattccgctacgctccg
	ctgtgctaggcattatctat	Bclx_B11_intron_27	25 nmole	gcagattccgctacgctccg
	gccttagctgatctgagaaa	Bclx_B11_intron_28	25 nmole	gcagattccgctacgctccg
	ttccacctagaatctccaaa	Bclx_B11_intron_29	25 nmole	gcagattccgctacgctccg
	acaaggtgcagtttttcagg	Bclx_B11_intron_30	25 nmole	gcagattccgctacgctccg
	gtatgacagcaacatgctgt	Bclx_B11_intron_31	25 nmole	gcagattccgctacgctccg

	gctttgtgaatgagccaaga	Bclx_B11_intron_32	25 nmole	gcagattccgctacgctccg
	tcctaggatgtcaattccaa	Bclx_B11_intron_33	25 nmole	gcagattccgctacgctccg
	cttggtgaaatctgccaagg	Bclx_B11_intron_34	25 nmole	gcagattccgctacgctccg
Cox4i2 intronic probe	gcaccagaatctgagactta	Cox4i2_B11_intron_01	25 nmole	gcagattccgctacgctccg
	tataagctcgttaacaggcc	Cox4i2_B11_intron_02	25 nmole	gcagattccgctacgctccg
	cgagaaacttggtccaggac	Cox4i2_B11_intron_03	25 nmole	gcagattccgctacgctccg
	acctggaatgaagagtctgc	Cox4i2_B11_intron_04	25 nmole	gcagattccgctacgctccg
	agaggtaaggtaagccacac	Cox4i2_B11_intron_05	25 nmole	gcagattccgctacgctccg
	ttaggaagtggagggtcttg	Cox4i2_B11_intron_06	25 nmole	gcagattccgctacgctccg
	agagaggacagttttcttcc	Cox4i2_B11_intron_07	25 nmole	gcagattccgctacgctccg
	cccagataatccatccaaag	Cox4i2_B11_intron_08	25 nmole	gcagattccgctacgctccg
	gaacgggtgatagattgtcc	Cox4i2_B11_intron_09	25 nmole	gcagattccgctacgctccg
	actgtgcacagttgtatctg	Cox4i2_B11_intron_10	25 nmole	gcagattccgctacgctccg
	cactgccacttaacatgcaa	Cox4i2_B11_intron_11	25 nmole	gcagattccgctacgctccg
	cttcattagagacagctggg	Cox4i2_B11_intron_12	25 nmole	gcagattccgctacgctccg
	atccattcgaaactgccatg	Cox4i2_B11_intron_13	25 nmole	gcagattccgctacgctccg
	ggtgaggaagggctgaaaga	Cox4i2_B11_intron_14	25 nmole	gcagattccgctacgctccg
	gggaagtctagtaaggcaga	Cox4i2_B11_intron_15	25 nmole	gcagattccgctacgctccg
	ctgtgttctttgggaagaca	Cox4i2_B11_intron_16	25 nmole	gcagattccgctacgctccg
H13L intronic probe	gttctgcactgtcaggaaag	H13L_B11_intron_01	25 nmole	gcagattccgctacgctccg
	cctgatgaagacagtgcttg	H13L_B11_intron_02	25 nmole	gcagattccgctacgctccg
	ggcagaaaccaggtagagag	H13L_B11_intron_03	25 nmole	gcagattccgctacgctccg
	ctagaatggccatgtgacac	H13L_B11_intron_04	25 nmole	gcagattccgctacgctccg
	gcatggcatttaaaaccgga	H13L_B11_intron_05	25 nmole	gcagattccgctacgctccg
	ggcttcatgtggacagtaag	H13L_B11_intron_06	25 nmole	gcagattccgctacgctccg
	agggcacctcaaaactgtat	H13L_B11_intron_07	25 nmole	gcagattccgctacgctccg
	gaagggaggagtgaagagca	H13L_B11_intron_08	25 nmole	gcagattccgctacgctccg
	gcttggtggaaggtttaagg	H13L_B11_intron_09	25 nmole	gcagattccgctacgctccg
	ctaagcttattcctggatct	H13L_B11_intron_10	25 nmole	gcagattccgctacgctccg
	aagaatctcttctctccagg	H13L_B11_intron_11	25 nmole	gcagattccgctacgctccg
	tcagggatatagccatctag	H13L_B11_intron_12	25 nmole	gcagattccgctacgctccg
	atgtctcggagaagtagacc	H13L_B11_intron_13	25 nmole	gcagattccgctacgctccg
	atgtctacctagagcaatgc	H13L_B11_intron_14	25 nmole	gcagattccgctacgctccg
	cactattcagggcagtaagg	H13L_B11_intron_15	25 nmole	gcagattccgctacgctccg
	ttgctattgtcagagggtac	H13L_B11_intron_16	25 nmole	gcagattccgctacgctccg
	ttgggcaatgtggaatgtcg	H13L_B11_intron_17	25 nmole	gcagattccgctacgctccg
	catgttcttgcctaagatgg	H13L_B11_intron_18	25 nmole	gcagattccgctacgctccg
	gcagggatggaaggtcaaac	H13L_B11_intron_19	25 nmole	gcagattccgctacgctccg
	tccttgtaggttttttgagg	H13L_B11_intron_20	25 nmole	gcagattccgctacgctccg
	agtaaagaggcatcgacctc	H13L_B11_intron_21	25 nmole	gcagattccgctacgctccg
	atctcggagataaatggcct	H13L_B11_intron_22	25 nmole	gcagattccgctacgctccg
	acaaagtgtactcgtggctt	H13L_B11_intron_23	25 nmole	gcagattccgctacgctccg
	tggacttggagggagtaagt	H13L_B11_intron_24	25 nmole	gcagattccgctacgctccg
	ctgcgtgttagtgatcattc	H13L_B11_intron_25	25 nmole	gcagattccgctacgctccg

	ctatctcatctgacctactt	H13L_B11_intron_26	25 nmole	gcagattccgctacgctccg
	gatgtgactcttgtcatctc	H13L_B11_intron_27	25 nmole	gcagattccgctacgctccg
	tcgcctattacctctgaaag	H13L_B11_intron_28	25 nmole	gcagattccgctacgctccg
	gagaaggtctaatgtcctgg	H13L_B11_intron_29	25 nmole	gcagattccgctacgctccg
	gctgggagaaaaggaaggca	H13L_B11_intron_30	25 nmole	gcagattccgctacgctccg
	aacagggctagagtcagaga	H13L_B11_intron_31	25 nmole	gcagattccgctacgctccg
	acagaggctagtgagggaag	H13L_B11_intron_32	25 nmole	gcagattccgctacgctccg
Tpx2 intronic probe	cagaaccctggaaaaacggc	Tpx2_B11_intron_01	25 nmole	gcagattccgctacgctccg
	ggttcccagaaataccaacg	Tpx2_B11_intron_02	25 nmole	gcagattccgctacgctccg
	cttacaccaacagtccttac	Tpx2_B11_intron_03	25 nmole	gcagattccgctacgctccg
	gaataagcttggtgcgggaa	Tpx2_B11_intron_04	25 nmole	gcagattccgctacgctccg
	attcaatggcagggctattt	Tpx2_B11_intron_05	25 nmole	gcagattccgctacgctccg
	actttgctatcccagacaaa	Tpx2_B11_intron_06	25 nmole	gcagattccgctacgctccg
	ctctacctcaattgtgttgg	Tpx2_B11_intron_07	25 nmole	gcagattccgctacgctccg
	cccacagtactatatgatct	Tpx2_B11_intron_08	25 nmole	gcagattccgctacgctccg
	ggaaaattgggtgtaagccc	Tpx2_B11_intron_09	25 nmole	gcagattccgctacgctccg
	ctgaggccacacacaagaat	Tpx2_B11_intron_10	25 nmole	gcagattccgctacgctccg
	tatgatctggggcaacttga	Tpx2_B11_intron_11	25 nmole	gcagattccgctacgctccg
	caaaggtcaattagttggcc	Tpx2_B11_intron_12	25 nmole	gcagattccgctacgctccg
	agcataccagaaaacccttg	Tpx2_B11_intron_13	25 nmole	gcagattccgctacgctccg
	ccatgagcaagatattgggt	Tpx2_B11_intron_14	25 nmole	gcagattccgctacgctccg
	tccacttctaaattgccaga	Tpx2_B11_intron_15	25 nmole	gcagattccgctacgctccg
	cttccctcttttaaatctca	Tpx2_B11_intron_16	25 nmole	gcagattccgctacgctccg
	ccagacacttcgaaaatcca	Tpx2_B11_intron_17	25 nmole	gcagattccgctacgctccg
	ctgctttctgagagtttgta	Tpx2_B11_intron_18	25 nmole	gcagattccgctacgctccg
	atatatgcagcctggttgtt	Tpx2_B11_intron_19	25 nmole	gcagattccgctacgctccg
	cttcctagacatccaattca	Tpx2_B11_intron_20	25 nmole	gcagattccgctacgctccg
	tttgctgccaacttagacag	Tpx2_B11_intron_21	25 nmole	gcagattccgctacgctccg
	atctagtttctcacacttgc	Tpx2_B11_intron_22	25 nmole	gcagattccgctacgctccg
	cattagcataaacttggcca	Tpx2_B11_intron_23	25 nmole	gcagattccgctacgctccg
	ggaccagcaagataatctga	Tpx2_B11_intron_24	25 nmole	gcagattccgctacgctccg
	gaacagacccaagagaagct	Tpx2_B11_intron_25	25 nmole	gcagattccgctacgctccg
	gtgtacaggctcatagtgta	Tpx2_B11_intron_26	25 nmole	gcagattccgctacgctccg
	caccacctttgtgaaaggat	Tpx2_B11_intron_27	25 nmole	gcagattccgctacgctccg
	ttatacaggatcttgggctg	Tpx2_B11_intron_28	25 nmole	gcagattccgctacgctccg
	ataactcacctggaagcagt	Tpx2_B11_intron_29	25 nmole	gcagattccgctacgctccg
	atttatgaagctggtatgct	Tpx2_B11_intron_30	25 nmole	gcagattccgctacgctccg
	caaggcagccataatttctc	Tpx2_B11_intron_31	25 nmole	gcagattccgctacgctccg
	attctggcttcaatccaaca	Tpx2_B11_intron_32	25 nmole	gcagattccgctacgctccg